


DIPLOMARBEIT

Multielemental Analysis of Coffee Samples Using Total Reflection X-ray Fluorescence (TXRF) and Energy-Dispersive X-ray Fluorescence (EDXRF) Methods

zur Erlangung des akademischen Grades

Diplom-Ingenieur/in

im Rahmen des Masterstudiums

Physikalische Energie- und Messtechnik

eingereicht von

Matthias Paul Weinberger, BSc.

Matrikelnummer: 01326345

ausgeführt am
Atominstitut der Fakultät für Physik, TU Wien in Zusammenarbeit mit dem Department für Chemie, Universität Girona

Betreuung:
Betreuer: Ao.Univ.Prof.i.R. Dipl.-Ing. Dr.techn. Peter Wobrauschek
Mitwirkung: Professora agregada Dra. Eva Marguí Grabulosa

Wien, am 29. September 2023

(Unterschrift Verfasser/in) (Unterschrift Betreuer/in)

Abstract

This Master's thesis focuses on the analysis of the multi-elemental composition of commercial coffee powder samples from Croatian supermarkets. The coffee samples come from three different categories: pure coffee, pure instant coffee and coffee with additives (e.g. milk, proteins). The analysis was performed using a Bruker Ranger S2 bench-top energy dispersive X-ray fluorescence (EDXRF) system and a total reflection X-ray fluorescence (TXRF) spectrometer custom-built at the Institute of Atomic and Subatomic Physics, TU Vienna, based on the WOBISTRAX design. Since there is no certified reference material (CRM) for coffee, the results obtained were verified and compared with inductively coupled optical plasma spectroscopy (ICP-OES) and flame atomic absorption spectroscopy (FAAS) measurements. The concentrations obtained showed acceptable agreement with the reference measurements. One of the novelties of this study is the detailed discussion of different sample preparation procedures. For the EDXRF analysis, pellets with and without different amounts of wax added for stabilization were compared to lose powder samples. For TXRF, we took the digest previously prepared for ICP measurements and added gallium as an internal standard. For the quantification of the EDXRF and TXRF measurements, we focused on the elements K, Ca, Mn, Fe, Cu, Zn, Sr and Rb. We applied a variety of fundamental parameter methods as well as empirical calibration methods. The obtained spectra and concentrations were then used for chemometric analysis, namely Principal Component Analysis (PCA) and Partial Least Square Discriminant Analysis (PLS-DA). The chemometrics were performed using SPSS, a commercial statistical software package. In contrast to many previous works on chemical fingerprinting of food samples, we also obtained chemometric results by inserting the raw spectra directly into the SPSS algorithms. This has the advantage that elemental concentrations do not have to be determined beforehand.

Key words: TXRF, EDXRF, coffee grain powders, multi-elemental analysis, chemometrics

Zusammenfassung

Diese Masterarbeit untersucht die multielementare Zusammensetzung von Kaffeepulverproben aus kroatischen Supermärkten. Die Kaffeeproben stammen aus drei verschiedenen Kategorien: purer Kaffee, purer Instantkaffee und Kaffee mit Zusatzstoffen (z.B. Milch, Proteine, etc.). Die Messungen wurden mit einem energiedispersiven Röntgenfluoreszenzsystem (EDRFA) von Bruker (Ranger S2) und einem Total-Reflexions-Röntgenfluoreszenzspektrometer (TRFA) durchgeführt, das am Atominstitut der TU Wien auf der Grundlage des WOBISTRAX-Designs entwickelt wurde. Da kein zertifiziertes Referenzmaterial (ZRM) für Kaffeepulver existiert, wurden die RFA Messergebnisse mit Hilfe von induktiv gekoppelten optischen Plasmaspektroskopie (ICP-OES)- Messungen und Flammen-Atomabsorptions-Spektroskopie (FAAS)- Messungen überprüft und verglichen. Die für die untersuchten Kaffeesorten erhaltenen Konzentrationen zeigten akzeptable Übereinstimmungen mit den Referenzmessungen. Eine der Neuheiten dieser Studie ist die detaillierte Diskussion der verschiedenen Probenvorbereitungsverfahren. Für die ED-RF-Analyse wurden Pellets mit und ohne unterschiedliche Mengen an Wachs, das zur Stabilisierung hinzugefügt wurde, mit losen Pulverproben verglichen. Für die TRF-Analyse wurden die zuvor für die ICP-Messungen vorbereiteten Digests verwendet und Gallium als interner Standard hinzugefügt. Bei der Quantifizierung der EDRFA- und TRRFA-Messungen konzentrierten wir uns auf die Elemente K, Ca, Mn, Fe, Cu, Zn, Sr und Rb. Wir verwendeten eine Reihe von Fundamentalparametermethoden sowie empirische Kalibrier-Methoden. Die erhaltenen Spektren und Konzentrationen wurden anschließend für chemometrische Analysen verwendet, insbesondere für die Hauptkomponentenanalyse (PCA) und die Regression der partiellen kleinsten Quadrate (PLS-DA). Die chemometrischen Analysen wurden mit SPSS, einem kommerziellen statistischen Softwarepaket, durchgeführt. Im Gegensatz zu vielen früheren Arbeiten über den chemischen Fingerabdruck von Lebensmittelproben erhielten wir auch chemometrische Ergebnisse, indem wir die Rohspektren direkt in die SPSS-Algorithmen einfügten. Dies hat den Vorteil, dass die Elementkonzentrationen nicht im Voraus bestimmt werden müssen.

Stichworte: TRFA, ED-RFA, Kaffeepulver, Multi-elementanalyse, Chemometrik

Parts of this thesis will be / were used for scientific publications and conference contributions:

Conferences:

- P. Wobrauschek, M. Weinberger, P. Kregsamer, E. Margui, J. Jablan and C. Streli. *Total Reflection X-Ray Fluorescence Analysis of Coffee samples*; presented at the Denver X-ray Conference 2023 through P. Wobrauschek (talk session).

- M. Weinberger, P. Wobrauschek, P. Kregsamer, E. Margui, J. Jablan and C. Streli. *Total Reflection X-Ray Fluorescence Analysis of Coffee samples*; presented at the International Conference of Total Reflection X-ray Fluorescence Analysis and Related Methods 2023 through P. Wobrauschek (poster session).

Publications:

- M. Weinberger, I. Queralt, C. Streli, P. Wobrauschek, E. Besalú, J. Jablan and E. Marguí. *Critical evaluation of energy dispersive X-ray fluorescence spectrometry for multielemental analysis of coffee samples: sample preparation, quantification and chemometric approaches.* 2023. Submitted to the Journal of Food Chemistry in July 2023, Manuscript Nr.: FOODCHEM-D-23-06473.

- M. Weinberger, I. Queralt , C. Streli, P. Wobrauschek, E. Besalú, J. Jablan and E. Marguí. *Critical evaluation of total reflection X-ray fluorescence spectrometry for multielemental analysis of coffee samples: sample preparation, quantification and chemometric approaches.* 2023. To be submitted to a thematically relevant scientific journal.

Contents

1 Introduction

1.1 General introduction

The first part of this thesis was carried out at the University of Girona, Spain, as part of an Erasmus+ internship from mid-September 2022 to mid-December 2022. During this period, the energy dispersive X-ray fluorescence (EDXRF) experiments were carried out. The total reflection X-ray fluorescence (TXRF) experiments were later performed at the Institute of Atomic and Subatomic Physics at the TU Wien.

1.2 Why do we analyze coffee-grain samples with X-ray fluorescence (XRF) analysis?

Coffee is one of the most widely consumed beverages in the world. For 2020/21, the International Coffee Organization (ICO) estimates global consumption at 164.5 million bags [1]. Given this immense number, it is surprising that little research has been done to determine the elemental concentrations of coffees using approaches other than induced coupled plasma (ICP) spectrometry (e.g. ICP-MS, ICP-OES), flame atomic absorption spectrometry (FAAS) and related techniques. In contrast to these approaches, X-ray fluorescence (XRF) techniques are generally non-destructive and do not necessarily require time-consuming digestion processes [2] [3]. Another advantage is that the exact same sample can be measured again later if re-analysis is necessary.
As traceability and product transparency become increasingly important in today's world, there is a growing demand for inexpensive, rapid multi-element analysis. Consumers and producers want to know what is in their products, not only to detect potentially toxic elements in coffees (e.g. Cd, Pb and Hg) from fertilizers or other sources of contamination [4], but also to estimate their macro- and micronutrient content. The concentrations of certain elements may be of interest from a health perspective, as Mn, Fe, Cu and Zn, for example, have antioxidant properties [5].

XRF techniques have proven to be useful tools for the multielemental analysis of other organic materials such as milk powders [6], wine [7] and blood samples [8][9]. However, the potential of XRF for the analysis of coffee grain samples has hardly been explored. Moreover, when XRF approaches are chosen, the literature often lacks information on why certain measurement conditions and

sample preparation techniques are preferred over others. Table 1 shows a comparison of the studies that have already been carried out using XRF methods for the elemental analysis of coffee beans. In order to have a broad basis of comparison for this study, a fundamental parameter method (FPM) and external calibration curves with 11 coffees as empirical standards, previously measured and quantified by ICP-OES, were used for energy dispersive X-ray fluorescence (EDXRF) and total reflection X-ray fluorescence (TXRF) analysis.

In addition, the elemental concentrations determined can be used as chemical fingerprints of the samples [10][11]. These plots can then be used for provenance and geographical origin studies. This has already been demonstrated for coffee by Worku et al. [12] and for bean seeds by Allegretta et al. [11]. For coffees, chemometric tools such as Principal Component Analysis (PCA), Linear Discriminant Analysis (LDA) or Partial Least Square Discriminant Analysis (PLS-DA) have been used for this task, as seen in Table 1. This study also explores the very novel strategy in the food field of using the raw EDXRF and TXRF spectra directly from the instrument. This approach eliminates the time-consuming process of elemental quantification. The use of the raw XRF spectra in food analysis has only been published in early 2023 [11].
The coffees in this master thesis come from three different categories (pure coffee, pure instant coffee and coffee with additives). In the future, the methods developed in this work could be used to distinguish not only between these types of coffee, which intuitively have different elemental compositions, but also between coffees from e.g. highland and lowland areas, and also between coffees from different growing regions in a fast and inexpensive way.

(a) (b)

Figure 1: Coffee plantation (a) and dried coffee beans (b) in Monteverde, Costa Rica (altitude ≈ 1300 m). Photos: Matthias Weinberger

Type of coffee	Analytes	Sample preparation	XRF system	Chemometric approach	Reference
Organic and commercial coffee	Mg, P, Cl, S, K, Ca, Cr, Mn, Ni, Cu,Zn, Br, Rb, Sr and Ba,	Coffee beans milled to powder, 40 mm diameter pellets, 5 g sample mass, no binder	EDXRF, epsilon 5 benchtop-system	PCA, PLS-DA	Fiamegos et al., 2021 [13]
Coffee samples from different Ethiopian markets (roasted, non-roasted comparison)	P, S, K, Ca, Mn, Fe, Cu, Zn, Se, Br, Rb, Sr	Three pellets of each sample, 200 mg sample mass, 13 mm diameter, 1-2 mm thickness	EDXRF, Rh anode, tube tension: 6-23 kV, tube current: 200 – 900 mA, Filter: none, titanium, iron, scan time: 200-600 s	None	Feleke et al., 2018 [14]
Commercial coffee samples from Brazil (Salvador region)	Mn, Fe, Cd, Pb	Three pellets of each sample, 5 g sample mass, 36 mm diameter pellets, 3 mm thickness	EDXRF, Ag anode, tube tension: 40 kV; tube current: 2 mA, Al 500 μ m filter for Pb, Mn, and Fe; Cu 300 μ m filter for Cd, scan time: 100 s	None	Almeida et al., 2021 [15]
Commercial coffee	K, Ca, Ti, Mn, Fe, Ni, Cu, Zn, As, Se, Br, Rb, Pb	Air dried at 85 °C, pressed into pellets, no diameter given	EDXRF, Mo anode, tube tension: 34 kV tube current: 18 mA, scan time: 2000 s	None	Orlić et al., 1986 [16]
Arabica coffee	Mg, Al, Si, P, S, Cl, K, Ca Fe, Mn, Cu, Ni, Zn, Rb, Sr	Pellets mixed with polypropylene wax binding agent 1:4, 40 mm diameter pellets	WDXRF; Rh tube for low atomic weight elements: tube tension: 25 kV, tube current: 160 mA; or high atomic weight elements: tube tension: 60 kV, tube current: 66 mA, no scan time given	LDA	Worku et al., 2019 [12]

Type of coffee	Analytes	Sample preparation	XRF system	Chemometric approach	Reference
Coffee grain samples	K, Ca, Cr, Mn, Fe, Ni, Cu, Zn, Br, Rb, Sr	6 replicates of each sample, 0.3 g sample mass, vanadium as internal standard, 10 μl pipetted on siliconized reflector (Serva silicon solution)	TXRF, EXTRA II TXRF spectrometer (Rich Seifert) scan time: 500 s	PCA, Cluster analysis	Haswell and Walmsley, 1998 [17]
Roasted ground coffee powders	25 elements	Samples dried in a vacuum oven for 3 h, at 110° C, loose powder analysis	Hand-held EDXRF system, Rh anode, Olympus Vanta C-sieries, scan time: 60 s	None	Denni and Joseph, 2019 [18]
Coffees from local markets (Rio de Janeiro, Brazil), roasted and ground coffees	P, S, Cl, K, Ca, Mn, Fe, Cu, Zn, Rb	Samples dried at 60° C, three pellets of each coffee, 1 g sample mass pressed into pellets of 2.2 - 2.4 mm thickness and 25.4 mm diameter	Ag anode, tube tension: 10-50 kV, tube current: 0,1-0,365 mA, scan time: 200 – 300 s, 500 μm Cu filter for Z >= 20	PCA	Machado et al. 2023 [19]
Commercial coffee powder and ground samples from Brazil, Venezuela and Peru	K, Rb, Ca, Cl, S, Sr, Fe	For coffee ground samples: 60 g of sample was passed by 90° C water, afterwards samples were dried at 100° C for 24 h.	Portable EDXRF system by Amptek, Ag anode, tube tension: 30 kV, tube current: 0,005 mA, scan time: 300 s	None	Guazzelli et al., 2022 [20]

Table 1: Summary of research already carried out in the context of coffees and X-ray florescence (XRF) analysis. Abbrevations: EDXRF = energy dispersive X-ray fluorescence, WDXRF = wavelength dispersive X-ray fluorescence, TXRF = total reflection X-ray fluorescence, PCA = principal component analysis, PLS-DA = partial least square-discriminant analysis, LDA = linear discriminant analysis), FP = fundamental parameters. Table used in similar form in [21].

2 Theory

2.1 Physical background of X-ray fluorescence (XRF) techniques

2.1.1 Basic principle of XRF

In X-ray fluorescence (XRF) methods, probes are irradiated with an X-ray beam and, if the beam energy is high enough, a primary photon can eject an inner electron from the atoms of the probe (**inner photoelectric effect**). If the remaining positive holes are then filled with electrons from the outer shells, the atoms can emit so-called "**characteristic X-ray radiation**". The probability of such an emission is a function of the atomic number Z and has a competing effect - the **Auger-Meitner effect** (visualized in Figure 3. The latter is a radiationless transition. When characteristic radiation is emitted, the energy of the photon is $E_{photon} = E_{previous} - E_{following}$. This transition is, as the name suggests, element specific because the different possible optical transitions are unique to each element. A schematic overview of this process and the possible transitions in *Siegbahn* and *IUPAC* notation is shown in Figure 4 and Figure 5. In this thesis the *IUPAC* notation is used. These emmited photons are then detected by a detector system and if the output signal is a function of the photon energy this is called "Energy-Dispersive X-ray Fluorescence" (EDXRF). The complementary method, where intensities are plotted over wavelengths, is called "Wavelength-Dispersive XRF" (WDXRF) [22] [23].

In addition to the X-ray line spectrum, there is also a continuous X-ray spectrum called the **bremsstrahlung** spectrum. This type of radiation is produced when an incoming electron is slowed down by inelastic coalitions with the nuclei of the anode. The continuous spectrum has an upper limit of $E_{max} = e \cdot U_0$ as this is the final energy the electron reaches when accelerated in an electric field. If all of the electron's energy is transferred to a photon, its energy becomes E_{max}. The range of the bremsstrahlung spectrum is therefore $0 \leq E_{photon} \leq E_{max}$.

In XRF experiments, a **side window X-ray tube** is usually used as the primary beam source (see Figure 2). An electric current is applied to a filament, usually made of tungsten (W), which heats up and emits electrons. A high voltage is applied between the cathode and anode of the X-ray tube and the electrons reach the energy $e \cdot U_0$ described above. When the electrons hit the anode

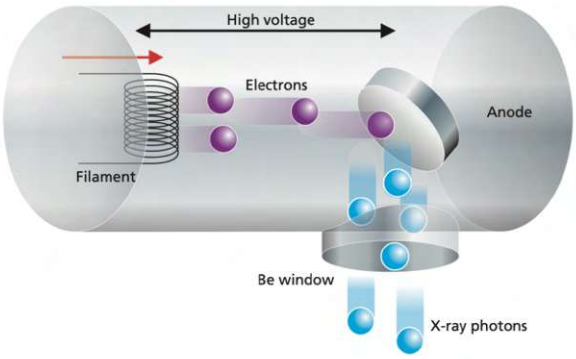

Figure 2: Classical side-widow X-ray tube with a beryllium (Be) window for the production of X-rays. Figure taken from [24].

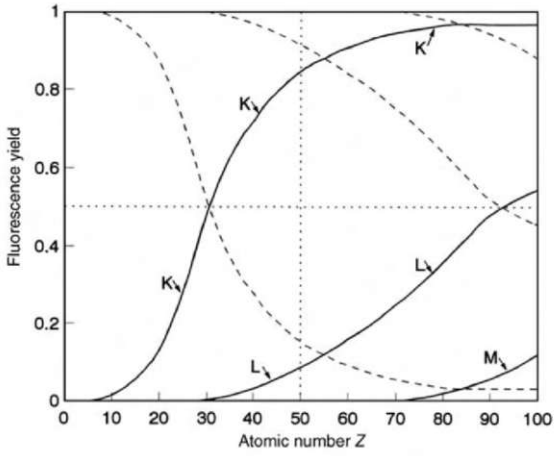

Figure 3: The photoelectric effect (black line) and its competing effect, the Auger-Meitner effect (dotted line). For light Z elements the Auger-Meitner effect is dominant, for heavier atoms the photoelectric absorption becomes the primary factor. Figure taken from [22].

material they produce *Bremsstrahlung* and X-rays characteristic of the anode material. Both then leave the tube through a thin beryllium (Be) window. Another common source of X-rays are synchrotrons, which use magnetic fields to force charged particles such as electrons into circular orbits. As synchrotron experiments were not part of this thesis, the author refers to the literature for further information [22].

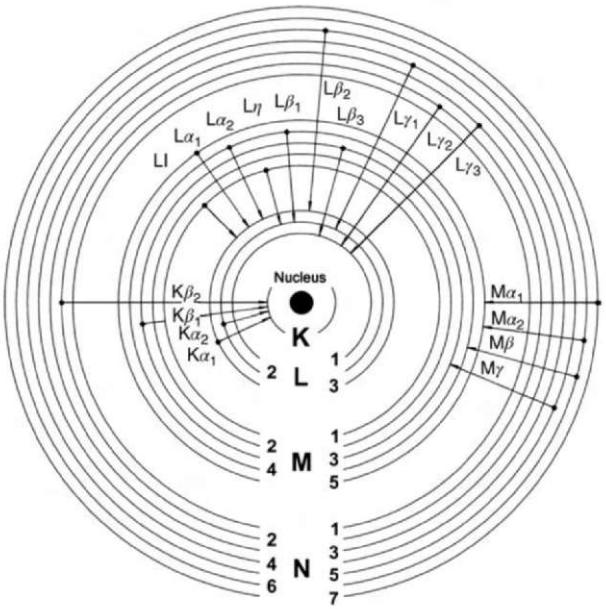

Figure 4: Schematic overview of the possible optical transitions of a heavy atom. Figure taken from [22].

Siegbahn	IUPAC	Siegbahn	IUPAC	Siegbahn	IUPAC	Siegbahn	IUPAC
$K\alpha_1$	K–L_3	$L\alpha_1$	L_3–M_5	$L\gamma_1$	L_2–N_4	$M\alpha_1$	M_5–N_7
$K\alpha_2$	K–L_2	$L\alpha_2$	L_3–M_4	$L\gamma_2$	L_1–N_2	$M\alpha_2$	M_5–N_6
$K\beta_1$	K–M_3	$L\beta_1$	L_2–M_4	$L\gamma_3$	L_1–N_3	$M\beta$	M_4–N_6
$K\beta_2^{I}$	K–N_3	$L\beta_2$	L_3–N_5	$L\gamma_4$	L_1–O_3	$M\gamma$	M_3–N_5
$K\beta_2^{II}$	K–N_2	$L\beta_3$	L_1–M_3	$L\gamma_4'$	L_1–O_2	$M\zeta$	$M_{4,5}$–$N_{2,3}$
$K\beta_3$	K–M_2	$L\beta_4$	L_1–M_2	$L\gamma_5$	L_2–N_1		
$K\beta_4^{I}$	K–N_5	$L\beta_5$	L_3–$O_{4,5}$	$L\gamma_6$	L_2–O_4		
$K\beta_4^{II}$	K–N_4	$L\beta_6$	L_3–N_1	$L\gamma_8$	L_2–O_1		
$K\beta_{4x}$	K–N_4	$L\beta_7$	L_3–O_1	$L\gamma_8'$	L_2–$N_{6,7}$		
$K\beta_5^{I}$	K–M_5	$L\beta_8$	L_3–$N_{6,7}$	$L\eta$	L_2–M_1		
$K\beta_5^{II}$	K–M_4	$L\beta_9$	L_1–M_5	Ll	L_3–M_1		
		$L\beta_{10}$	L_1–M_4	Ls	L_3–M_3		
		$L\beta_{15}$	L_3–N_4	Lt	L_3–M_2		
		$L\beta_{17}$	L_2–M_3	Lu	L_3–$N_{6,7}$		
				Lv	L_2–$N_{6,7}$		

Figure 5: IUPAC and Siegbahn notation of the possible optical transitions of a heavy atom. Figure taken from [22].

In addition to the Auger-Meitner process and the inner photoelectric effect, there are scattering and pair production processes that occur when X-rays interact with matter. However, pair production is only present when the primary photon has an energy of at least 1.022 MeV and is therefore irrelevant for the current study [25]. However, Compton and Rayleigh scattering play an important role, since the ratio between these two peaks can be used to determine the effective atomic number Z_{eff} of the sample matrix [26] [27]. This method is further explained in section 4.7.2. Figure 6 visualizes these two effects at the atomic level. The Rayleigh peak has a higher energy because the scattering is elastic in this case. The primary beam photon collides with a strongly bound inner-shell electron but does not transfer any energy. Compton scattering, on the other hand, is an inelastic phenomenon. The primary photons interact with weakly bound outer-shell electrons and transfer some of their energy to the ejected electron. The Compton peak therefore has a lower energy than the Rayleigh peak [24] [28] [29]. The energy loss can be calculated with [28], where φ is the scattering angle in the electron rest system, c is the velocity of light, and m_e is the electron mass.

$$\frac{E'}{E} = \frac{1}{\left(1 + (1 - cos(\varphi) \cdot \frac{E}{m_e \cdot c^2}\right)} \tag{1}$$

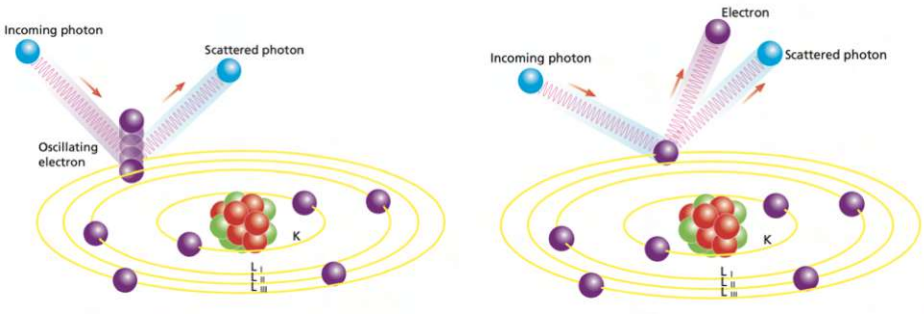

(a) (b)

Figure 6: Schematic Rayleigh- (a) and Compton-scattering process (b). Figures taken from [24]

If all the fundamental parameters contributing to the fluorescence intensity of an element i in a sample are known, it is possible to calculate the fluorescence intensity of a given line from them. Figure 7 shows the main components of the equation 2. The red line corresponds to the primary attenuation, the green line to the secondary attenuation, the yellow line to the sample/detector attenuation and the blue line to the fluorescence cross section [30] [31] [32] [33].

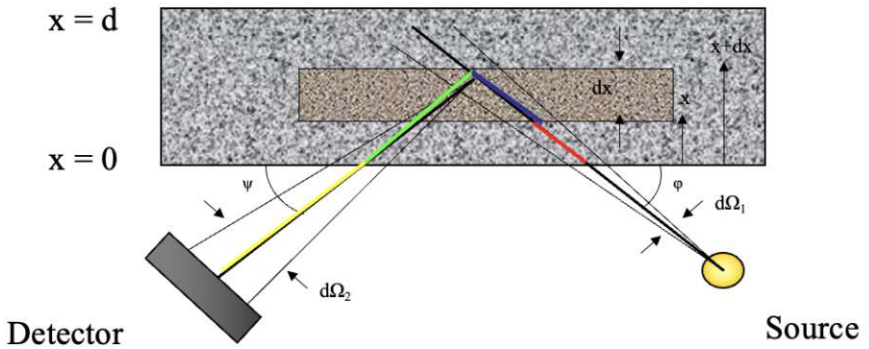

Figure 7: Contributions to the measured fluorescence intensity of an element i. Figure taken from [34].

$$I(E^i_{K_\alpha}) = \int_{E^i_{abs}}^{E_{max}} \int_0^d \underbrace{I_0(E)}_{\text{primary intensity}} \cdot \underbrace{\frac{A}{4\pi r^2}}_{\text{geometry factor } G_1} \cdot \underbrace{\frac{I_{int}(\varphi, E)}{I_0(E)}}_{\text{standing wave field}} \cdot \rho(x) \cdot$$
$$\underbrace{\frac{\tau^i_K(E)}{\rho} \cdot \omega^i_K \cdot p^i_\alpha}_{\text{fluorescence cross-section}} \cdot \underbrace{c^i}_{\text{concentration of element i}} \cdot \underbrace{G_2(\psi)}_{\text{secondary geometry factor}} \cdot$$
$$\underbrace{V^i(E)}_{\text{secondary excitation}} \cdot \underbrace{e^{-\left(\frac{\mu(E)}{\rho \cdot sin(\varphi)} + \frac{\mu(E^i_K)}{\rho \cdot sin(\psi)}\right)\rho \cdot x}}_{\text{primary + secondary attenuation}} \cdot$$
$$\underbrace{f(E^i_{K_\alpha})}_{\text{sample/detector attenuation}} \cdot \underbrace{\epsilon(E^i_{K_\alpha})}_{\text{detector efficiency}} \cdot dx \cdot dE \tag{2}$$

2.1.2 Total reflection X-ray fluorescence (TXRF)

If we irradiate the samples below the critical angle for total reflection, we get a double excitation (TXRF). This effect increases the signals for particles by a factor of ≈ 2 and therefore, together with the low background radiation, the detection limits [35]. Both XRF and TXRF are non-destructive methods [22] [31].

It is important to note that for X-rays, air or vacuum is optically denser than solids [22]. The refractive index can be written as $n = 1 - \delta - i\beta$, where δ is the decrement of the refractive index and β is the absorption term (which can be neglected for total reflection). The critical angle is calculated as suggested in [35] and [22]:

$$\alpha_{crit} \approx \sqrt{2\delta} \approx \frac{1.65}{E}\sqrt{\frac{Z}{A}\rho} \tag{3}$$

where E is the energy of a photon from the incoming beam [in keV], Z is the atomic number, A is the atomic weight [g/mol] and ρ is the density of the substrate material (in our case silicon).

The principle of EDXRF and TXRF measurements is shown in Figure 8: A polychromatic X-ray beam hits a first spectrum modifier, usually a multilayer monochromator. The now monochromatic radiation irradiates the sample, which in TXRF is placed on a reflector with an angle below the critical angle. The characteristic X-rays emitted are then detected by a solid-state detector system. A major advantage of TXRF is, that the detector can be placed very close to the sample without interfering with the measurement. As a result, the solid angles of the fluorescence signals are very large. This in combination with the double excitation and the low scattering background leads to low detection limits [3] [31] [35].

TXRF approaches work best for thin and homogeneous samples [35]. If these assumptions are fully satisfied and we use a monochromatic excitation, we can drop the integrals in equation 2. The primary and secondary attenuation as well as the secondary excitation can also be neglected. If we rewrite the geometry factor G_1, the density $\rho(x)$ and the concentration c^i as $\frac{1}{4\pi r^2} \cdot \frac{dm^i(x)}{dx}$, the equation 2 can be simplified to [32] [33]:

$$I(E^i_{K_\alpha}) = m^i \cdot \frac{I_0(E)}{4\pi r^2} \cdot \frac{I_{int}(\varphi, E)}{I_0(E)} \cdot \frac{\tau^i_K(E)}{\rho} \cdot \omega^i_K \cdot p^i_\alpha \cdot G_2(\psi) \cdot f(E^i_{K_\alpha}) \cdot \epsilon(E^i_{K_\alpha}) \tag{4}$$

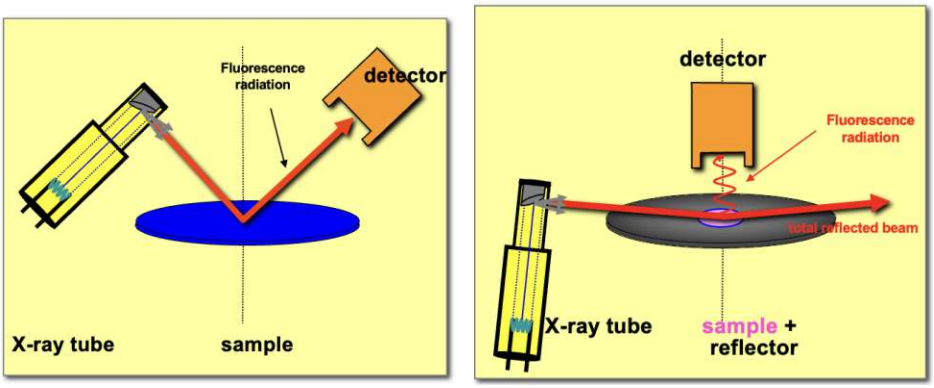

(a) (b)

Figure 8: Schematic EDXRF (a) and TXRF measurement setup (b). Figures designed by S. Pahlke (private communication).

Where m^i is the elemental sample mass, $I_{0(E)}$ is the primary intensity, $\frac{I_{int(\varphi,E)}}{I_{0(E)}}$ is the mean standing wave field, $\frac{G_2(\psi)}{4\pi r^2}$ a geometry factor, $f(E^i_{K_\alpha})$ the sample determined attenuation and $\epsilon(E^i_{K_\alpha})$ the efficiency of the detector. $\left(\frac{\tau^i_K(E)}{\rho} \cdot \omega^i_K \cdot p^i_\alpha\right)$ is the fluorescence cross section, where $\frac{\tau^i_K(E)}{\rho}$ is the photoelectric absorption coefficient, ω^i_K is the fluorescence yield, and p^i_α is the emission probability of a given element depending on the incoming excitation.

The thin film approximation can also be used to determine elemental concentrations with relative ease. This is done by using an internal standard with a known concentration of an element not present in the sample [6] [22]. For example vanadium (V), gallium (Ga), rhodium (Rh) and yttrium (Y) can be used as an internal standard depending on the exciting beam and on the investigated elements [6]. The sensitivity of an element i is defined as:

$$S^i = \frac{I^i}{c^i} = \frac{I^i}{m^i} \tag{5}$$

and the ratio of the sensitivity of an element i to the sensitivity of the internal standard is called "relative sensitivity": [36]

$$S_{rel} = \frac{S^i}{S^{st}} \tag{6}$$

If we now calculate the relative sensitivity of the KL_3 lines of the investigated

element and the internal standard, we get

$$S_{rel} = \frac{I(E^i_{KL_3})}{I(E^{st}_{KL_3})} \cdot \frac{c^{st}}{c^i} \tag{7}$$

The intensities $I(E^i_{KL_3})$ are calculated with the equation 15 and the geometry factors as well as the standing wave fields cancel out. What remains is the formula for the calculation of the element concentration i: [32] [33] [35]

$$c^i = \frac{I(E^i_{KL_3})}{I(E^{st}_{KL_3})} \cdot c^{st} \cdot \frac{1}{S_{rel}} \tag{8}$$

Another important formula for the analysis of X-ray spectra is the limit of detection (LOD) [3] [37]:

$$LOD^i = \frac{3 \cdot \sqrt{N^i_{background}}}{N^i_{peak}} \cdot c^i \tag{9}$$

For the background counts $N^i_{background}$ usually the total background intensity is taken. In this work, however, the background value proposed by Marguí et al. [26] for the LOD was chosen. This approach uses the fluctuations on the background base level instead of the total background value as seen in Figure 9 because the element peaks are often clearly visible despite the relatively high background base level.

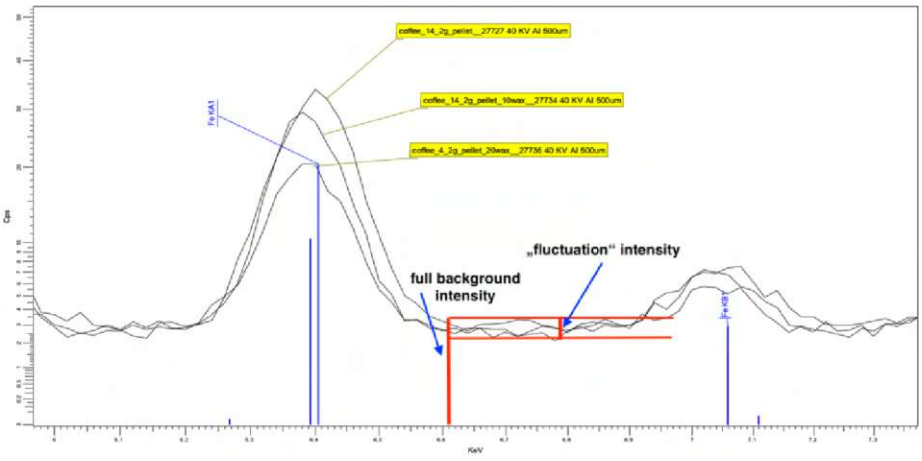

Figure 9: Proposed value for the background intensity needed to calculate the limit of detection of a certain element (in this case Fe).

2.1.3 X-ray reflectometry (XRR)

The following two subsections are not essential for understanding the concepts used in this paper. However, since Gracing Incidence X-ray Fluorescence (GIXRF) plays an important role in the Radiation Physics group at the Institute of Atomic and Subatomic Physics, TU Wien, and because of its general importance, it should be mentioned. To determine if samples are truly homogeneous and the thin film approximation is valid, one could use a scanning electron microscope (SEM) or an atomic force microscope (AFM) to take a close look at the samples. However, X-ray reflectometry in combination with GIXRF can also be used, as shown by D. Ingerle [38] [39]. The XRR measurements provide insight into the layer thickness and roughness of the samples. This is done by varying the angle of incidence of the X-ray beam and detecting the resulting interference signal produced by the reflections at the interface of each layer. Figure 10 shows a typical XRR signal. From the period of the resulting oscillation pattern, the thickness of the layer can be calculated. The slope of the oscillation gives the roughness of the interface between the sample and the substrate material. Since the resulting pattern is directly related to the electron density of the material, this technique works only for materials with different electron densities [40][41].

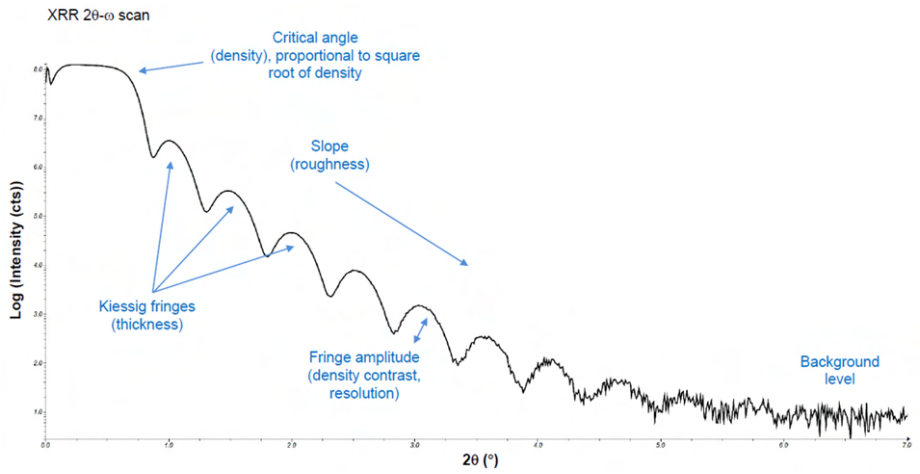

Figure 10: Typical XRR signal with the most important measurement outputs. Figure taken from [41].

2.1.4 TXRF signals and sample structure

When the thin-film approximation is satisfied, the information obtained by XRR can be combined with fluorescence data to overcome the ambiguity problem (= two or more different solutions for layer thickness and implant distribution result in good fitting) [38]. Figure 11 shows three possible signals caused by different structures: [35]

- **Residue:** Residues on the reflector surface behave like particles as their fluorescence signal doubles up to the critical angle. This is caused by the total reflected beam and the primary beam resulting in double excitation.
- **Surface layer:** The signal is similar to that of an XRR measurement because the reflected X-rays at the surface and bottom of a monolayer interfere to produce a standing wave field (see Figure 12). Since the intensity of the reflected beam is proportional to the fluorescence yield, this can result in a maximum almost four times as high as the primary fluorescence intensity.
- **Bulk Material:** Usually the bulk material is a quartz reflector made of SiO_2. The function shown is made of silicon. Up to the critical angle the bulk is hardly penetrated. The fluorescence intensity increases exponentially near the critical angle as more photons penetrate the surface and excite silicon atoms. After passing the critical angle, the signal increases steadily until the refractive maximum of the X-ray beam is reached.

The fluorescence intensity is directly proportional to the intensity of the standing wave field [35]. The distance between two periodic points is calculated by Bragg's law, as it is the prerequisite for constructive interference (equation 10). Therefore, D is the distance between the nodal and antinodal planes [22]. The height of the field above the substrate and the decay below the substrate surface vary as a function of the angle of incidence ϕ (see Figure 12 (b)).

$$n \cdot \lambda = 2 \cdot D \cdot sin(\phi) \tag{10}$$

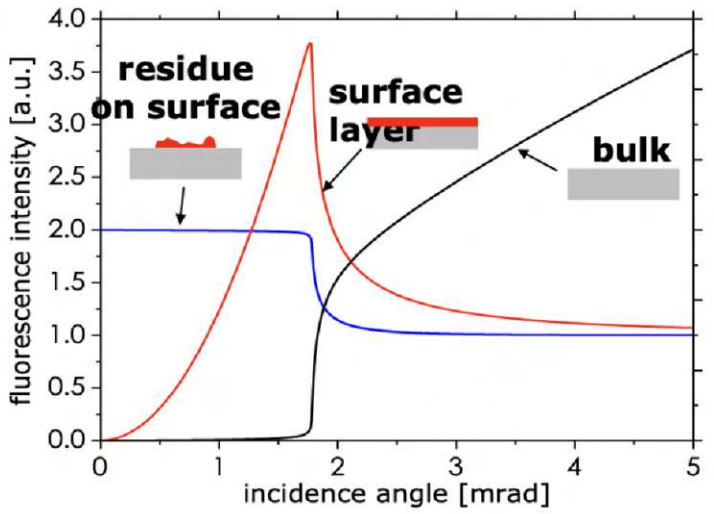

Figure 11: TXRF signal around the critical angle (here just before 2 mrad) from different structured samples. Figure taken from [30].

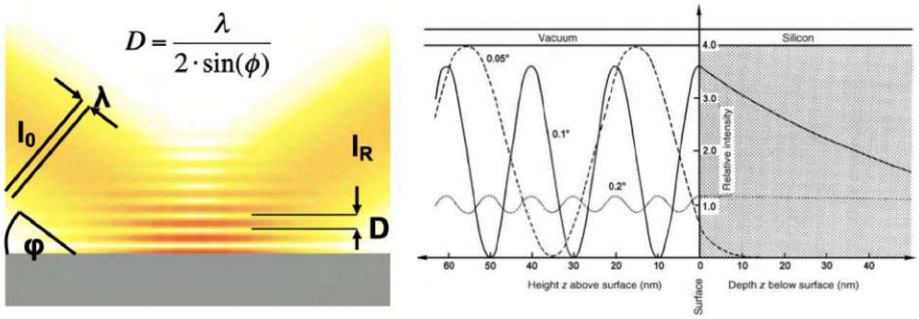

(a) (b)

Figure 12: Standing wave field created by the reflected beam at the surface and the reflections at the interfaces between layers (a) [30]. Different angles result in different relative intensities above and below the surface of the reflector (b) [22].

2.2 Liquid inductively coupled plasma optical emission spectroscopy (Liquid ICP-OES)

Liquid inductively coupled plasma optical emission spectroscopy (ICP-OES) is a very popular analytical technique for analyzing the elemental composition of a wide range of pharmaceutical and environmental samples. However, this method requires liquid samples [1]. Therefore, solid samples, such as coffee grain powder, must be digested with acids such as HNO_3, H_2O_2, HCl and H_2SO_4 before measurement.

The schematic principle and its differences to liquid inductively coupled plasma mass spectroscopy (Liquid - ICP-MS) are shown in Figure 13. For both methods the liquid sample is pumped into a nebulizer or other sample injection device such as a spray chamber or drain. Here the sample is converted into an aerosol and sprayed into an ICP torch. There an argon plasma state is created by applying radio frequencies (RF) to the argon gas. The two RF generators used are piezoelectric quartz crystal generators and free-running generators. The operating frequency ranges from 27 to 56 MHz and is transmitted to the plasma torch via a load coil. The temperature of the coils is regulated by either gas or water cooling. For ICP-OES the plasma temperature reaches 8000 - 10,000 K and, in combination with the high electron density, vaporizes and dissolves the sample molecules into atoms. In these conditions electrons are easily excited and ionized and when they fall back to lower energy levels they emit element specific radiation.

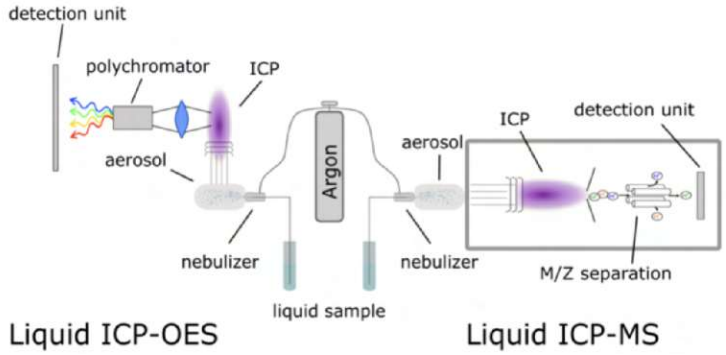

Figure 13: Schematic principle of ICP-OES and ICP-MS. Figure taken from [42].

[1] Other ICP related methods also work with gaseous samples

This characteristic radiation is then collected by focusing optics (concave lens or convex mirror) and presented to a wavelength-dispersive detector system. The incoming light must first be separated in a spectrometer using a diffraction grating. This grating is implemented in a mirror and the light is scattered at different angles depending on its wavelength (see Figure 14). Shorter wavelengths and lower line densities of the grating generally result in smaller reflection angles. Both polychromators and monochromators are used to spread the incoming white light. Polychromators have the advantage of being able to analyze all wavelengths simultaneously (typically 20 to 30) and therefore have a high throughput rate. Monochromators have a lower throughput rate, but are more suitable when background correction techniques are required. This is due to the monochromator's ability to focus on any wavelength within its working range at any time.

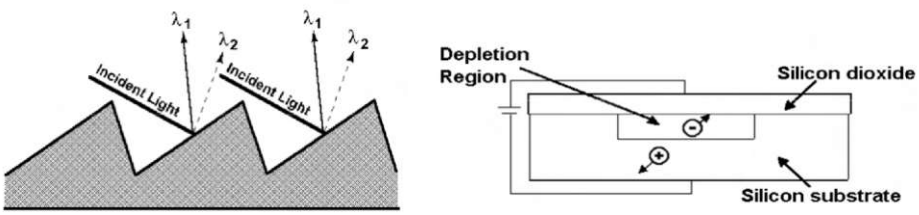

(a) (b)

Figure 14: (a) Diffraction grating principle for two wavelengths, where $\lambda_2 > \lambda_1$. Shorter wavelengths and a lower grit density result in smaller deflection angles. (b) Principle of a charge transfer device (CTD). Figures taken from [43].

The detectors used are photomultiplier tubes, array detectors, photodiode arrays or, from the large class of charge transfer devices (CTDs), charge injection devices (CIDs) or charge coupled devices (CCDs). Since the Agilent 5100 ICP-OES system used in this study has a CCD detector, only the CTD class will be discussed here.

A schematic diagram of a CTD is shown in Figure 14 (b). The substrate is a silicon (Si) crystal with a silicon oxide (SiO_2) layer on its surface, the latter being non-conductive. This structure is also known as a metal-oxide-silicon (MOS) capacitor. When light from the diffraction grating hits the crystal, it breaks the electrochemical bonds between the Si atoms, creating an electron-hole pair. A voltage is applied to the crystal and the electrons and holes drift in opposite

directions. This current can be measured and is proportional to the intensity of the incident light. A CTD detector unit typically contains 512 x 512 to 4096 x 4096 individual MOS capacitors, called pixels. For CIDs each of these pixels can be read during the measurement process without destroying its charge. However, CIDs require extensive cooling down to down to 77 K (the temperature of liquid nitrogen at atmospheric pressure) to reduce the background noise. The huge advantage of CCDs over CIDs is that they do not require extensive cooling. [43] [44] [45].

Liquid ICP-MS, as shown in Figure 13, also uses an ICP to ionize and atomize samples. The most commonly used selection device in ICP-MS is a quadrupole consisting of four rods. After passing through the ICP torch, the now gaseous sample is transferred to an electromagnetic quadrupole; a direct bias current is applied to one pair of rods, an RF field to the other. Depending on these two fields, only atoms/molecules with a certain mass-to-charge ratio can pass through the quadrupole configuration and reach the detector. This process is then repeated for every other possible m/z ratio of the analytes [44] [46].

2.3 Chemometrics

Chemometrics is an integral part of this thesis; the two methods used were Principal Component Analysis (PCA) and Partial Least Squares Discriminant Analysis (PLS-DA). These statistical methods are closely related and have been used extensively in chemical research to visually distinguish different groups of samples, creating so-called chemical fingerprints. PLS-DA can be thought of as an improved version of PCA that takes into account the different labels, or classes, of each sample [47] [48] [49] [50] [51]. In our case, these classes were pure coffees, pure instant coffees, and coffees with additives (e.g. milk, proteins, ...).

2.3.1 Principal component analysis (PCA)

This subsection follows the article "*From Periodic Properties to a Periodic Table Arrangement*" by Emili Besalú [50] and its "*Guide for Instructor*" in the Supporting information. For many scientists with no previous experience in chemometrics, including the author, the concept of a PCA can seem quite abstract if explained only theoretically without an example. The calculations from the article are slightly adapted and reproduced here to illustrate the principles of PCA. The goal of this example is to take the atomic properties from Table 2 and transform it into something close to the well-known periodic table of the elements using the PCA method. However, instead of using 35 elements as in [50], this calculation includes just elements present in coffee samples employed in this study, namely: P, S, Cl, K, Ca, Mn, Fe, Cu, Zn, Br, Rb, and Sr. The transition metals Mn, Fe, Cu, Zn were not studied in [50]. The chosen atomic properties, however, are the same as in [50]; atomic weight (in amu), covalent atomic radius, first ionization potential, first electron affinity and electronegativity (see Table 2).

PCA tries to reduce dimensions (in this case we have five dimensions, our atomic properties) in a way that retains most of the information contained [47] [52]. This allows us to explore relationships that may not have been obvious before. The goal in this particular case is to reduce the data to a 2D space so that we can visualize and plot it, while losing as little information as possible.

No.	Atomic Number	Symbol	Atomic weight (amu)	Atomic Radius (pm)	First IP (kJ/mol)	First EA (kJ/mol)	Electroneg. (Pauling)
1	15	P	30,97	100	1011	72	2,2
2	16	S	32,06	100	1000	200	2,6
3	17	Cl	35,45	100	1255	349	3,2
4	19	K	39,10	220	418	48	0,8
5	20	Ca	40,08	180	590	2	1,3
6	25	Mn	54,94	140	717	-50	1,6
7	26	Fe	55,84	140	759	16	1,8
8	29	Cu	63,55	135	785	118	1,9
9	30	Zn	65,41	135	906	-58	1,6
10	35	Br	79,9	115	1140	325	3
11	37	Rb	85,47	235	402	47	0,8
12	38	Sr	87,62	200	548	5	1,0
Mean value			55,86	150,00	791,31	99,17	1,82
Scaled deviation			68,89	157,80	916,90	423,60	2,68

Table 2: Atomic properties used for the exemplary PCA. Atomic radii taken from [53], originally from [54]. The First EA for Mn and Zn was taken from [55]. Other data taken from [56].

First, the values from Table 2 must be transformed to make them dimensionless. This requires calculating the mean of each atomic property x_i' and the corresponding scaled deviation:

$$\sigma_i = \sqrt{\sum_{n=1}^{N=12} (x_n - x_i')^2} \tag{11}$$

Then each value is subtracted by the mean of each respective column and divided by the scaled deviation of that column. The now dimensionless matrix A is shown in Table 3.

The means of this new dimensionless matrix are zero, and the scaled deviation becomes:

$$\sigma_s = \frac{1}{\sqrt{N}} = \frac{1}{\sqrt{12}} = 0.289 \tag{12}$$

To obtain the correlation matrix C (Table 4, which gives information about the positive or negative correlation between the atomic properties, we have to calculate the scalar product of each column with the others. For example, the scalar product of the atomic weight vector times the atomic weight vector

No.	Atomic Number	Symbol	Atomic weight	Atomic Radius	First IP	First EA	Electronegativity
1	15	P	-0,361	-0,317	0,240	-0,064	0,142
2	16	S	-0,346	-0,317	0,228	0,238	0,292
3	17	Cl	-0,296	-0,317	0,506	0,590	0,515
4	19	K	-0,243	0,444	-0,407	-0,121	-0,372
5	20	Ca	-0,229	0,190	-0,220	-0,229	-0,193
6	25	Mn	-0,013	-0,063	-0,081	-0,352	-0,100
7	26	Fe	0,000	-0,063	-0,031	-0,199	0,004
8	29	Cu	0,112	-0,095	-0,050	0,047	0,030
9	30	Zn	0,138	-0,095	0,126	-0,097	-0,063
10	35	Br	0,349	-0,222	0,380	0,533	0,441
11	37	Rb	0,430	0,539	-0,425	-0,123	-0,372
12	38	Sr	0,461	0,317	-0,265	-0,222	-0,324
Mean value			0,00	0,00	0,00	0,00	0,00
Scaled deviation			0,289	0,289	0,289	0,289	0,289

Table 3: Dimensionless matrix A obtained by subtracting the mean value x_i' and dividing by the scaled deviation σ_i. The mean values now become zero and the scaled deviation of each column is $\sigma_s = \frac{1}{\sqrt{N}}$

gives $a_{11} = 1$; the atomic weight vector times the atomic radii vector gives $a_{21} = 0.444$, and so on.

The resulting 5 x 5 matrix is symmetric and is shown in Table 4. It is important to note that the atomic radius is strongly negatively correlated with the first ionization potential (-0.928) and the electronegativity (-0.895). However, the first ionization potential is strongly positively correlated with the first electron affinity (0.771) and the electronegativity (0.966). The electronegativity and the first electron affinity are also strongly positively correlated (0.848). The correlation between each atomic property and itself is logically 1.

	Atomic weight	Atomic Radius	First IP	First EA	Electronegativity
Atomic weight	1	0,444	-0,325	-0,125	-0,330
Atomic Radius	0,444	1	-0,928	-0,555	-0,895
First IP	-0,325	-0,928	1	0,771	0,966
First EA	-0,125	-0,555	0,771	1	0,848
Electronegativity	-0,330	-0,895	0,966	0,848	1

Table 4: Correlation matrix C.

It can be shown that a symmetric matrix can be diagonalized with an invertible matrix B with $B^{-1}CB = D$. The matrix elements $a_{11}, a_{22}, ..., a_{nn}$ of a diagonalized n x n matrix are its eigenvalues $\lambda_1, \lambda_2, ..., \lambda_n$. Furthermore, if $\lambda_1 \neq \lambda_2 \neq ... \neq \lambda_n$, then the corresponding eigenvectors are linearly independent, orthogonal and form a so-called "eigenbasis" [57] [58]. We now want to transform our correlation matrix C in Table 4 into this new basis. For convenience, we diagonalize the matrix C with an online diagonalization tool [59].

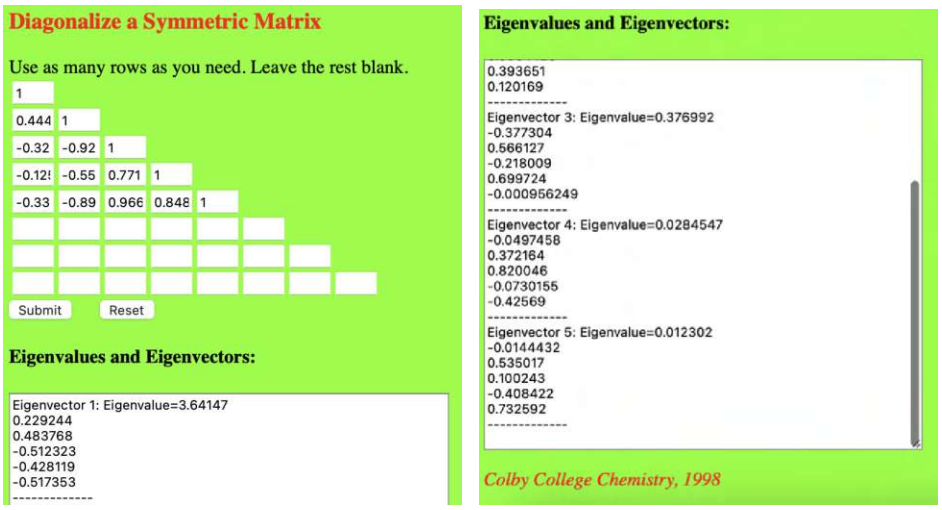

(a) (b)

Figure 15: Online matrix diagonalization tool from Colby College [59]. Through the diagonalization process we obtain the eigenvalues and eigenvectors.

	Eigenvalues	Percentage	PC1	PC2
	3,641	72,83	-0,229	-0,896
	0,941	18,82	-0,484	-0,144
	0,377	7,54	0,512	-0,086
	0,028	0,57	0,428	-0,394
	0,012	0,25	0,517	-0,120
Sum	5,000	100,00		

Table 5: Eigenvalues and their respective percentages (left) and the first two columns (PC 1 and PC 2) of the loadings matrix L (right).

The eigenvectors and their percentages (cumulated variance) are shown on the left side of Table 5. The first eigenvalue carries 72.83 % of the total information, the second eigenvalue carries 18.82 % of the total information. The cumulative variance of the first two eigenvalues therefore contains an astonishing $72.83\% + 18.82\% = 91.65\%$ of the total information. Principal component (PC) 1 and 2 are the first two columns of the so-called loadings matrix L. These loadings are now multiplied by the adimensional matrix A (Table 3) to obtain the score matrix S:

$$\underbrace{S}_{5x2} = \underbrace{A}_{5x5} \cdot \underbrace{L}_{5x2} \tag{13}$$

The entries of the score matrix are now our new 2D coordinates for our initial data (see Table 6) and vary from -1 to 1. Note that the signs of the eigenvectors have been changed to get a graph with the same orientation as the periodic table.

We now plot the score matrix and connect the points of the respective groups and periods of the periodic table. Of course, Figure 16 differs from the original Figure [60], but the connection is still clearly visible.

No.	Atomic Number	Symbol	PC1 coordinate	PC2 coordinate
1	15	P	0,405	0,357
2	16	S	0,602	0,207
3	17	Cl	0,999	-0,027
4	19	K	-0,612	0,282
5	20	Ca	-0,350	0,310
6	25	Mn	-0,210	0,179
7	26	Fe	-0,068	0,090
8	29	Cu	0,031	-0,104
9	30	Zn	0,005	-0,075
10	35	Br	0,678	-0,576
11	37	Rb	-0,822	-0,333
12	38	Sr	-0,658	-0,309

Table 6: Score matrix S for the elements P, S, Cl, K, Ca, Mn, Fe, Cu, Zn, Br, Rb, and Sr.

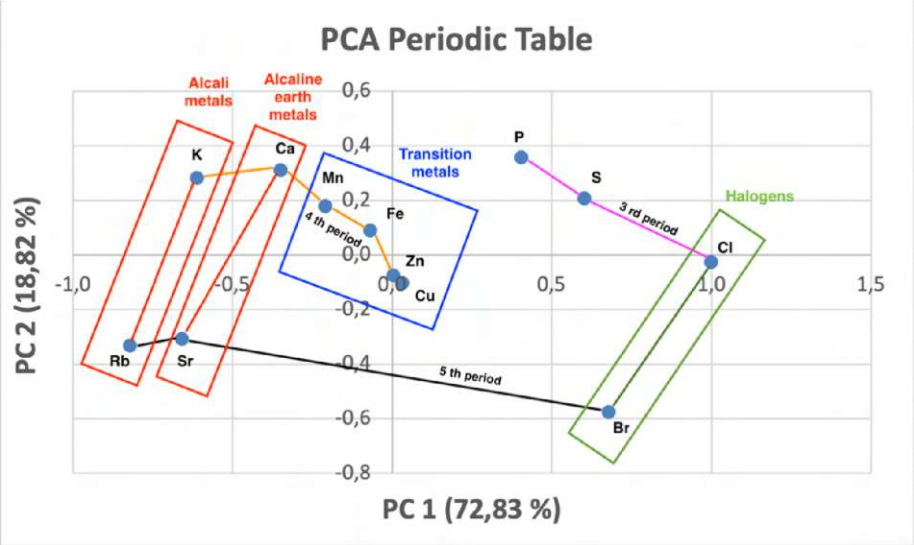

Figure 16: Plotted score matrix S. The representation is similar to the well known periodic table of the elements [60].

2.3.2 Partial least squares-discriminant analysis (PLS-DA)

PLS-DA can be interpreted as an improved version of a PCA, with full knowledge of the class labels used. A PLS-DA must reduce dimensions like a PCA and also provide a model for prediction, such as the cross-validation leave-one-out (LOO) procedure. The PCs are called latent variables (LVs) here and are our new orthogonal axes. In the LLO method, each sample is hidden once when the model is computed and inserted into the latent variable model to test whether the classification is accurate for each "unknown" sample. In practice, two algorithms are used for PLS-DA: PLS-DA1, when there are two classes involved (e.g., two categories of coffee), or PLS-DA2, when there are three or more classes, as in our case. The number of discriminant functions obtained from PLS-DA is n-1, where n is the total number of classes. The algorithms are iterative, so the results of the previous PLS component become the new input and output data (the output data in this case is a dummy matrix made up of the class labels). The final plot of a PLS-DA should show a grouping of the different classes [51] [61] [62] [63]. The values of the discriminant functions can be interpreted as a sample belonging to a particular class [64].

3 Experimental setup

3.1 Agilent ICP-OES 5100 Synchronous Vertical Dual View (SVDV) Spectrometer at the University of Girona

The key data and operating parameters of the Agilent ICP-OES 5100 used for our study were:

- **Sample Aggregate State**: Liquid
- **Radio Frequency (RF) power**: 1200 W
- **Plasma Gas Flow Rate**: 12 l/min
- **Torch Configuration**: Axial
- **Nebulizer:** Concentric
- **Analytical lines:** K (766.491 nm), Ca (317.933 nm), Mn (257.610 nm), Fe (238.204 nm), Cu (327.295 nm), Rb (780.026 nm), Sr (407.771 nm for CRMs and 460.733 nm for coffees), Zn (213.857 nm)
- **Gas**: Argon (Ar) gas is used for the plasma, the nebulizer and the optics interface purge. The polychromator assembly can be operated with argon or nitrogen gas.

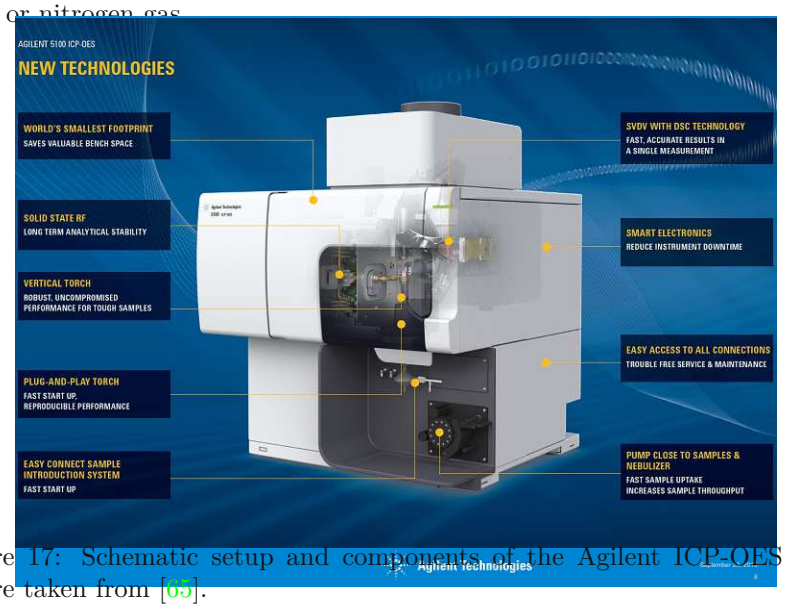

Figure 17: Schematic setup and components of the Agilent ICP-OES 5100. Figure taken from [65].

3.2 Bruker AXS Ranger S2 at the University of Girona

The EDXRF analysis was performed with a commercially available benchtop EDXRF spectrometer (S2 Ranger, Bruker AXS, GmbH, Karlsruhe, Germany). The anode of the X-ray tube is made of palladium (Pd). The system features the XFLASH-LE™ Silicon Drift Detector (SDD) with an ultra-thin beryllium (Be) window. The resolution is typically around 141 eV for the Mn-KL3 line at a count rate of 100,000 cps. The Ranger S2 has nine primary filters and can be operated in vacuum or helium flush mode. The X-ray tube requires no external cooling, which is both convenient and cost-effective. The control software *Spectra EDX* also comes from Bruker AXS, GmbH and can perform all necessary tasks from fitting to deconvolution. It uses intensity correction when inter-element effects occur and is capable of performing quantitative routines such as fundamental parameter approaches using varying alpha coefficients. The specification of the instrument and all measurement conditions are summarized in the following list [66] [67]:

- **X-ray tube anode material**: Palladium (Pd), Z=46
- **Measurement mode**: Vacuum mode for pellets, He flush mode for loose powder samples
- **Measuring time**: 200 s
- **Voltage:** Range 10-50 kV, 40 kV selected for experiments
- **Current**: 1-1000 μA, max. 2 mA
- **Filters evaluated:** 5 μm Ag, 200 μm Al, 500 μm Al, 100 μm Cu, 200 μm Cu, None; primary filter used for experiments: 500 μm Al
- **Detector**: XFLASH-LE™ Silicon Drift Detector (SDD)
- **Detector Specifications**:
  - **Window**: High transmission polymer window
  - **Active Area**: 20 mm^2.
  - **Resolution**: Typically 141 eV for Mn-KL3 at 100,000 cps
  - **Element Range:** In theory C (Z=6) to U (Z=92); practically with the used control unit: F (Z=9) to U (Z=92)
  - **Cooling:** Maintenance free electric Peltier cooling

Figure 18: Ranger S2 EDXRF benchtop system.

3.3 WOBISTRAX at the Institute of Atomic and Subatomic Physics, TU Wien

For the TXRF experiments we used a spectrometer based on the WOBISTRAX design, developed at the Roentgenlab at the Institute of Atomic and Subatomic Physics, TU Wien [68] [69] [70]. Figures 19, 20 and 21 show the setup in detail. The measurement time was set to 1000 s for each sample. The main components and settings for the WOBISTRAX spectrometer are

- **X-ray Generator**: IfG Control and Supply Unit (CSU) (Adlershof, Berlin, Germany, now part of Helmut Fischer GmbH).
- **X-ray Tube**: Warrikhoff MCB50-0.7G, 35 W Rhodium (Rh) anode, air cooled, long fine focus, IfG IMOXS tube housing.
- **Operating Conditions:** 50 kV / 700 μA
- **Multilayer Monochromator**: Diameter: 25.4 mm (1 inch), 100 layers of Pd/B_4C (d = 3.24 nm) on polished quartz SiO_2 substrate. ϕ_{bragg}=

0.66 deg.

- **Sample changer / reflector**: The sample changer is mobile and can hold 12 sample carriers (= reflectors) for sequential measurements. The reflectors are usually made of quartz (SiO_2), but can be any 30 mm diameter reflectors.
- **Vacuum**: Rough vacuum membrane pump ($\approx$ 2 mbar)
- **Limits of detection**: $<$ 100 ng Sr ($<$ 10 ppb for a 10 μl droplet)
- **Detector**: X-123 complete X-ray spectrometer silicon drift detector (SDD) with a Si-PIN (Amptek Inc., Bedford, MA, USA) with a 25 mm^2 and 8 μm thick beryllium window collimated to 17 mm^2. It has a 5 mm diameter silver (Ag) end cap control hole. The resolution is 139 to 260 eV FWHM at 5.9 keV [71].
- **Beam Monitor**: Fluorescent film in the beamline monitored by a carged coupled device (CCD) camera connected to the computer.
- **Electronic safety contact** that closes the shutter of the incoming X-ray beam if the door is accidentally opened while the X-ray beam is on.
- **Software**: Customized WOBISTRAX control software with graphical user interface (GUI).

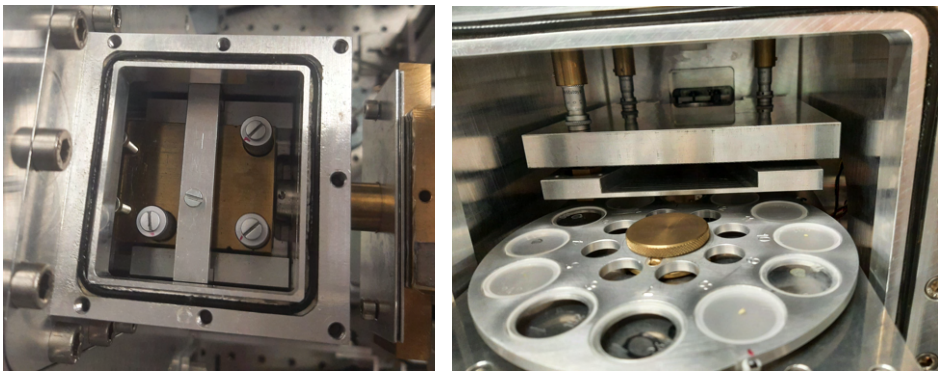

(a) (b)

Figure 19: Monochromator adjustable with 3 plane defining screws (a) and horizontal view of samples inside the sample changer (b).

From the X-ray tube mounted on the left side of the chamber, the emitted polychromatic X-rays hit the multilayer, which acts as a monochromator. The beam then passes through an Al filter, which suppresses the Rh-L lines. The angle for the first order Bragg reflection of the Rh-KL3 line, according to Bragg's law for n=1 and E=20.02 keV, is ϕ_{bragg}= 0.66 deg.

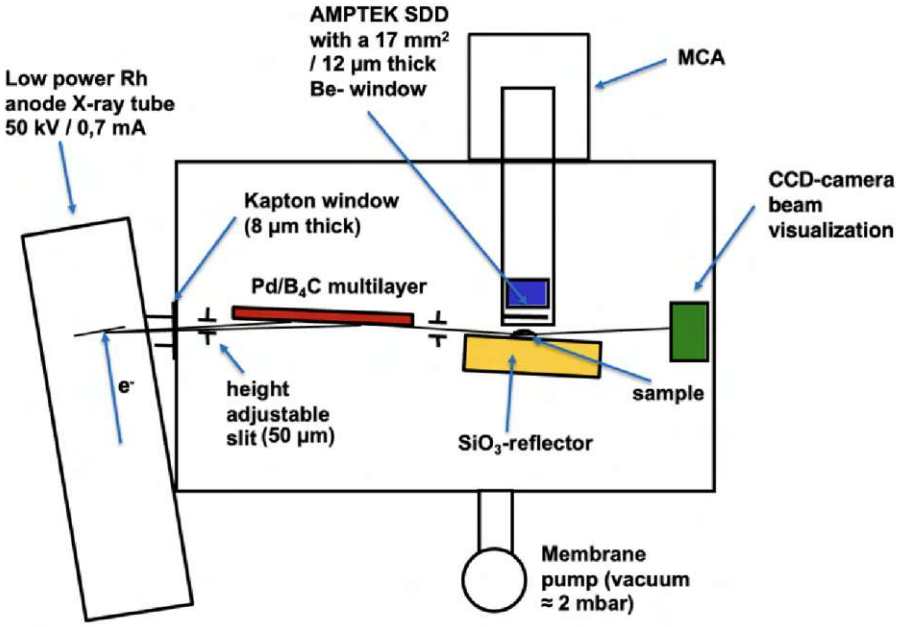

Figure 20: Schematic layout and beamlines in the WOBISTRAX spectrometer chamber.

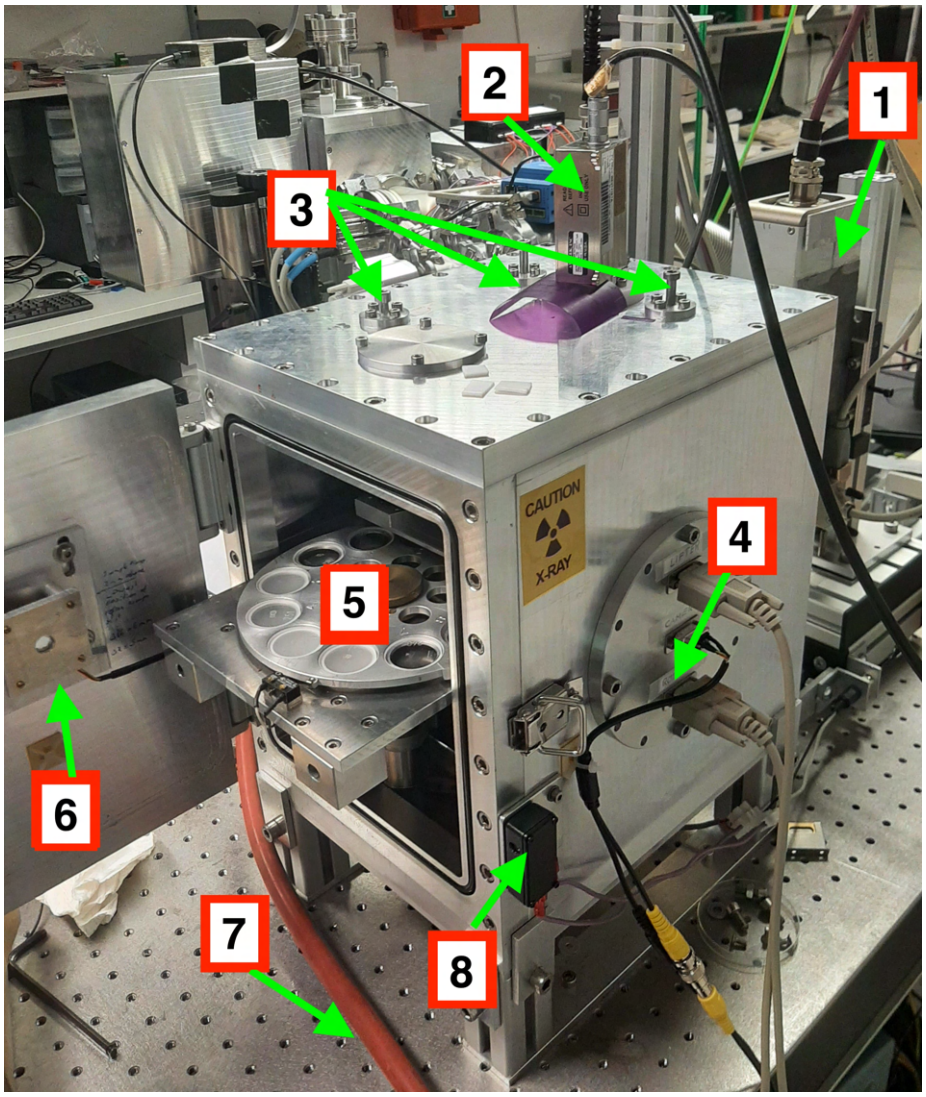

Figure 21: The WOBISTRAX setup at the Institute for Atomic and Subatomic Physics at the TU Wien. The marked components are: (1) Rh anode X-ray tube, (2) Amptek XR-100SDD detector, (3) 3 screws for adjusting the sample changer plane, (4) motor signal cable, (5) sample changer, (6) CCD camera for beam monitoring, (7) hose to vacuum pump, and (8) electronic safety contact.

4 Methods

4.1 Analysis strategy for EDXRF experiments

This subsection can be seen as a graphical summary (Figure 22 and Figure 23) of this work. Since many publications on coffee powder analysis using XRF methods (Table 1) did not report the exact measurement conditions and/or sample preparation steps, we wanted to fill this knowledge gap. The exact process of developing the experimental methodology is explained in more detail below in the next subsection.

For the sample preparation for the EDXRF analysis, we compared pressed pellets with and without various amounts of CEROX wax added to loose powder samples. Loose powders require the least preparation time and were presented to the Bruker Ranger S2 in a Teflon ring with a transparent film. Since the loose powder particles could damage the instrument if used in a vacuum, the helium flush mode had to be used instead. However, the loose powder did not provide sufficiently precise and accurate results.

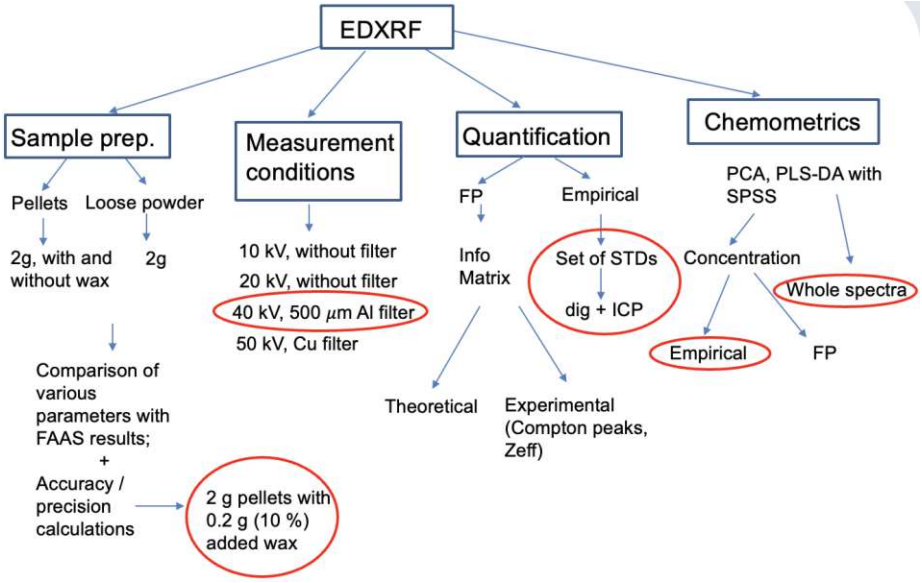

Figure 22: Visualization of the experimental approach for the EDXRF measurements of this thesis. The measurements were carried out at the Department of Chemistry, University of Girona using a Bruker Ranger S2 benchtop EDXRF system. The red circles mark the finally chosen modes/configurations.

In the end, 2 g of pellets with 0.2 g (10 %) of wax added was the best compromise between pellet durability and trueness (= precision + accuracy). The qualified measurement conditions of the Bruker S2 Ranger are 10 kV without filter; 20 kV without filter; 50 kV with Cu filter and 40 kV with 500 μm Al filter. The latter were found to be the most suitable.

The quantification process was particularly difficult because coffee powders are, by their nature, not homogeneous in composition. This is especially true for the class of coffees with additives (milk, proteins, etc.). To be able to compare our results in the absence of a certified reference material (CRM), we performed ICP-OES measurements. For the quantification of the EDXRF spectra, we used two different fundamental parameter (FP) approaches and one with empirical calibration curves. For the first FP method, we used a reported coffee extract formula to calculate the effective atomic number Z_{eff}, which is required for the FP calculation software provided by the Ranger S2 instrument. The second FP approach used the Rayleigh to Compton peak ratio of known materials pressed into pellets to calculate the Z_{eff}. However, as expected, the calibration curves prepared using empirical standards previously measured by ICP-OES showed the best agreement with the reference ICP-OES results.
Chemometrics were performed using SPSS (Statistical Package for the Social Sciences), a commercial statistical software package from IBM. Both PCA and PLS-DA were used to analyze the empirical concentration values and the full spectra. To date, very few publications have used the full XRF spectra for chemometrics. The advantage of this approach is, that it is no longer necessary to first determine the elemental concentrations (by whatever method) if one is only interested in chemical fingerprints.

4.2 Analysis strategy for TXRF experiments

The TXRF measurements were performed at the Institute of Atomic and Subatomic Physics at the TU Wien. A custom built spectrometer chamber based on the WOBISTRAX design was used. We used the digestions previously prepared for the ICP-OES analysis and added 25 μl of 200 ppm Ga as internal standard to 1 ml of the digest. This results in a final Ga concentration of 4 ppm. Depending on the sample type and element abundance, 10 or 30 μl of sample were pipetted onto a quartz (SiO_2) reflector. The chosen measurement conditions were 50 kV / 700 μA with a 50 μm Al filter. The original plan was to also prepare suspensions, as these sample types do not require prior time-consuming digestion processes. However, in order not to go beyond the scope of this work, this step was omitted and will be tested for a future publication.

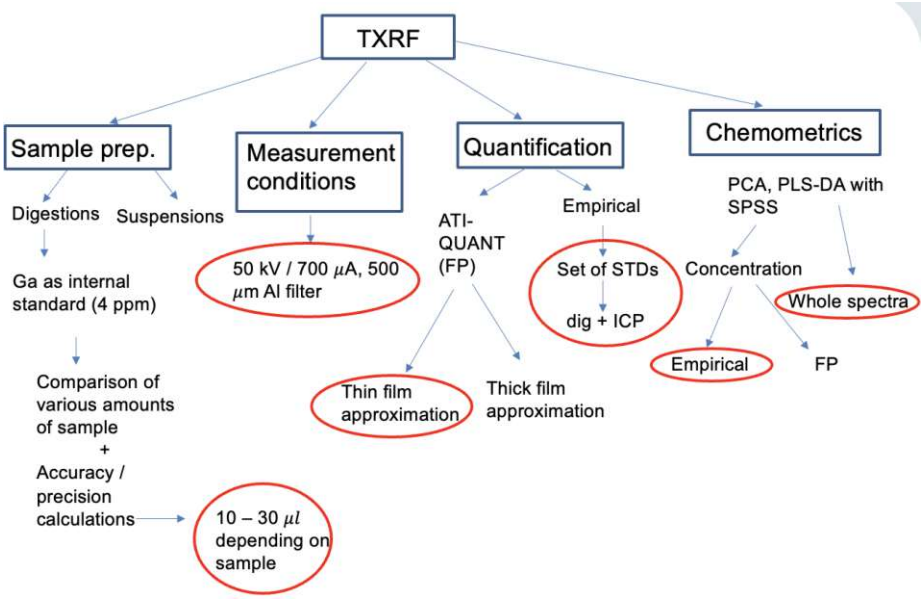

Figure 23: Visualization of the experimental approach for the TXRF measurements of this thesis. The measurements were carried out at the spectrometer chamber based on the WOBISTRAX design, custom-made at the Institute for Atomic and Subatomic Physics, TU Wien. The red circles mark the finally chosen modes/configurations.

For the quantification of the TXRF spectra, as for the EDXRF data, we compared an FP approach with empirically derived calibration curves. For the FP approach we used ATI-QUANT, a software developed at the Institute of Atomic

and Subatomic Physics, TU Wien. The thin film approximation mode was used. The empirical calibration curves contained the same standards as the EDXRF empirical calibration. The spectra fitting for both approaches was done with PyMca, an open source software for XRF analysis (developed by the European Synchrotron Radiation Facility).

4.3 Coffee samples

The coffee samples were purchased in Croatian supermarkets and come from three different categories: pure coffee, pure instant coffee and coffee with additives (e.g. milk, proteins, etc.). For the EDXRF study 48 coffees were used, 11 of them as empirical standards. Of these 48 coffees, 19 were pure coffee, 8 were pure instant coffee, and 21 were coffees with additives. For 19 of these 48 samples, FAAS data were already available for comparison. For the remaining 29 coffees, reference measurements were required as there is no certified reference material (CRM) for coffee. ICP-OES was chosen for this task due to its availability at the University of Girona and the reliability of the method. In addition to these 29 samples, 3 of the first 19 samples were also analyzed by ICP-OES, since these samples were available in relatively large quantities and had been extensively studied during the sample preparation test procedure. This results in 32 coffees that were finally measured by ICP-OES. For each of these coffees, two independently prepared samples were made.

We produced enough of the coffee digests for the ICP-OES measurement so that the remaining liquid could be used for the TXRF analysis. Of the 32 coffees for TXRF analysis, 10 were pure coffee, 7 were pure instant coffee, and 15 were coffees with additives.

4.4 Materials

The following materials (other than coffee samples) were used in the study:

- **Stock solutions of the elements K, Ca, Mn, Fe, Cu, Zn, Rb, Sr and Ga (internal standard)** (1000 mg/L, ROMIL PrimAg® Monocomponent Reference Solutions) for the preparation of calibration standards for ICP-OES analysis.
- **Ultrapure deionized water** (Millipore Corp., Bedford, Massachusetts, USA) for diluting stock solutions and coffee sample digests.
- **Nitric acid** (69%, HIPERPUR, Panreac, Spain) and **hydrogen peroxide solution** (30%, TraceSELECT®, Sigma-Aldrich, Spain) for digesting coffee samples and reference materials for ICP-OES and TXRF analysis.
- **Hoechst wax C micropowder** ($C_{38}H_{76}N_2O_2$, Merck KGaA, Germany) to stabilize the coffee pellets and make them more durable for future analysis, if needed.+
- **Boric acid** (H_3BO_3, ACS 99.5% Merck KGaA, Germany) to calculate the calibration curve for the mean effective atomic number (Z_{eff}) of the coffee samples for the semi-FP EDXRF approach.
- **Potassium nitrate** ($KNO_3, ACS > 99.0\%$, Merck KGaA, Germany) to calculate the calibration curve for the mean effective atomic number (Z_{eff}) of the coffee samples for the semi-FP EDXRF approach.
- **Lithium tetraborate** ($Li_2B_4O_7, > 99.0\%$ trace metal basis, Merck KGaA, Germany) to calculate the calibration curve for the mean effective atomic number (Z_{eff}) of the coffee samples for the semi-FP EDXRF approach.
- **Cellulose** ($C_{12}H_{22}O_{11}$, microcrystalline powder $< 20\mu$m, Merck KGaA, Germany) to calculate the calibration curve for the mean effective atomic number (Z_{eff}) of the coffee samples for the semi-FP EDXRF approach.
- 4.0 μm-thick Prolene® **X-ray film** (Chemplex Industries, Inc., Palm City, FL, USA) to support loose powder samples.

In addition, in the absence of a CRM for coffee, the following other organic reference materials for ICP-OES and TXRF measurements were purchased from the National Analysis Center for Iron and Steel in Beijing, China:

- **CBW07604 (poplar leaves)**
- **NCS ZC73036 (green tea)** and
- **NCSZC73031 (carrot)**

4.5 Sample preparation and measurement conditions

4.5.1 ICP-OES

A microwave acid digestion method was used to digest the coffee samples to make them suitable for ICP-OES analysis. Dalipi et al. [72] have already shown that this method is reliable for the digestion of vegetation matrices. We took 250 mg of each coffee sample and weighed each one on a microbalance to record the exact mass. The samples were then transferred to a Teflon vessel and 9 ml of the aforementioned nitric acid and 1 ml of hydrogen peroxide were added. The closed vessels were placed in a microwave system (speedwave XPERT, Berghof Products + Instruments GmbH, Germany, see Figure 24) and digested according to the following scheme: in a first step (5 min) the samples were heated to 180°C; in a second step the program stayed at 180°C for 10 min. Finally, after the cooling phase, the digested sample solutions were transferred to 30 ml vessels and diluted to this volume with ultrapure water. The exact dilution factor of each sample was then calculated. One random vessel was always used as a blank sample. The analysis was performed on the aforementioned Agilent ICP-OES 5100 Synchronous Vertical Dual View (SVDV) spectrometer.

(a) (b)

Figure 24: (a) Speedwave XPERT microwave system and (b) PE-MAN manual hydraulic press with pellet preparation equipment.

4.5.2 EDXRF

The coffee grain powder samples were pressed into pellets of 40 mm diameter. Since sometimes only small amounts of sample mass were available, we

finally decided to mix 2 g of powder sample (instead of e.g. 5 g) with 0.2 g of Hoechst Wax C micropowder for stabilization and durability. We pressed the 2.2 g mixture at 200 kN (20 metric tons) for 60-90 s in a hydraulic manual press (PE-MAN, LGC Limited, Teddington, England) shown in Figure 24. For comparison, loose coffee powder samples were also analyzed by EDXRF (Figure 26). For this, 2 g of coffee powder was transferred into a Teflon cup supported by a 4.0 μm-thick Prolene® X-ray film (Chemplex Industries, Inc., Palm City, FL, USA). The helium (He) flush mode of the Bruker S2 Ranger was chosen for the loose powder analysis to prevent damage to the instrument. To ensure the quality of the measurements, the system was calibrated daily using reference standards.

To determine the best measurement conditions available on the Bruker Ranger S2, a pressed pellet of a pure coffee sample was analyzed. The measurement time was generally set to 200 s as this seemed to be a good compromise between repeatability and analysis time. Figure 42 shows a comparison between four different conditions: (1) 50 kV with a 100 μm Cu filter; (2) 40 kV with a 500 μm Al filter; (3) 20 kV without filter and (4) 10 kV without filter. For the elements K and Ca, the best signal-to-noise (S/N) ratio was obtained using condition (3), and for the elements Mn, Fe, Cu, Zn, Rb, and Sr, the best condition was (2). However, since the focus of this study is on multi-element analysis, condition (2), 40 kV with a 500 μm Al filter, was selected as the best overall condition.

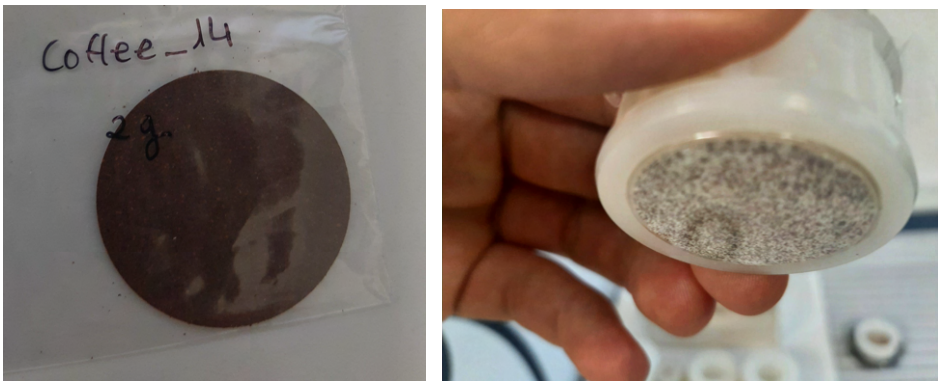

(a) (b)

Figure 25: (a) Pressed coffee pellet and (b) loose powder sample in a Teflon cup, coated with a thin film suitable for XRF analysis.

4.5.3 TXRF

For the TXRF analysis, the same digests were used as for the ICP-OES analysis. Gallium (Ga) was used as the internal standard. 1 ml of the 1000 ppm Ga stock solution was diluted with 4 ml of ultrapure water to obtain a 200 ppm Ga solution. For sample preparation, 25 μl of this Ga solution was mixed with 1 ml of digest. This results in a concentration of approximately 4 ppm Ga in the sample. The exact weight for this ratio was measured and recorded for each sample.

Each blank reflector was measured for 100 seconds to ensure that there was no contamination on the reflector. Prior to pipetting the liquids onto the reflectors, they were vortexed for one minute to ensure homogeneity. Sample volumes ranged from 10 μl to 30 μl. This depended on the element concentration of the sample and whether the droplet actually stayed in the center of the reflector after drying on an 80°C hot plate. After each 10 μl drop, the reflectors were dried before the next drop was added.

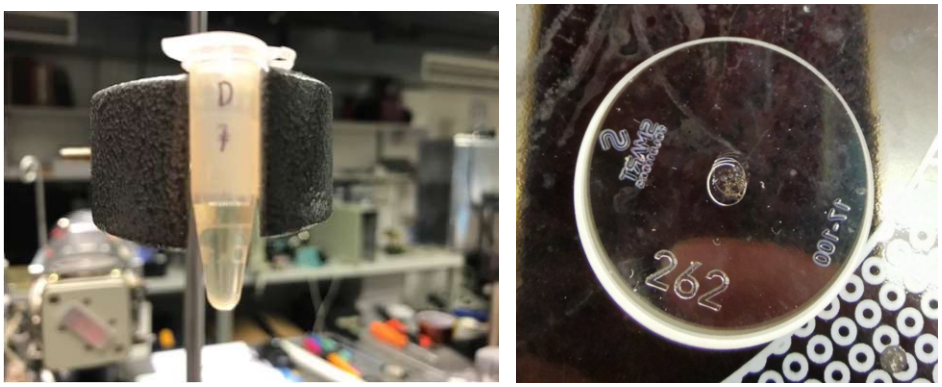

(a) (b)

Figure 26: A digested coffee sample that appears to be a perfectly clear liquid (a), but the dried residue on the reflector indicates that it is more likely a suspension (b).

4.6 ICP-OES quantification

For ICP-OES quantification, we focused on the elements K, Ca, Mn, Fe, Cu, Zn, Rb, and Sr for both certified reference materials (CRMs) and coffee samples. We prepared 8-12 standard solutions for each element with 1000 ppm stock solutions. The different amounts of stock solutions were mixed with 7 ml of HNO_3 to have more or less the same matrix as the digested coffee samples. The solution was then made up to volume (15 g) with ultrapure water. The measured intensities of the stock solution were then plotted against the known concentrations to obtain empirical calibration curves. The points were then linearly interpolated. The resulting function of the form $y = kx + d$ must then be solved for $x = \frac{y}{k} - d$, where y is the measured intensity from the K-KL3 line, k is the slope of the linear function, d is the offset, and x is the corresponding concentration. In some cases we had to split the calibration curves into different ranges (low and high concentration) due to the different concentrations within the samples.

For the quantification of the CRMs, we used the same approach. However, since the concentration levels were different from those of the coffee samples, a new set of calibration curves was required, again using two different ranges (low and high concentration). An example calibration curve is shown in Figure 27. It is important to note that the concentrations obtained from this curve still need to be multiplied by the correct dilution factor for each sample ($DF \approx 60$ for coffee samples and ≈ 80 for CRMs) to obtain the correct element concentrations in the coffees.

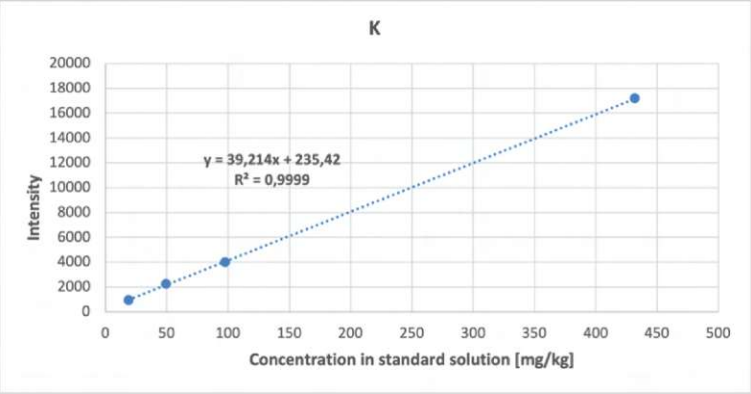

Figure 27: Experimental calibration curve for K for the quantification of the ICP-OES measurements. Only the higher K concentration range was considered.

4.7 EDXRF quantification approaches

In absence of a certified standard reference material (CRM) for coffee we chose a semi-empirical fundamental parameter approach and an empirical calibration approach for quantification of the EDXRF spectra.

4.7.1 Calibration curves using empirical standards (EDXRF)

For the EDXRF calibration curves for the elements K, Ca, Mn, Fe, Cu, Zn, Rb and Sr, we selected 11 coffees analyzed by ICP-OES, which provided a wide range of concentrations for all elements. These 11 coffees are called empirical standards. Then we created an application using the Bruker *Spectra EDX* software. The intensities of each element were plotted against the concentrations obtained from the ICP-OES measurements for the selected coffee samples. If a data point was clearly out of range, it was removed from the plot. The offset d was set to zero. The final calculations were performed by the software. An example plot is shown in Figure 28 for potassium (K). The white squares mark the net intensities and the blue hourglasses mark the corrected values for the K-KL3 line.

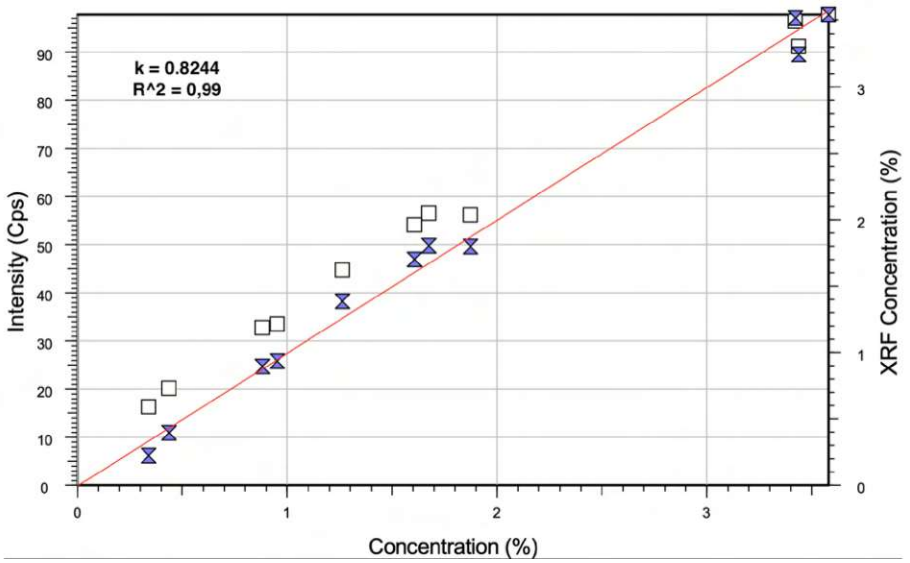

Figure 28: Experimental calibration curve for K using 11 coffees as empirical standards.

4.7.2 Semi-empirical fundamental parameter approach

For this semi-empirical fundamental parameter approach, the Bruker Ranger S2 software was used. However, the software requires the effective atomic number Z_{eff} of the sample matrix for quantification. To determine this Z_{eff}, we used the ratio between the Compton and Rayleigh scattering peaks of known materials, since these signals carry information about the sample matrix. This approach has already been shown by [26]. Z_{eff} is defined as

$$Z_{eff} = \frac{\sum(W_i \cdot Z_i \cdot A_i)}{\sum(W_i \cdot A_i)} \tag{14}$$

where W_i is the weight fraction of element k in the compound, Z_i is the atomic number of element k, and A_i is the atomic mass of element k in atomic mass units (amu). To obtain a calibration curve like the one in Figure 29, we calculated the Z_{eff} according to equation 14 for known materials and measured their EDXRF spectra using 5 g pellets to obtain the Compton to Rayleigh ratio (x-axis).

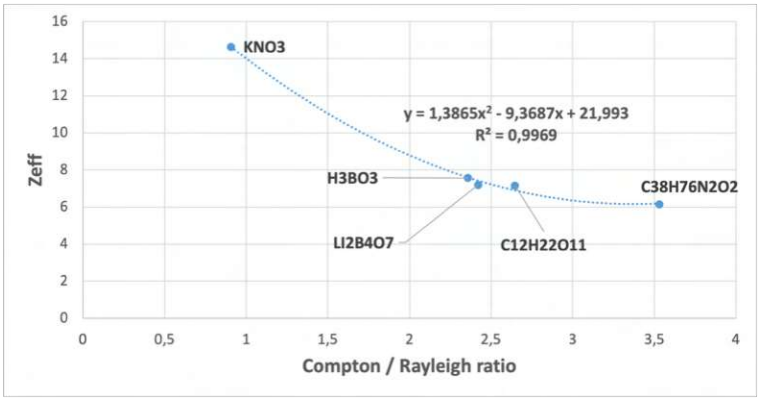

Figure 29: Experimental calibration curve with known materials to determine an effective atomic number (Z_{eff}) for each coffee from the ratio of Compton to Rayleigh scattering peaks.

The points were then parabolically fitted using Microsoft Excel 365. To obtain the Z_{eff} for each coffee, we calculated the Compton to Rayleigh ratio and entered it into the 2^{nd} order fit function $y = Z_{eff} = 1.3865x^2 - 9.3687x + 21.993$. The materials used were: potassium nitrate (KNO_3), boric acid (H_3BO_3), lithium borate ($Li_2B_4O_7$), cellulose ($C_{12}H_{22}O_{11}$), and Hoechst Wax C micropowder ($C_{38}H_{76}N_2O_2$). The range of Z_{eff} was from 14.7 (KNO_3) to 6.2 ($C_{38}H_{76}N_2O_2$).

4.8 TXRF quantification approaches

4.8.1 Empirical calibration curves (TXRF)

For the empirical calibration curves, the same set of 11 empirical coffee standards was used as in section 4.7.1. Approximately 4 ppm Ga was added to 1 ml of the digest of the empirical coffee standards. The exact weight of both the digest and added internal standard was recorded to calculate the concentration of the internal standard in the sample (Table 30). This factor is needed for an accurate calculation.

Two independently prepared digests were available for all 11 coffees used as standards. These 22 coffee standards were then measured with the WOBIS-TRAX system using the sample preparation techniques and measurement conditions described above. Figure 30 shows a calibration curve used to quantify the TXRF spectra. Since an internal standard was used, the y-axis is no longer just the intensity of an element i, but the corrected intensity $\frac{I(E_K^i)}{I(E_K^{st})}$ times the concentration of the internal standard c^{st} (see also equation 8). The mean of the two independent standards was taken to obtain a point on the calibration curve. Then the points were fitted linearly again.

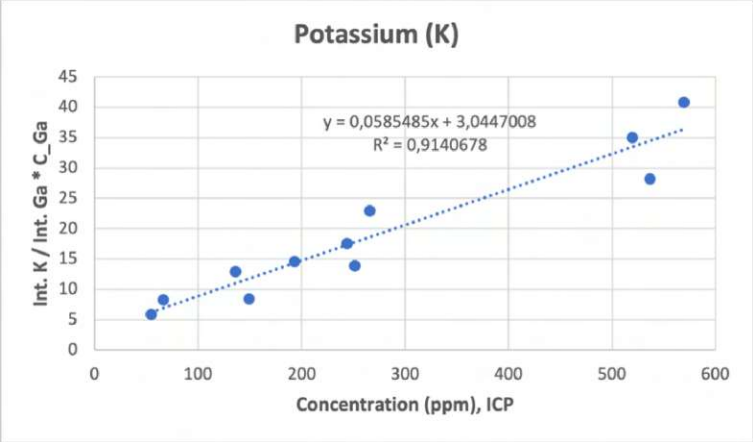

Figure 30: Experimental calibration curve for K using 11 coffees as empirical standards.

PyMca was used to deconvolve the spectra. It is important to note that the fluorescence peak area for the entire K shell was used instead of just the KL3/KL2 lines. However, this makes **no difference** when used for all calibration curves and all samples. This approach does not apply to L-lines and their entire tran-

sitions which is the result given by PyMca.
To obtain the correct concentration for each element of the coffee samples, the measured peak area must be divided by the internal standard peak area and multiplied by the respective internal standard concentration. The final step is to calculate the mean and standard deviation of each element for each sample. Microsoft Excel was used to perform the calculations.

4.8.2 Fundamental parameter approach (ATI-QUANT)

The ATI-QUANT software was developed by B. Grossmayer [73], P. Necker [74] and E. Holub [75] at the Institute of Atomic and Subatomic Physics, TU Wien. The application is able to perform quantification of TXRF spectra using only fundamental parameters. We used the thin-film approximation mode, which is described by the formula explained in section 2.1.2:

$$I(E^i_{K_\alpha}) = m^i \cdot \frac{I_0(E)}{4\pi r^2} \cdot \frac{I_{int}(\varphi, E)}{I_0(E)} \cdot \frac{\tau^i_K(E)}{\rho} \cdot \omega^i_K \cdot p^i_\alpha \cdot G_2(\psi) \cdot f(E^i_{K_\alpha}) \cdot \epsilon(E^i_{K_\alpha}) \quad (15)$$

The software is very easy to use, but not yet publicly available. It allows the user to precisely describe the measurement conditions such as tube parameters, information about filters (source and detector) and the detector itself, as well as to implement known sample compositions, if any. In order to make XRF spectra usable for ATI-QUANT, they must first be fitted with PyMca. The .fit files received must then be converted into an .asr file with an in-house program. If AXIL is used for fitting and peak deconvolution, the fit result is already in .asr format.
The ATI-QUANT results can be exported to Microsoft Excel. There we have to correct the results for the internal standard concentration by dividing it by the Ga result and then multiplying the element concentration by the individual dilution factor and the internal standard concentration of each sample. Figure 31 shows the ATI-QUANT user interface and Figure 32 shows the calculated tube spectrum and detector efficiency.

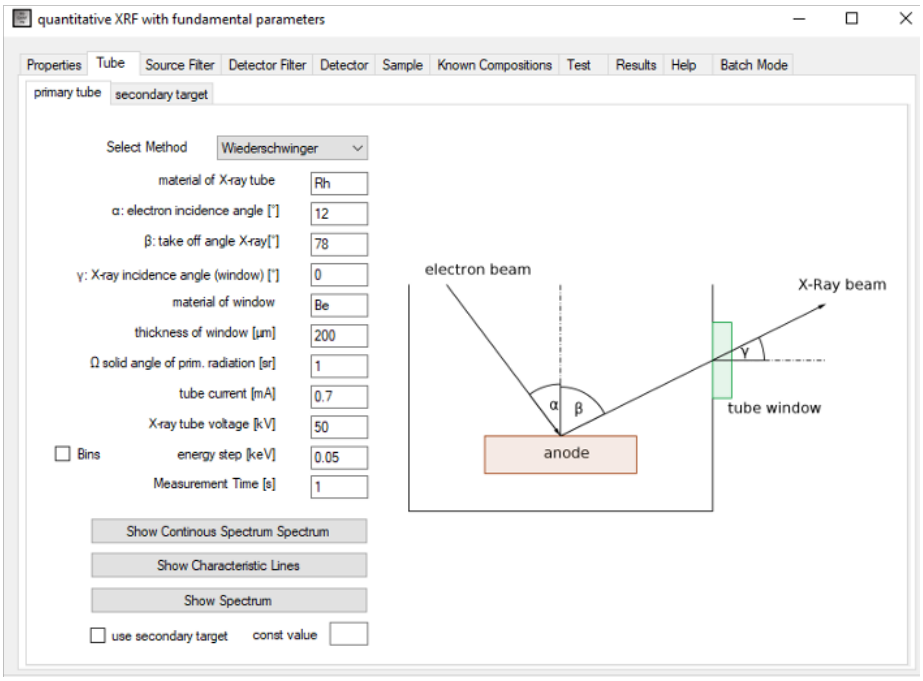

Figure 31: User interface of the ATI-QUANT software.

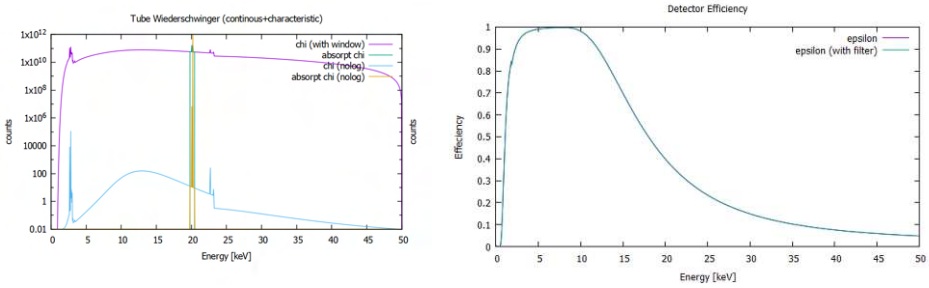

(a) (b)

Figure 32: Simulated spectrum of the Warrikhoff MCB50-0.7G X-ray tube with the selected Rh-KL3 line (a) and simulated detector efficiency (b). Figures created with ATI-QUANT.

4.9 Chemometric analysis

We used the IBM SPSS version 28 to conduct the chemometric experiments. Principal component analysis (PCA) and partial least squares combined with discriminant analysis (PLS-DA) were chosen as analytical techniques. However, before the data in the form of .txt files from the spectrometer could be loaded into SPSS, they had to be processed by an in-house Fortran 95 application (Lahey/Fujitsu Fortran 95 express v 7.20.00 compiler).

5 Results and Discussion

5.1 ICP-OES measurements

5.1.1 ICP-OES calibration curves for certified reference materials (CRMs)

The CMRs had to be further diluted compared to the coffee samples. Therefore, two different sets of calibration curves were used. The Figures 33 - 36 show the calibration curves for the quantification of the analyzed certified reference materials CBW07604 (poplar leaves), NCS ZC73036 (green tea) and NCSZC73031 (carrot) for the elements K, Ca, Mn, Fe, Cu, Zn, Rb and Sr. In the case of the carrot standards, an extra curve was calibrated for Ca because the concentrations were relatively low. The calibration curve for K is already shown in section 4.6 (Figure 27). The linear regression values R^2 are all above 0.99.

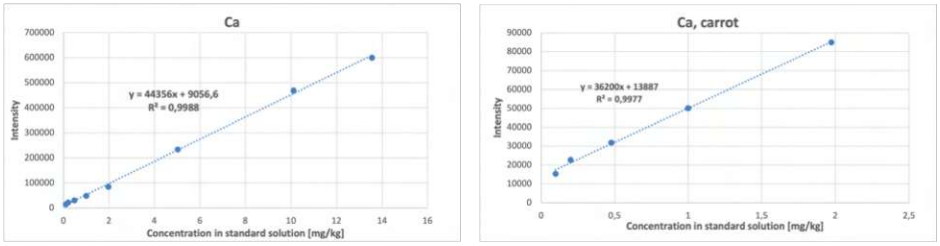

(a) (b)

Figure 33: (a) Calcium (Ca) calibration curve for quantification of ICP-OES measurements for the poplar leaf and green tea CMRs. (b) Calibration curve for calcium (Ca) quantification of ICP-OES measurements for carrot CRM using low concentration Ca standards.

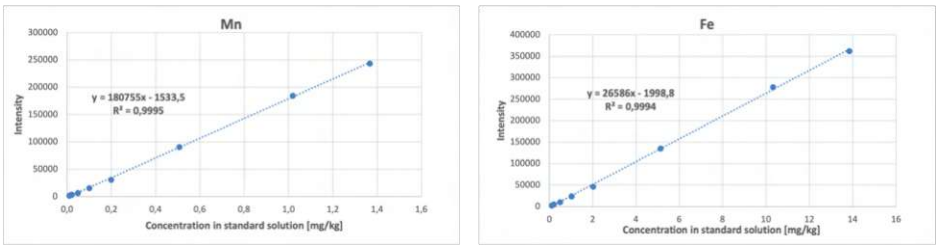

(a) (b)

Figure 34: (a) Calibration curve for manganese (Mn) and (b) iron (Fe) quantification of the ICP-OES measurements using standard solutions.

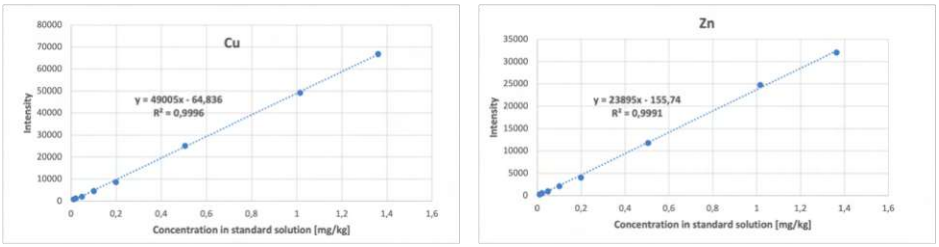

(a) (b)

Figure 35: (a) Calibration curve for copper (Cu) and (b) zinc (Zn) quantification of the ICP-OES measurements using standard solutions.

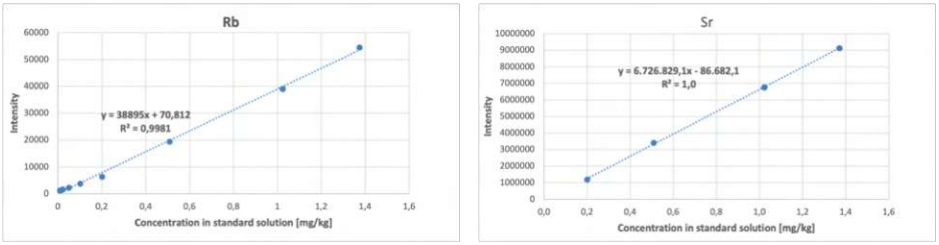

(a) (b)

Figure 36: (a) Calibration curve for rubidium (Rb) and (b) strontium (Sr) quantification of the ICP-OES measurements using standard solutions.

5.1.2 ICP-OES calibration curves for coffee samples

The Figures 37 - 41 show the calibration curves for the quantification of the analyzed coffee samples for the elements K, Ca, Mn, Fe, Cu, Zn, Rb and Sr. In the case of Mn, Rb and Sr, two calibration curves were used; one for low and one for high concentrations of the respective element. The linear regression values R^2 are all above 0.99.

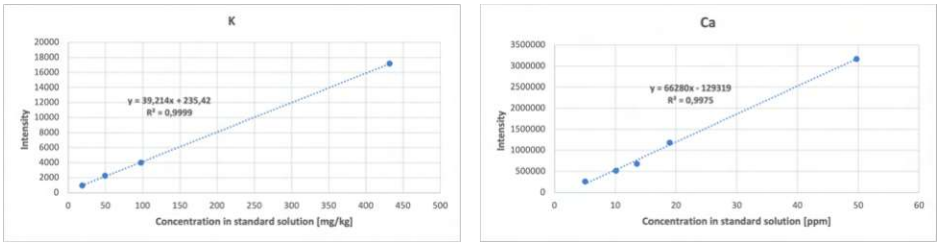

(a) (b)

Figure 37: (a) Calibration curve for the quantification of the ICP-OES measurements of coffee samples for potassium (K) and (b) for calcium (Ca) using standard solutions.

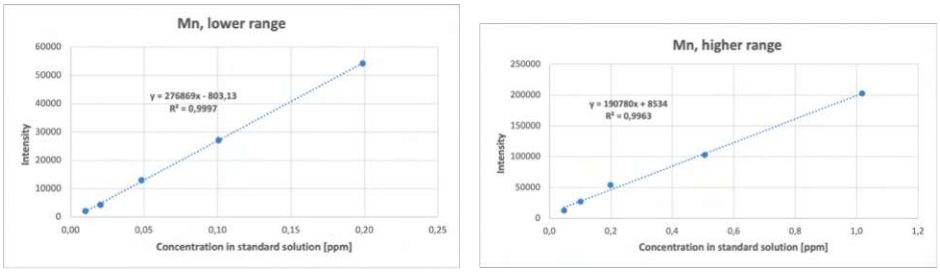

(a) (b)

Figure 38: (a) Calibration curve for the quantification of the ICP-OES measurements of coffee samples for low concentrations of manganese (Mn) and (b) for high concentrations of Mn using standard solutions.

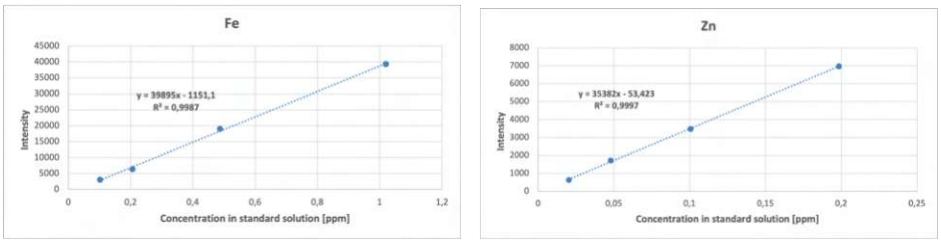

(a) (b)

Figure 39: (a) Calibration curve for the quantification of the ICP-OES measurements of coffee samples for iron (Fe) and (b) for zinc (Zn) using standard solutions.

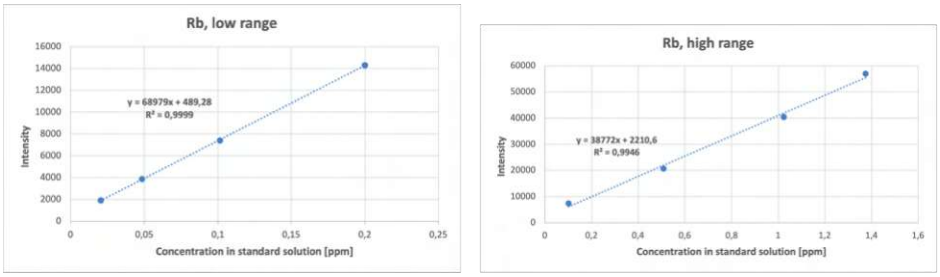

(a) (b)

Figure 40: (a) Calibration curve for the quantification of the ICP-OES measurements of coffee samples for low concentrations of rubidium (Rb) and (b) for high concentrations of Rb using standard solutions.

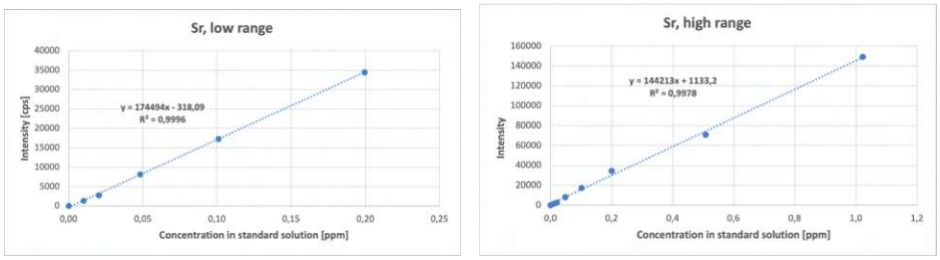

(a) (b)

Figure 41: (a) Calibration curve for the quantification of the ICP-OES measurements of coffee samples for low concentrations of strontium (Sr) and (b) for high concentrations of Sr using standard solutions.

5.1.3 ICP-OES results for certified reference materials (CRMs)

The ICP-OES elemental concentration analysis of the available organic CMRs with the obtained calibration curves from subsection 5.1.1 showed very good agreement with the reference data. The results are summarized in Table 7. Because of the excellent agreement, we decided to use the ICP-OES data of the coffee samples as reference values.

Element	CBW07604 (Poplar leaves)		NCS ZC73036 (Green tea)		NCS ZC73031 (Carrot)	
	ICP-OES [ppm]	Reference [ppm]	ICP-OES [ppm]	Reference [ppm]	ICP-OES [ppm]	Reference [ppm]
K	13400 ± 100	13800 ± 700	15600 ± 1500	15500 ± 700	9900 ± 1000	10800 ± 400
Ca	17600 ± 1600	18100 ± 1300	11200 ± 600	12100 ± 300	2500 ± 100	2500 ± 100
Mn	38.8 ± 0.3	45 ± 4	1258 ± 97	1170 ± 60	10.8 ± 0.9	12.1 ± 0.5
Fe	290 ± 26	274 ± 17	357 ± 12	322 ± 23	171 ± 12	148 ± 15
Cu	9.1 ± 0.1	9.3 ± 1.0	25.9 ± 4.7	24 ± 1	4.4 ± 0.3	4.1 ± 0.3
Zn	37.2 ± 2.0	37 ± 3	33.6 ± 2.0	35 ± 2	11.7 ± 1.0	11.2 ± 0.5
Rb	7.88 ± 0.05	7.6 ± 0.8	83.9 ± 8.5	89 ± 9	8.0 ± 0.4	6.9 ± 0.5
Sr	192 ± 18	154±9	29.0 ± 0.9	36±2	19.0±1.4	22±2

Table 7: ICP-OES results of our main analytes K, Ca, Mn, Fe, Cu, Zn, Rb and Sr of our three CRMs compared to their respective reference data. Table also used in [21].

5.1.4 ICP-OES results for coffee samples

The results for the ICP-OES measurements are implemented in the following subsections 5.2.5 (ICP-OES vs. EDXRF) and subsection 5.3.3 (ICP-OES vs. TXRF). They are also listed in detail in Appendix A and B.

5.2 EDXRF measurements

5.2.1 Measurement conditions

To evaluate the different measurement conditions available: 100 μm Cu filter at 50 kV, 500 μm Al filter at 40 kV, no filter at 20 kV, and no filter at 10 kV, we measured the spectra of a pressed coffee pellet for 200 s with the Ranger S2 system. The maximum intensity was automatically set to 100,000 cps. The result is shown in Figure 42. Note that the y-axis represents the logarithmic intensity. The effect of the filters is clearly visible as elements with Z less than K are almost completely blocked. When the Cu filter is used, the signal of the main elements K and Ca is drastically reduced. If no filters are used, the characteristic radiation of the light elements reaches the detector unhindered. However, the heavier elements such as Rb and Sr are hardly visible (poor signal-to-noise ratio). Therefore, since this study focuses on multi-element analysis, the mode with the 500 μm Al filter at 40 kV was chosen as the final measurement condition. It clears the spectrum of light elements not of interest in this study, but still allows strong K and Ca signals and allows the detection of heavier elements as well.

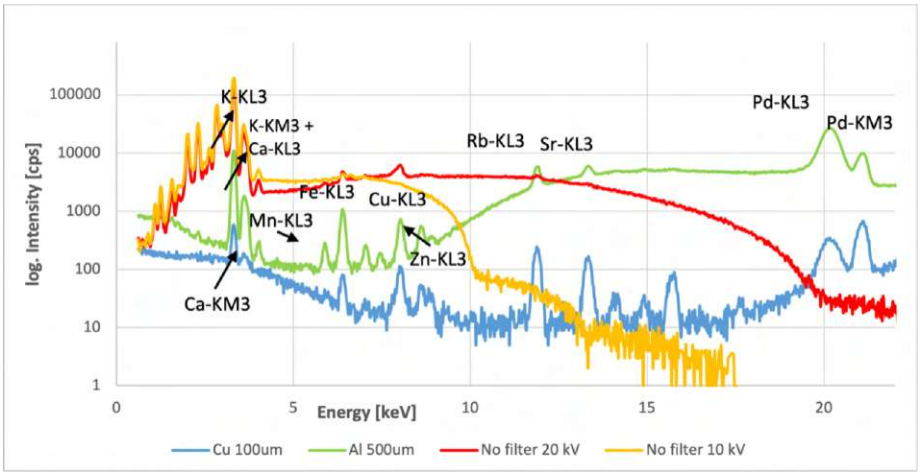

Figure 42: Effect of four different measurement conditions on the spectra of a pressed pellet: μm Cu filter at 50 kV (blue), 500 μm Al filter at 40 kV (green), no filter at 20 kV (red) and no filter at 10 kV (yellow). Figure in similar form used in [21].

5.2.2 Sample preparation

In addition to analyzing the chemometric and quantitation approaches, this study also focused on the different sample preparation options. As shown in Table 1, there is no general consensus on the best way to prepare coffee powder samples. Most studies use pressed pellets with and without wax as a binder. The advantages of wax are that it is an organic compound and that it helps to stabilize samples [76]. This is also useful when re-measurement is required. However, it is also possible to present the loose powder to the instrument. This approach is less time consuming as it requires little sample preparation. Both approaches have been tested, as well as the effect of different amounts of wax (in percent of sample mass). The latter is shown in Table 8 (mean values, n=2). The data show a steady decrease in signal-to-noise ratio with increasing amount of wax. This is particularly problematic in the case of trace element analysis in the category of coffee with additives, since the element concentrations are already very low and can be below the limit of detection. This effect can be explained by the dilution of the sample as the wax content increases (see Figure 43). In addition, since wax is composed of light elements, it can increase scattering and thus contribute to a higher background intensity. The sample mass was set at 2 g for all samples because many of the coffees studied were only available in small quantities. Better overall results could be obtained by using 5 g due to the indefinite-thickness-of-sample approximation then in use.

Element	**Instant coffee**			**Pure coffee**			**Coffee with additives**		
	0%	**10%**	**20%**	**0%**	**10%**	**20%**	**0%**	**10%**	**20%**
K	50.6	44.9	36.7	44.8	38.9	29.5	23.0	15.5	14.8
Ca	8.7	5.3	4.0	7.4	5.7	5.0	13.1	8.7	7.5
Mn	2.9	1.9	1.9	2.5	1.9	1.5	1.4	0.4	N.D
Fe	5.4	3.3	3.2	9.2	9.9	7.8	2.9	1.0	0.9
Cu	2.4	1.8	1.9	5.0	4.8	4.9	N.D	N.D	N.D
Zn	2.2	1.1	1.1	2.9	1.8	1.6	2.1	0.9	0.7
Rb	1.8	0.9	0.7	1.4	0.5	0.4	1.2	0.1	0.08
Sr	1.1	0.8	0.8	1.1	0.6	0.6	N.D	N.D	N.D

Table 8: Effect of different amounts of wax binder (0%, 10% and 20% of sample mass) on the signal-to-noise-ratio for the elements K, Ca, Mn, Fe, Cu, Zn, Rb and Sr for pure instant coffees, pure coffees and coffees with additives. Table also used in [21].

The results of the loose powder analysis are shown in Figures 44 and 45 for the trace elements Mn, Fe, Cu and Zn. The fundamental parameter approach was chosen for quantification as it was the first method available at this early stage of the study. Both the powder and the pressed pellet (10% wax) show large deviations from the mean ICP-OES values. However, because Mn was once undetectable by the powder method, despite being present in relatively large amounts, the pressed pellets with 10% wax added were chosen as our final sample preparation technique for EDXRF measurements.

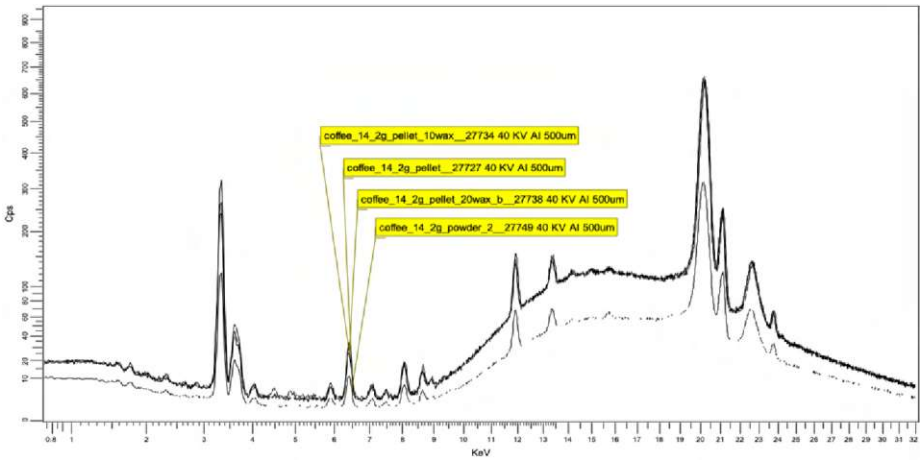

Figure 43: Comparison of different sample preparation techniques (from highest to lowest curve): (1) pellet with 0% wax, (2) pellet with 10% wax, (3) pellet with 20% wax, and (4) loose powder sample.

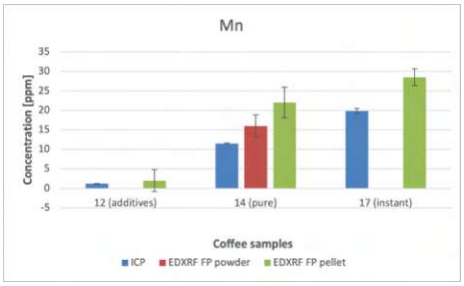

(a)

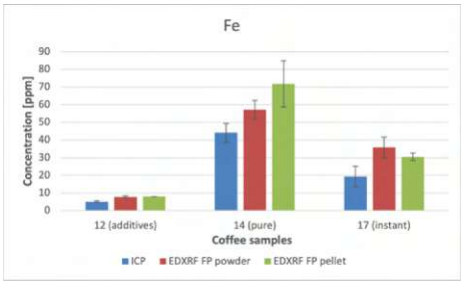

(b)

Figure 44: Comparison of FP quantification results for Mn (a) and Fe (b) for loose powder samples and pellets with 10% wax added with ICP-OES values.For means and SD of all ICP-OES data and pellet data for samples 12 and 17: n=2. For means of powder samples and pellet data for sample 14: n=5.

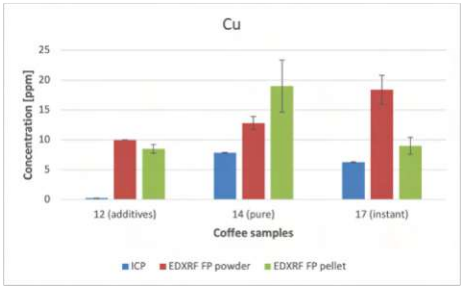

(a)

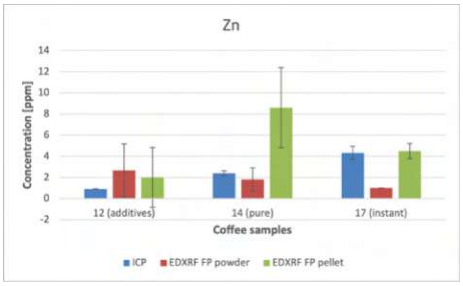

(b)

Figure 45: Comparison of FP quantification results for Cu (a) and Zn (b) for loose powder samples and pellets with 10% wax added with ICP-OES values. For means and SD of all ICP-OES data and pellet data for samples 12 and 17: n=2. For means of powder samples and pellet data for sample 14: n=5.

5.2.3 Limits of detection

Detection limits have not been extensively studied in this work, but it is interesting to show the difference in results from different forms of background calculations (as described in Figure 9). The comparison is shown in Figure 46. For Mn, Fe and Cu, the conventional background calculation gives about five times higher detection limits compared to when the standard deviation of 5-6 background points is inserted into the equation 9. For Zn the difference is smaller, but the detection limit still drops by 50%. The latter approach can be understood as a subtraction of the background level from the fluctuations.

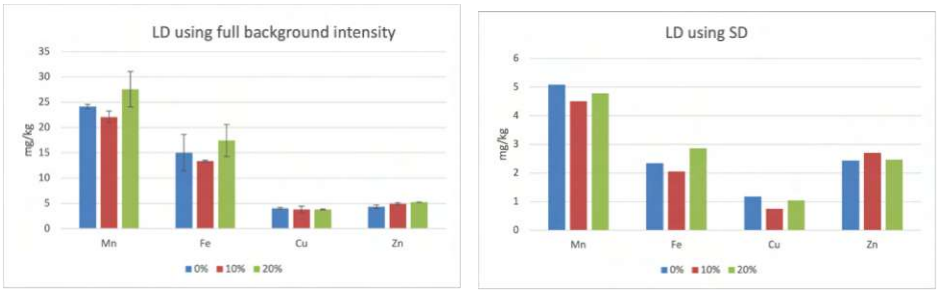

(a) (b)

Figure 46: Different results for the detection limit of Mn, Fe, Cu and Zn of a pressed pure coffee pellet with added 10% wax: (a) LOD calculation using the full background intensity and (b) LOD calculation using the standard deviation of different points of the background intensity.

5.2.4 Calibration curves for EDXRF

The Figures 47 - 50 show the calibration curves for the quantification of the analyzed EDXRF spectra of coffee samples for the elements K, Ca, Mn, Fe, Cu, Zn, Rb and Sr. The linear regression values R^2 are all between 0.88 and 0.99.

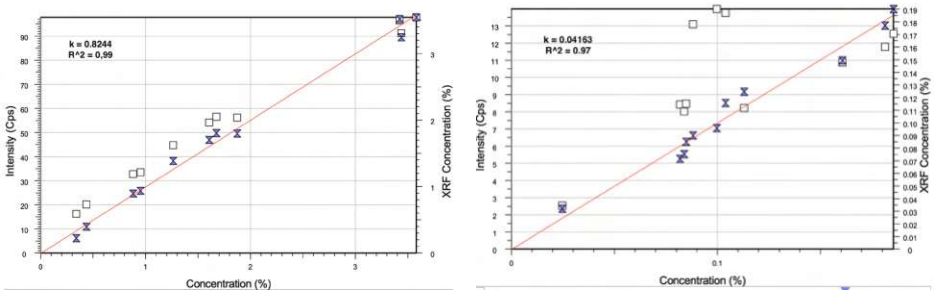

(a) (b)

Figure 47: (a) Empirical calibration curve for potassium (K) using 11 coffee samples as empirical standards.(b) Empirical calibration curve for calcium (Ca) using 11 coffee samples as empirical standards.

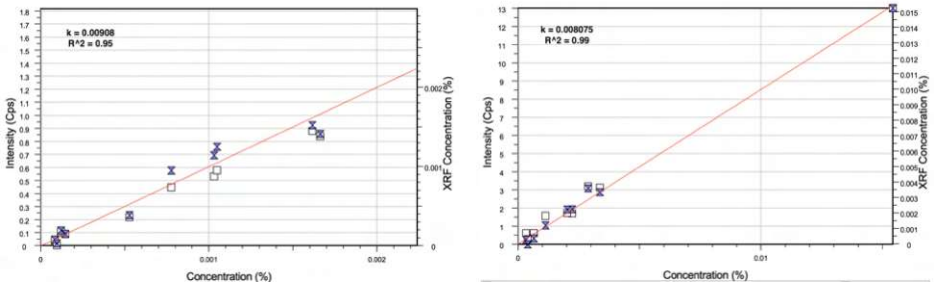

(a) (b)

Figure 48: (a) Empirical calibration curve for manganese (Mn) using 10 coffee samples as empirical standards.(b) Empirical calibration curve for iron (Fe) using 9 coffee samples as empirical standards.

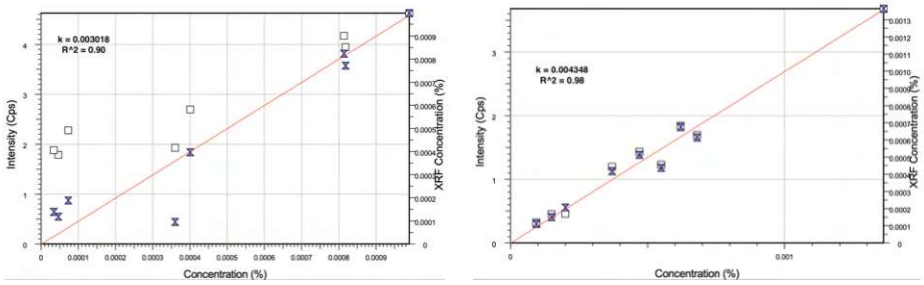

(a) (b)

Figure 49: (a) Empirical calibration curve for copper (Cu) using 8 coffee samples as empirical standards.(b) Empirical calibration curve for zinc (Zn) using 9 coffee samples as empirical standards.

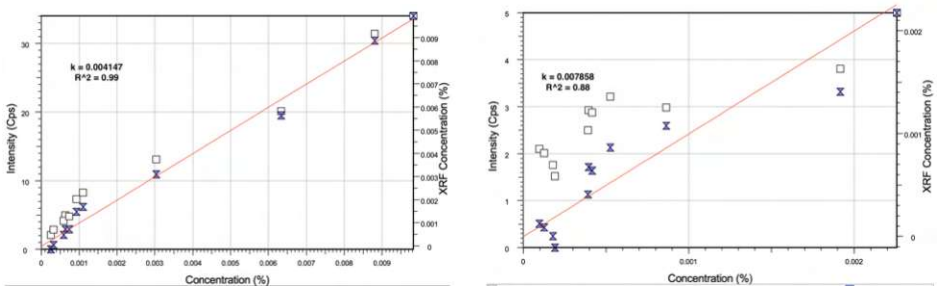

(a) (b)

Figure 50: (a) Empirical calibration curve for rubidium (Rb) using 11 coffee samples as empirical standards.(b) Empirical calibration curve for strontium (Sr) using 11 coffee samples as empirical standards.

5.2.5 ICP-OES vs. EDXRF quantification approaches

For the semi-empirical fundamental parameter approach, we used the Bruker Ranger S2 software, which requires a Z_{eff}. Therefore, we estimated this number using the method described in section 4.7.2. We calculated the Compton to Rayleigh peak ratios of 19 samples which resulted in a Z_{eff} for pure coffee of 6.92 ± 0.16 with n=10, for pure instant coffee in a Z_{eff} of 7.01 ± 0.13 with n=2 and for coffee with additives in a Z_{eff} of 6.88 ± 0.19 with n=7). Since there were hardly any differences, we chose a mean $\overline{Z_{eff}}$ of 6.916 (n=19). However, the software requires a chemical formula, so we created a dummy matrix using the equation 14 of exactly this Z_{eff}, namely $C_{25}H_{32}N_{10}O_{12}$.

The results of this semi-FP approach were then compared with the results of the empirical approach using calibration curves (section 4.7.1). Both sets of data were plotted against the reference ICP-OES values. These plots can now be analyzed using a linear regression method, also used in [21]. The ideal linear curve should have an R^2 value of 1, a slope of 1 and an intercept of 0. It is obvious that neither of the two approaches satisfies these conditions. Particularly problematic are the trace elements Mn, Fe, Cu and Zn, which were greatly overestimated by the semi-FP approach. Zn and Fe were also overestimated by the empirical calibration method. However, the empirical calibration method showed better results overall compared to the semi-FP approach. The following plots show the results in detail, the blue curves mark the results of the EQUAE measurements[2], the orange curves mark the concentrations of the empirical calibration approach.

[2]EQUAE is the name of the semi-FP application on the Ranger S2 system

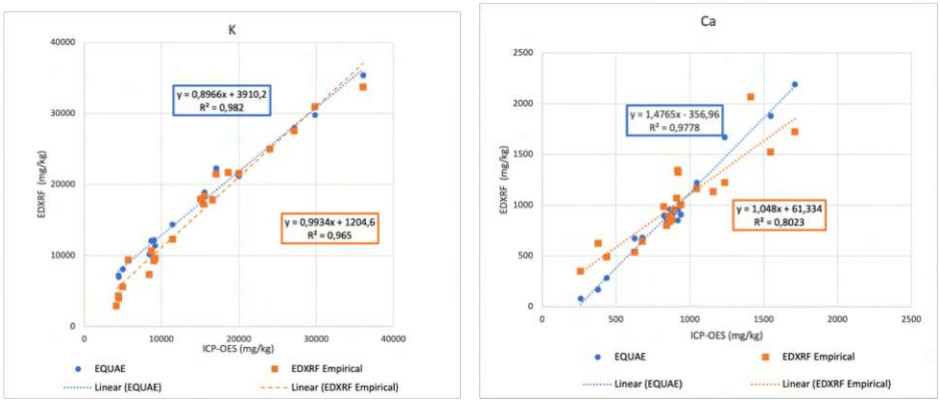

(a) (b)

Figure 51: Comparison between the EDXRF results obtained by the semi-empirical FP approach (EQUAE, blue) and the empirical calibration curves (orange) for the elements K (a) and Ca (b).

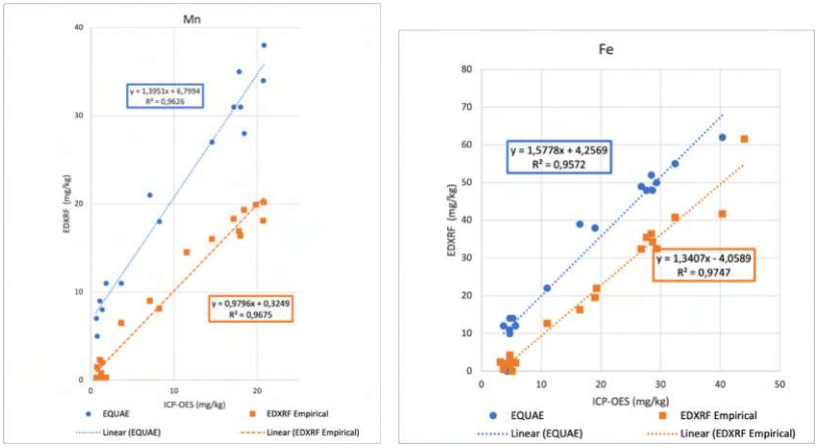

(a) (b)

Figure 52: Comparison between the EDXRF results obtained by the semi-empirical FP approach (EQUAE, blue) and the empirical calibration curves (orange) for the elements Mn (a) and Fe (b).

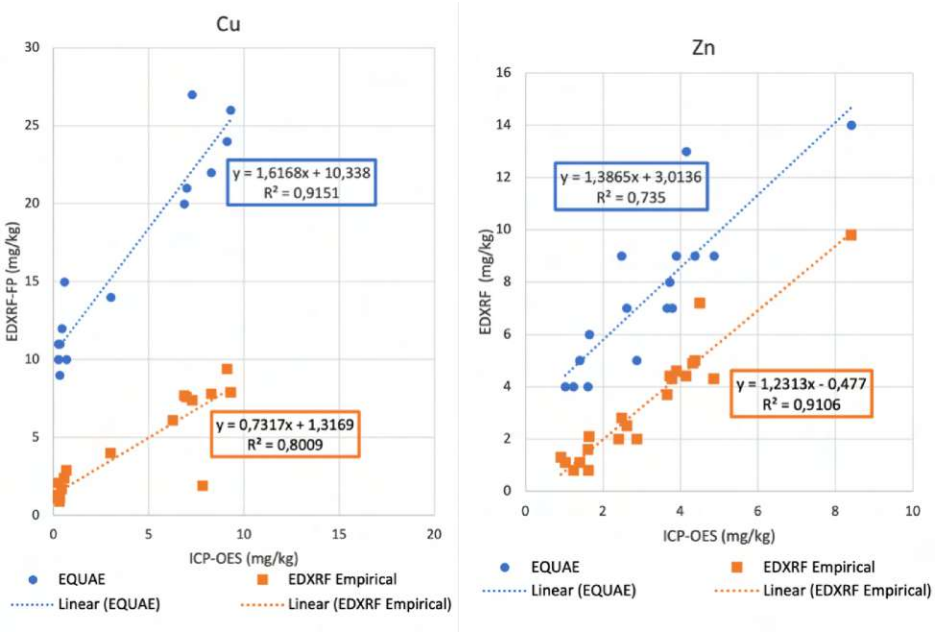

(a) (b)

Figure 53: Comparison between the EDXRF results obtained by the semi-empirical FP approach (EQUAE, blue) and the empirical calibration curves (orange) for the elements Cu (a) and Zn (b).

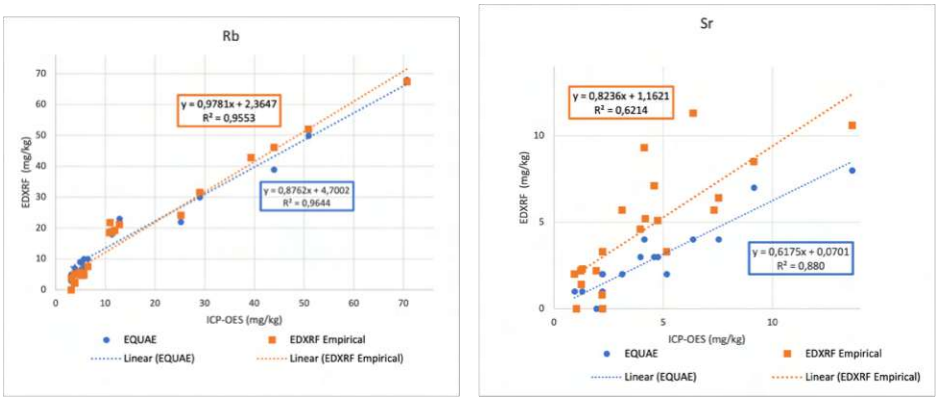

(a) (b)

Figure 54: Comparison between the EDXRF results obtained by the semi-empirical FP approach (EQUAE, blue) and the empirical calibration curves (orange) for the elements Rb (a) and Sr (b).

5.2.6 Chemometric results EDXRF

PCA

PCA can be used in a variety of contexts for XRF analysis, see for example [77] or [78]. Also for coffee analysis by XRF, PCA has been used relatively often for chemometric analysis, as shown in Table 1. For the PCA with the classical approach of using the mean values of the elemental concentrations, we used the EDXRF data of 37 samples obtained by the empirical calibration method (see table 20). The result are given in Figure 55 (a) next to the PCA result of the 1570 energy channels as variables Figure 55 (b).
In the case of the concentrations used as variables, the first three principal components contain about 86% of the total variability. Looking at the loading matrix shown in Table 9, we see that the first PC is strongly defined by the K, Mn, Fe, Cu, Rb and Sr contents, but weakly correlated with Ca and Zn. The latter two variables almost exclusively define the second PC. The clustering of the samples is clearly visible. The category of coffee with additives is the most dispersed, since its composition depends strongly on the additive (milk, chocolate, ...).
Using the raw spectra, we gain only 42% of information within the first 3 PCs. The clustering disappears and therefore this strategy is not usable for raw spectra analysis.

Variable	PC 1	PC 2	PC 3
K	0,799	-0,162	0,475
Ca	-0,1	0,915	0,328
Mn	0,902	0,082	-0,199
Fe	0,797	0,098	-0,441
Cu	0,819	0,086	-0,499
Zn	0,1	0,969	-0,053
Rb	0,687	-0,031	0,198
Sr	0,75	-0,103	0,617

Table 9: Loadings matrix for the first three PCs.

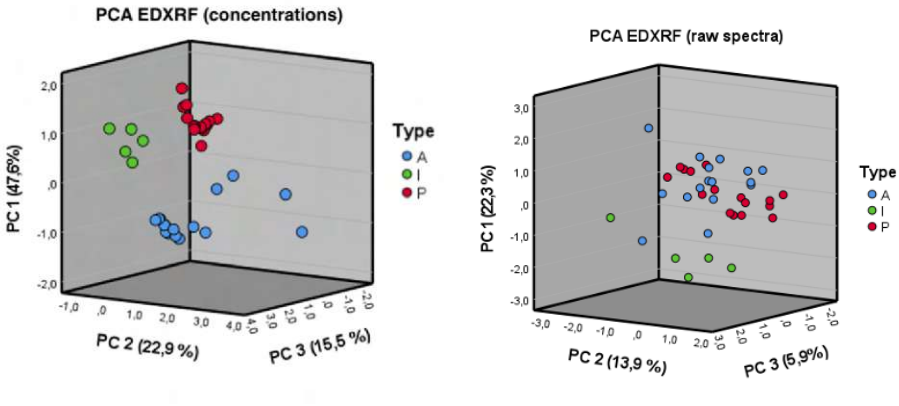

(a) (b)

Figure 55: Score plot of the PCA of the elemental concentration obtained by the EDXRF empirical calibration approach (a) and by presenting the raw spectra to the algorithm (b). The blue dots represent coffees with additives, the red dots represent pure coffees, and the green dots represent pure instant coffees.

PLS-DA

Since the PCA method was not able to cluster the raw EDXRF spectra, we tried to develop a PLS-DA approach using leave-one-out (LOO) cross-validation for this task. The PLS-DA of the raw EDXRF spectra was performed using 3 and 5 latent variables. We used all 37 available spectra for this analysis. The results are shown in the Figures 56 and 57. It can be seen that Function 1 separates coffees with additives from pure coffees. Function 2 separates instant coffees from pure coffees. Using 3 LVs results in less precise clustering than using 5 LVs. It was very surprising to the author that when PLS-DA was performed with bad labeling (incorrect labeling of the three categories, which happened by chance), both approaches still produced similar plots to the Figures 56 and 57. This is probably due to the immense amount of data available to the algorithm, which is then able to find a seemingly good model.

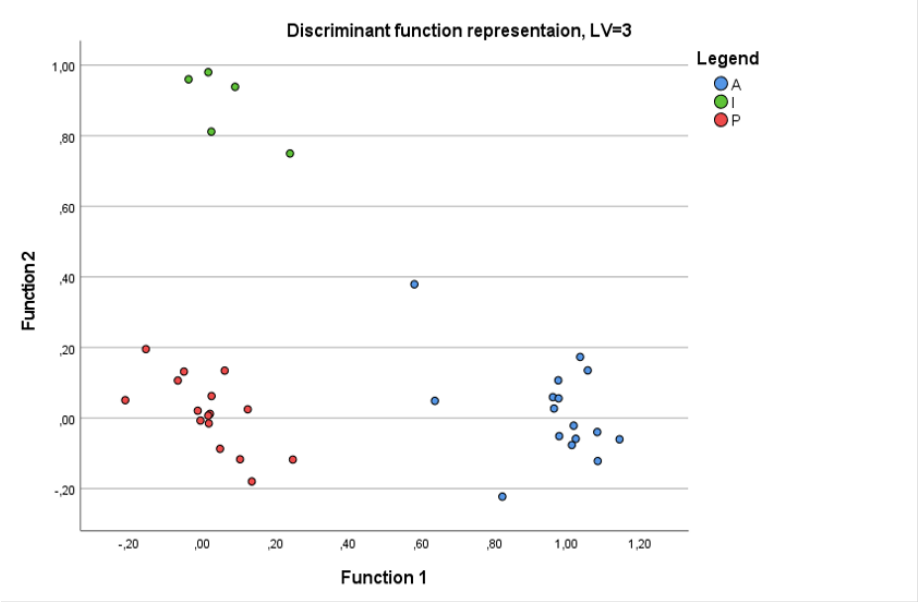

Figure 56: Training/fit of PLS-DA with 3 latent variables using the energy channels of the raw spectra as variables. The blue dots represent coffees with additives, the red dots represent pure coffees, and the green dots represent pure instant coffees

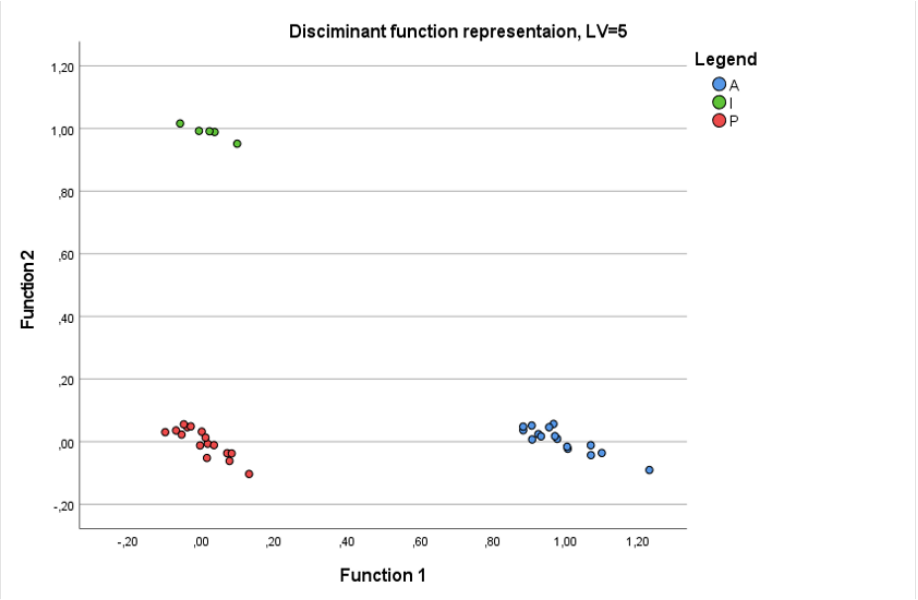

Figure 57: Training/fit of PLS-DA with 5 latent variables using the energy channels of the raw spectra as variables. The blue dots represent coffees with additives, the red dots represent pure coffees, and the green dots represent pure instant coffees

However, when it comes to making predictions, the bad labeling fails miserably. The predictions were done by hiding one sample at a time from the input data and computing the model without it. Then, the hidden sample is inserted into the model and the data point is plotted. The result is the LOO cross validation shown in Figure 58. The process was automated with an in-house Fortran 95 code. This approach worked best for 3 LVs. A sample belongs to the additive category if its Function 1 value is above 0.5 and its Function 2 value is below 0.5. A sample belongs to the pure coffee category if both its Function 1 and 2 values are below 0.5. A sample belongs to the instant category if its Function 1 value is below 0.5 and its Function 2 value is above 0.5. As can be seen in Figure 58, all predictions were successful. The additive category is again the least compact and the most widely spread.

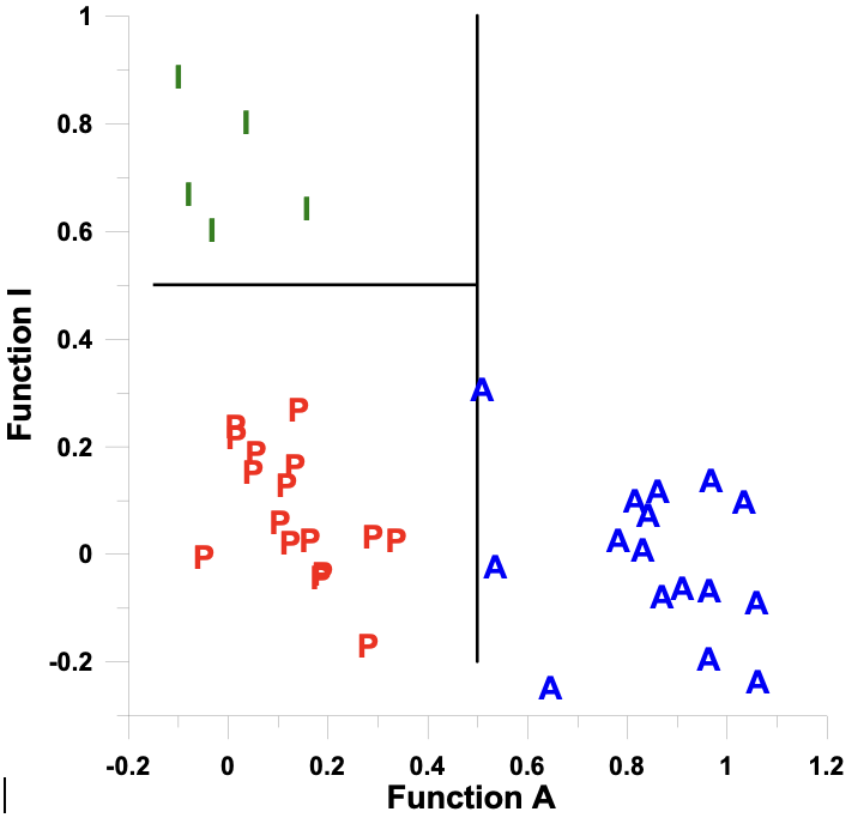

Figure 58: LOO cross-validation using a model based on 3 LVs. Figure taken from [21], created by E. Besalu.

5.3 TXRF measurements

For the TXRF measurements the custom-built WOBISTRAX spectrometer was used. Figure 59 shows a typical registered spectrum with logarithmic y-axis. Remarkable is the very low background intensity. Table 10 shows the deconvoluted peak area for each element (full K-shell) obtained by PyMca.

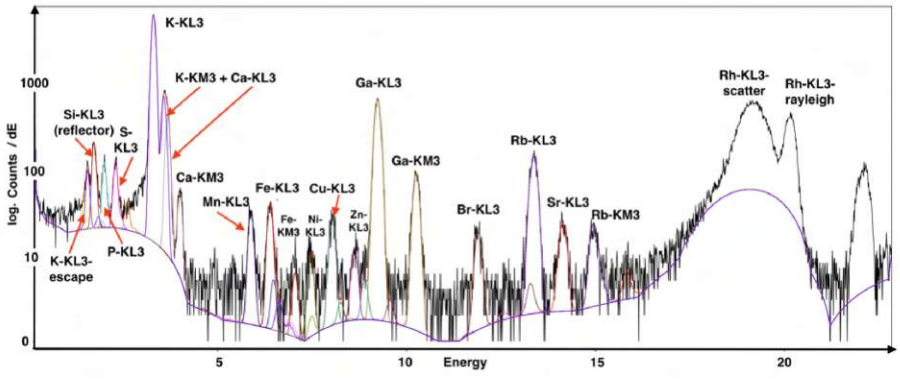

Figure 59: TXRF spectrum of a coffee sample, with Ga as internal standard.

Elements of interest (K-shell)	Peak area (PyMca)
K	77646
Ca K	5155
Mn	469
Fe	620
Cu	477
Zn	189
Rb	3130
Sr	510
Ga	11818

Table 10: Deconvoluted peak areas for the TXRF spectrum seen in Figure 59.

5.3.1 Validation of TXRF measurements

The only approaches completely independent of ICP-OES are the FP approaches. To validate our thin-film FP used by the ATI-QUANT software, we analyzed the digests of all three available CRMs (carrot, poplar leaves and green tea). Duplicates were used for the analysis. Deviation is defined as

$$DEV = 100 \cdot (C_{measured} - C_{reference})/C_{reference} \tag{16}$$

Carrot standard

Figure 60 shows a comparison between elemental concentration reference values from the data sheet, ATI-QUANT results, and ICP-OES data for the carrot standard. The comparison shows acceptable agreement with the reference and ICP-OES concentrations with deviations less than 30% for all elements (see Figure 61). The highest deviation is seen for the elements K and Ca with values significantly lower than the reference. This indicates some sort of self-absorption effect. The suspense nature of the solution (it is not a perfectly clear digest) is also problematic when pipetting, leading to variations in the amount of sample pipetted.

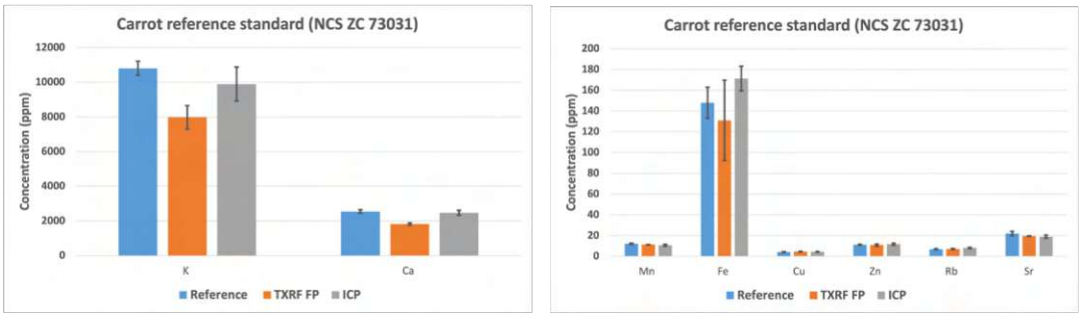

(a) (b)

Figure 60: Comparison of the obtained elemental concentrations of K and Ca (a) and Mn, Fe, Cu, Zn, Rb and Sr (b) of the carrot standard with the reference values; n=2.

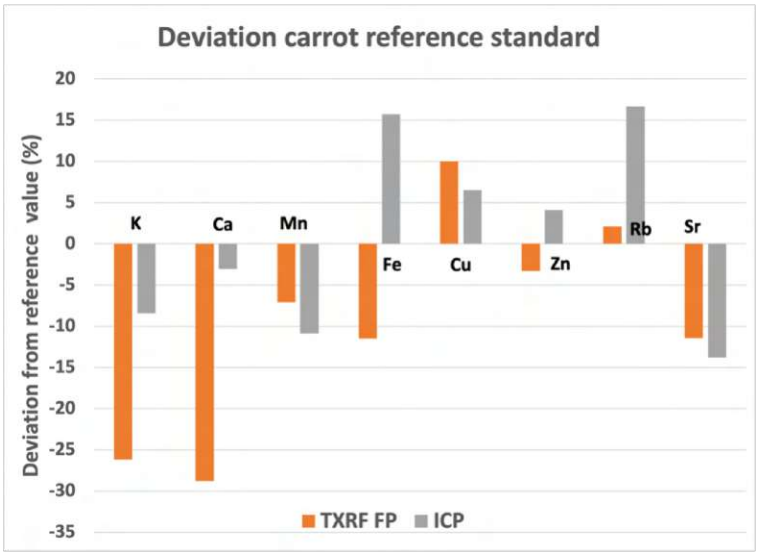

Figure 61: Deviations from the certified reference values of the carrot standard for the concentrations obtained by ICP-OES and ATI-QUANT; n=2.

Poplar leaves standard

The evaluation of the poplar leaf standards showed similar results to the carrot standard with a deviation below 20% for K, Ca, Mn, Cu and Zn (see Figures 62 - 64). The concentrations obtained for K and Ca were again lower than the reference data, which can be explained by self-absorption effects. However, the deviation for Fe is immense with more than 60%, which could indicate some kind of Fe contamination of the samples.

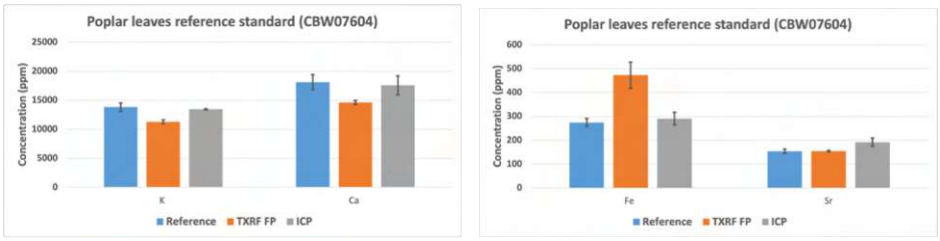

(a) (b)

Figure 62: Comparison of the obtained elemental concentrations of K and Ca (a) and Fe and Sr (b) of the poplar leaves standard with the reference values; n=2.

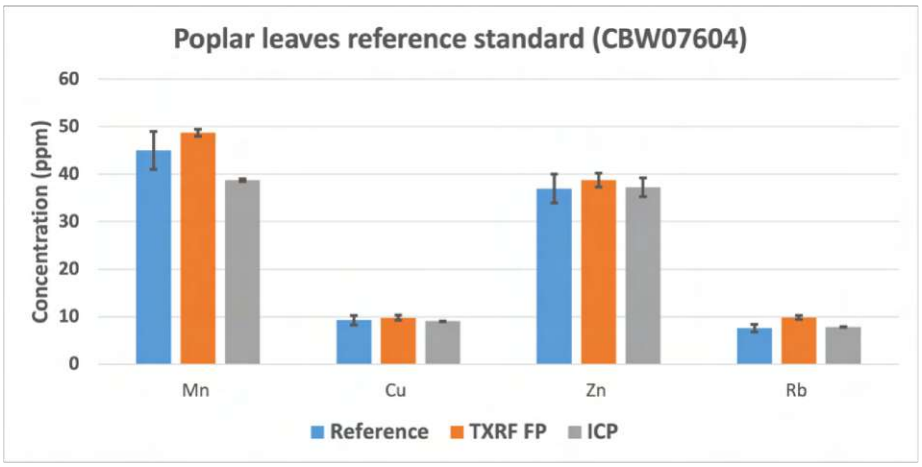

Figure 63: Comparison of the obtained elemental concentrations of Mn, Cu; Zn and Rb of the poplar leaves standard with the reference values; n=2.

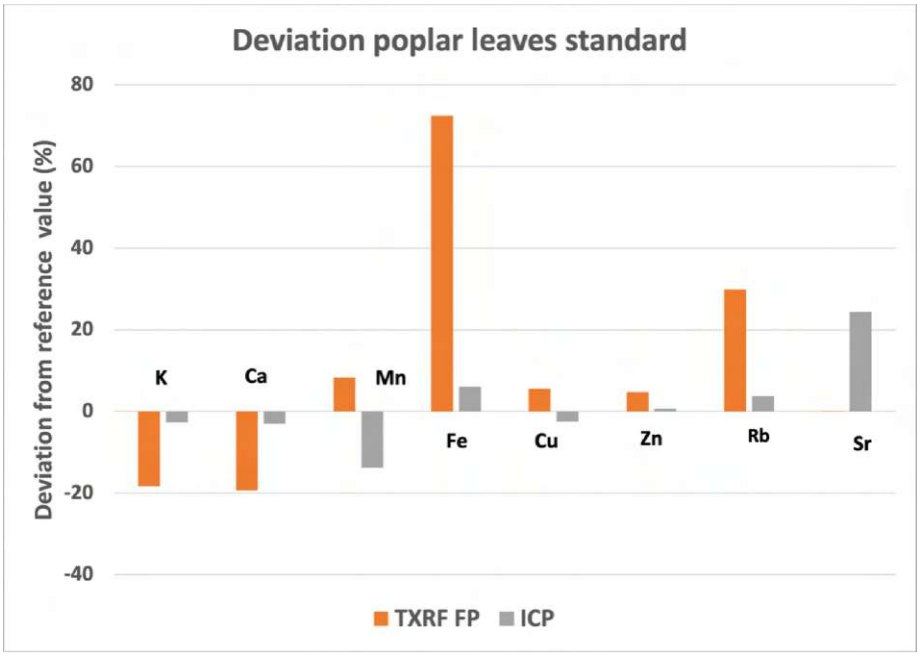

Figure 64: Deviations from the certified reference values of the poplar leaves standard for the concentrations obtained by ICP-OES and ATI-QUANT

5.3.2 Empirical calibration curves (TXRF)

The Figures 65 - 68 show the calibration curves for the quantification of the analyzed TXRF spectra of coffee samples for the elements K, Ca, Mn, Fe, Cu, Zn, Rb and Sr. The linear regression values R^2 range between 0.89 and 0.99.

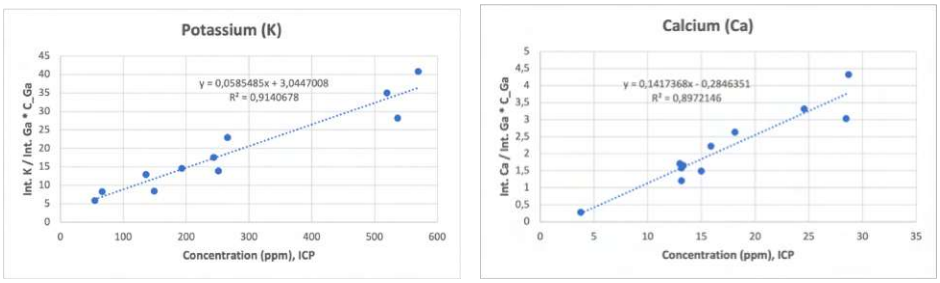

(a) (b)

Figure 65: (a) Empirical calibration curve for potassium (K) using 11 coffee samples as empirical standards. (b) Empirical calibration curve for calcium (Ca) using 11 coffee samples as empirical standards.

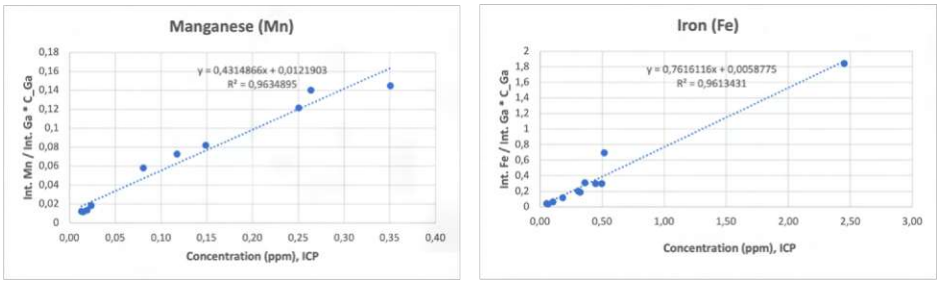

(a) (b)

Figure 66: (a) Empirical calibration curve for manganese (Mn) using 10 coffee samples as empirical standards. (b) Empirical calibration curve for iron (Fe) using 11 coffee samples as empirical standards.

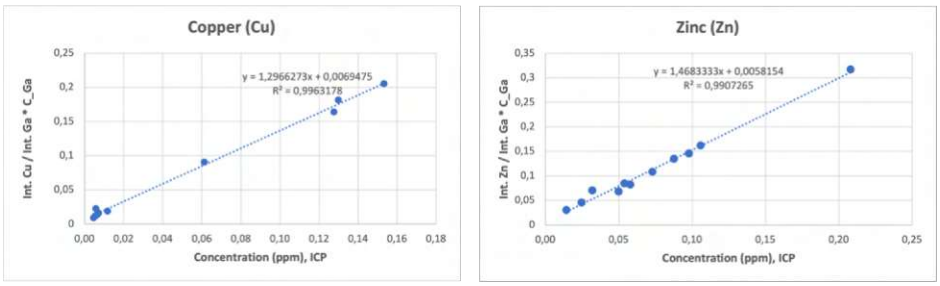

(a) (b)

Figure 67: (a) Empirical calibration curve for copper (Cu) using 11 coffee samples as empirical standards. (b) Empirical calibration curve for zinc (Zn) using 11 coffee samples as empirical standards.

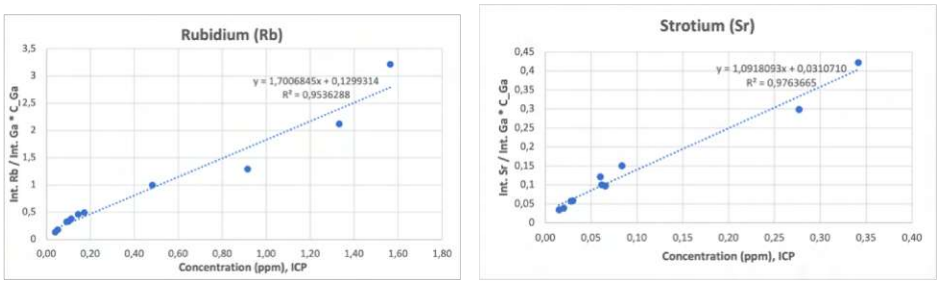

(a) (b)

Figure 68: (a) Empirical calibration curve for rubidium (Rb) using 11 coffee samples as empirical standards. (b) Empirical calibration curve for strontium (Sr) using 10 coffee samples as empirical standards.

5.3.3 ICP-OES vs. TXRF quantification approaches

The results of the ATI-QUANT FP approach are compared with the results of the empirical approach using calibration curves in the same way as for the EDXRF concentrations in section 5.2.5. Both data sets are again plotted against the reference ICP-OES values. These plots are analyzed using the linear regression method. The ideal linear regression curve should have an R^2 value of 1, a slope of 1, and an intercept of 0. Again, neither approach meets these conditions. However, the empirical TXRF concentration values have a higher overall trueness (= accuracy + precision). The trace elements Mn, Fe, Cu and Zn are again problematic, as they are strongly overestimated by the FP approach, but show relatively good agreement with the empirical TXRF approach. The following plots show the results in detail, the blue curves mark the results of the ATI-QUANT measurements, the orange curves mark the concentrations of the empirical calibration approach.

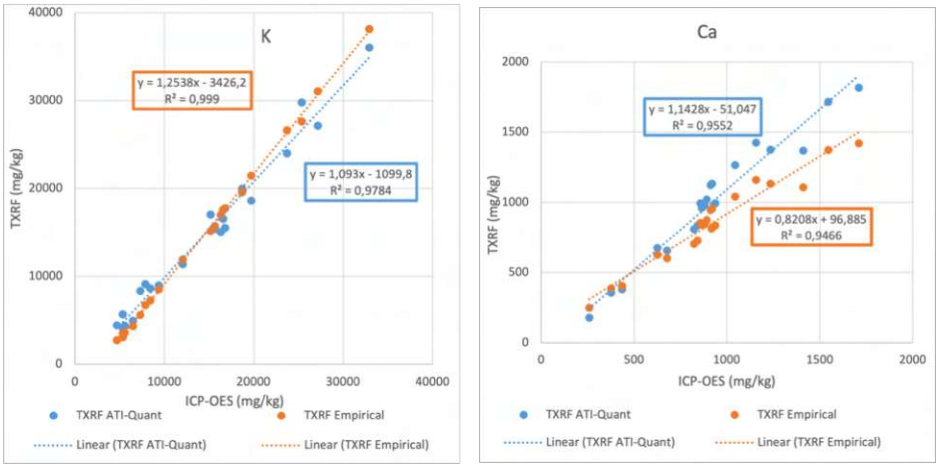

(a) (b)

Figure 69: Comparison between the TXRF results obtained by the FP approach (ATI-QUANT, blue) and the empirical calibration curves (orange) for the elements K (a) and Ca (b).

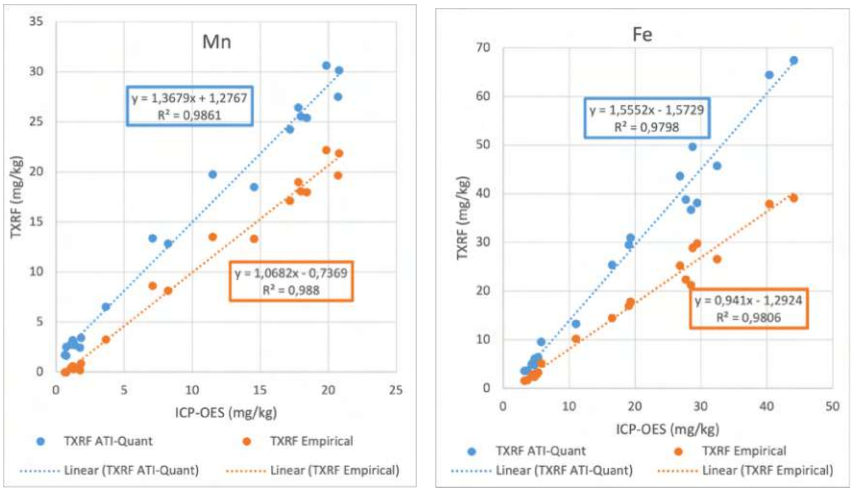

(a) (b)

Figure 70: Comparison between the TXRF results obtained by the FP approach (ATI-QUANT, blue) and the empirical calibration curves (orange) for the elements Mn (a) and Fe (b).

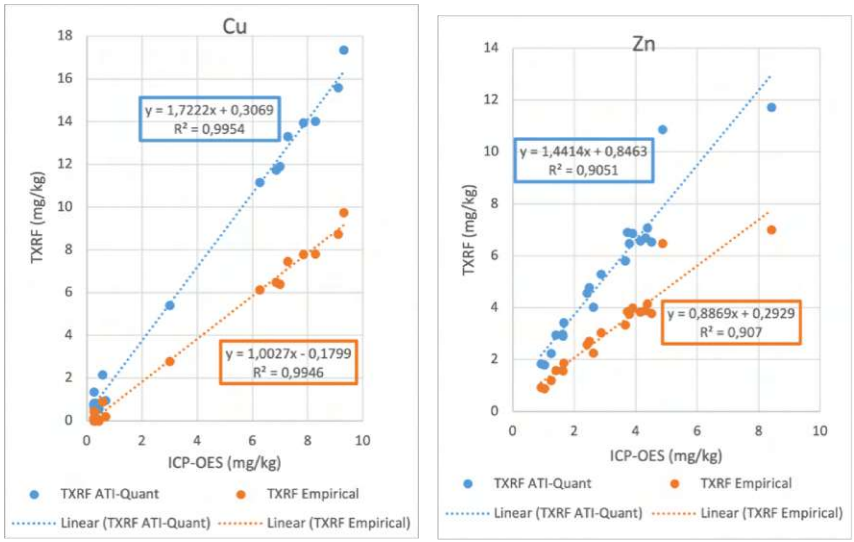

(a) (b)

Figure 71: Comparison between the TXRF results obtained by the FP approach (ATI-QUANT, blue) and the empirical calibration curves (orange) for the elements Cu (a) and Zn (b).

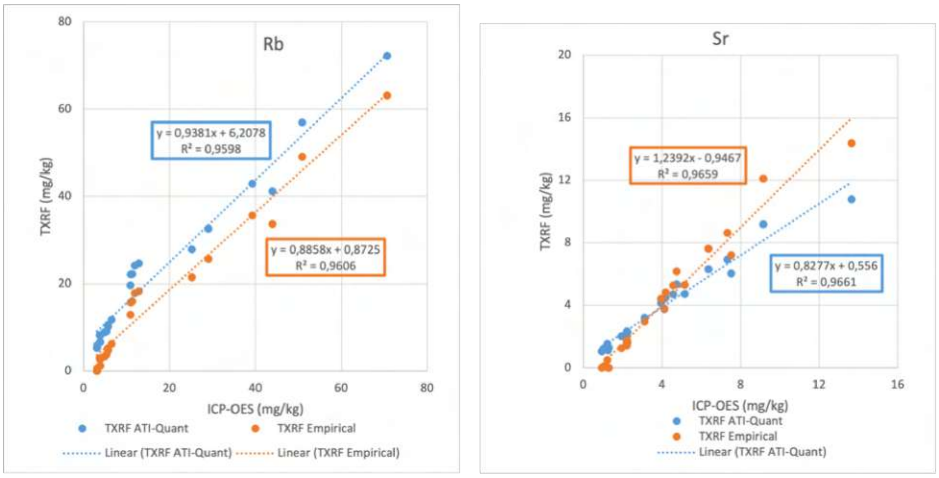

(a) (b)

Figure 72: Comparison between the TXRF results obtained by the FP approach (ATI-QUANT, blue) and the empirical calibration curves (orange) for the elements Rb (a) and Sr (b).

5.3.4 Chemometric results TXRF

PCA

As stated in section 5.2.6, PCA works best when using mean values of concentrations (see Table 31). The results are shown in Figure 73 and in the loadings matrix (Table 11). 21 samples were used for this analysis. In this case, almost 92 % of the variability is contained in the first 3 PCs. The first PC is defined by all element concentrations except Ca. The second PC is again dependent on all elements except Mn, and again not on Ca, which almost exclusively defines the third PC. The score plot shows a good clustering of the three coffee categories, but the instant coffee category is not as separated from the pure coffee category as in section 5.2.6.

Variable	PC 1	PC 2	PC 3
K	0,872	-0,461	-0,083
Ca	0,144	-0,073	0,957
Mn	0,928	0,147	-0,113
Fe	0,81	0,493	-0,081
Cu	0,715	0,606	-0,164
Zn	0,47	0,654	0,341
Rb	0,807	-0,573	0,018
Sr	0,872	-0,462	0,056

Table 11: Loading's matrix for the first three PCs.

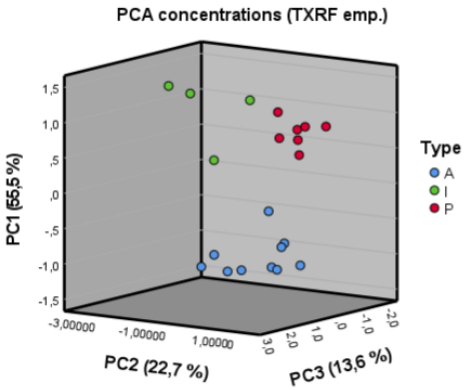

Figure 73: Score plot of a PCA using TXRF concentration data. The blue dots represent coffees with additives, the red dots represent pure coffees, and the green dots represent pure instant coffees.

PLS-DA

Unfortunately, at the time of writing, it was not possible to complete the chemometric analysis of the raw TXRF spectra. This analysis will be included in another planned publication. However, it is interesting to show the PLS-DA training/fit using elemental concentrations (Figure 74) instead of the raw spectra analysis in section 5.2.6. The clustering is accurate, but as for the PCA score plot in Figure 73, the difference between instant and pure coffee is small.

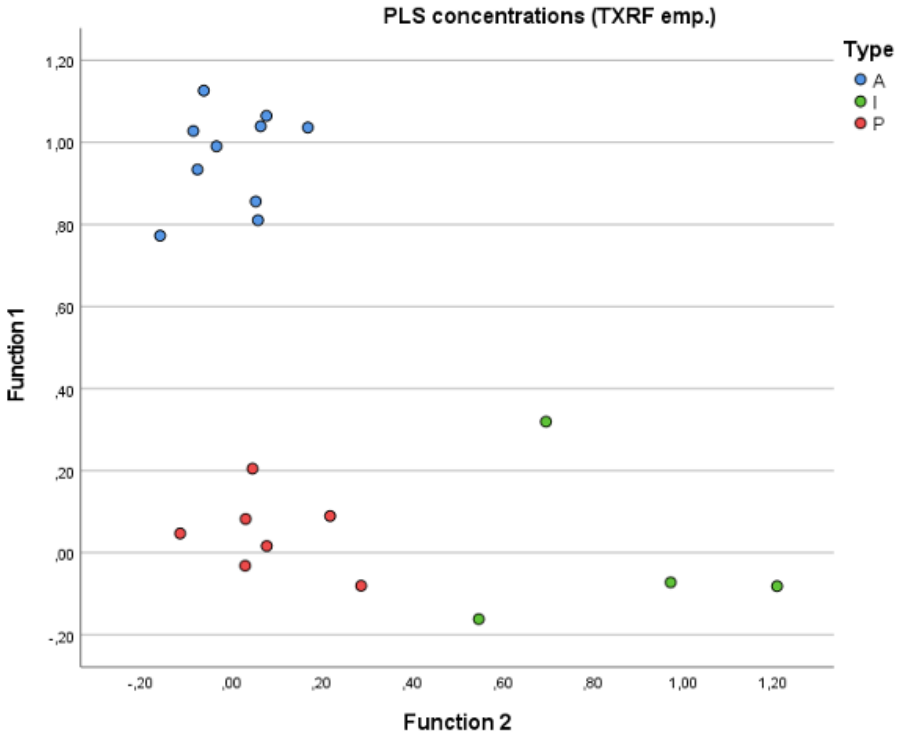

Figure 74: Training/fit of PLS-DA with 3 latent variables using the elemental concentrations of 21 samples from TXRF analysis. The blue dots represent coffees with additives, the red dots represent pure coffees, and the green dots represent pure instant coffees.

5.4 Comparison of all quantification approaches

The Figures 75 - 82 compare all 21 coffee samples quantified by ICP-OES, FP approach for TXRF (ATI-QUANT), empirical calibration method for TXRF, semi-empirical FP approach for EDXRF and empirical calibration method for EDXRF. For Cu, the semi-empirical FP approach for EDXRF results are not shown because they are much too high and interfere with the analysis. It is important to note that the FP approaches are the only ones that are completely independent of the ICP-OES results.

All the techniques used give results with deviations up to ±30% from the reference values, except for the EDXRF FP approach whose deviations can be much worse. In general, the variations are probably due to the samples themselves. The grain size of the pellets may be too large, and the TXRF samples are suspensions rather than perfectly clear digests. The ICP-OES experiments have the advantage of using several ml of sample. For TXRF the sample mass is in the low μl range. In general, the more sample mass used, the more representative the result. However, TXRF results could be improved by increasing the vortexing time to 2 minutes and then pipetting the samples immediately onto the reflectors. We also increased the volume pipetted from 10 μl to 3 x 10 = 30 μl.

Coffees with additives generally show lower concentrations of all elements because they are more diluted. Cappuccino samples show higher Ca concentrations, probably due to the added milk. Cappuccino Hazelnut shows higher concentrations of all elements except Rb compared to the other coffees with additives. Instant coffees show higher concentrations of K, Ca, Rb, Sr.

For unknown reasons, the metals Mn, Fe, Cu and Zn show much too high concentrations when analyzed with ATI-QUANT. Deconvolution and fitting have been checked several times and are fine. The ATI-QUANT results deviate not only from the ICP-OES values but also from the TXRF empirical calibration method. These latter deviations must be due to the evaluation itself, since both use the same spectra as a basis. Perhaps the empirical calibration method takes into account different sample properties that the FP approach cannot. This should result in lower elemental concentrations due to self-absorption, as seen for example in the deviations of K and Ca of the carrot standard (Figure 61). However, what we see for Mn, Fe, Cu and Zn is the exact opposite, namely much too high estimates when quantified with FP approaches.

The three categories pure coffee, pure instant coffee and coffee with additives show large differences in the concentrations of K, Ca, Rb and Sr. This allows a possible grouping for e.g. K (from highest to lowest range):

- **Pure instant coffee:** 25000 - 35000 ppm
- **Pure coffee:** 15000 - 20000 ppm
- **Coffee with additives:** 5000 - 12000 ppm

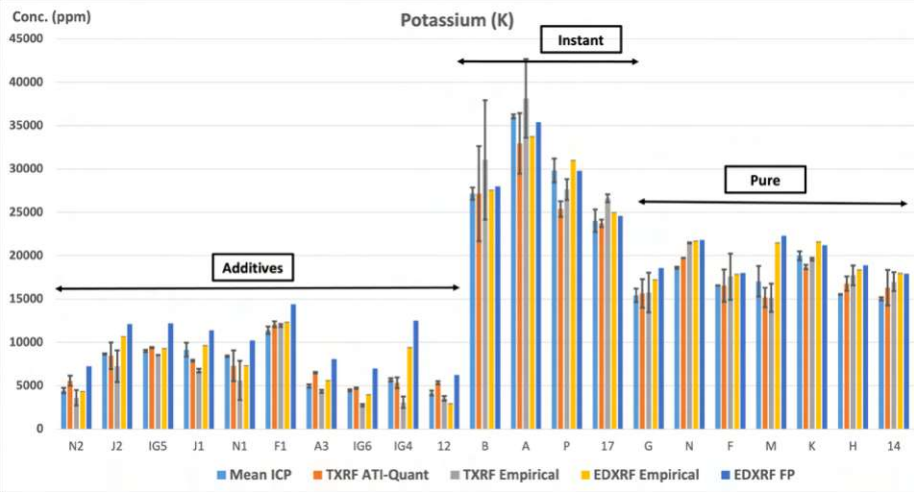

Figure 75: Comparison of the concentrations obtained with their standard deviation for K.

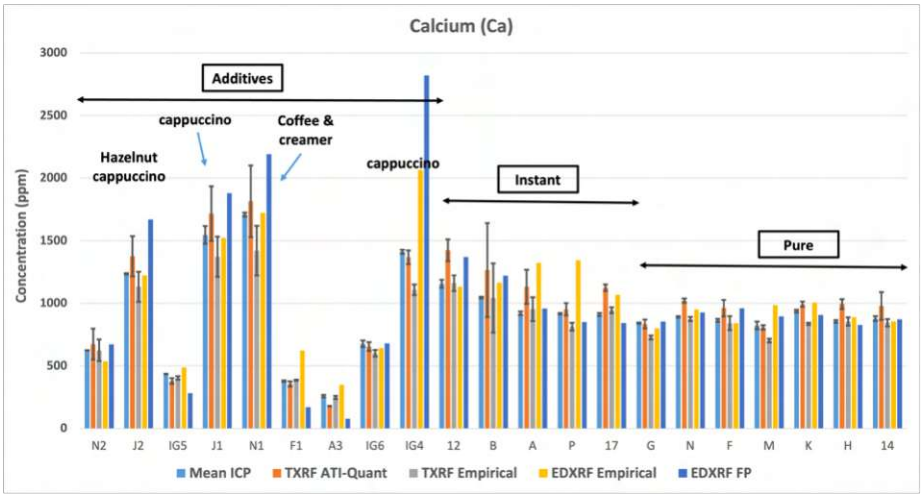

Figure 76: Comparison of the concentrations obtained with their standard deviation for Ca.

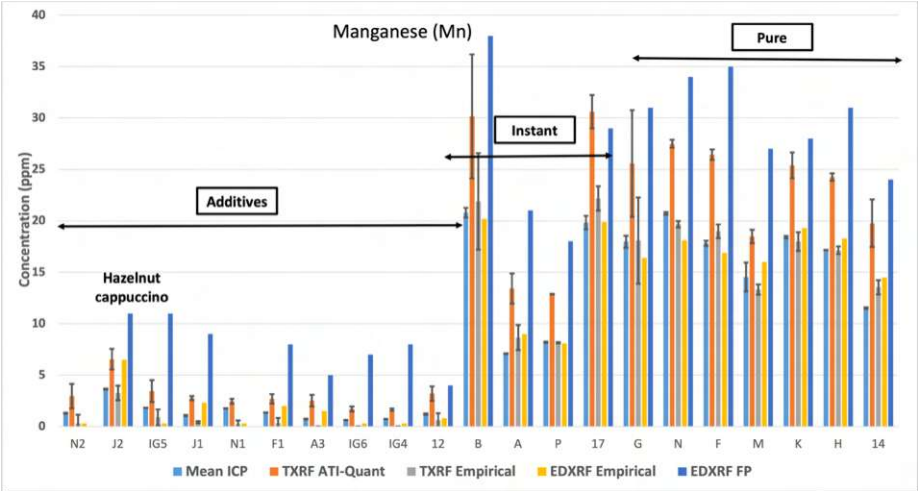

Figure 77: Comparison of the concentrations obtained with their standard deviation for Mn.

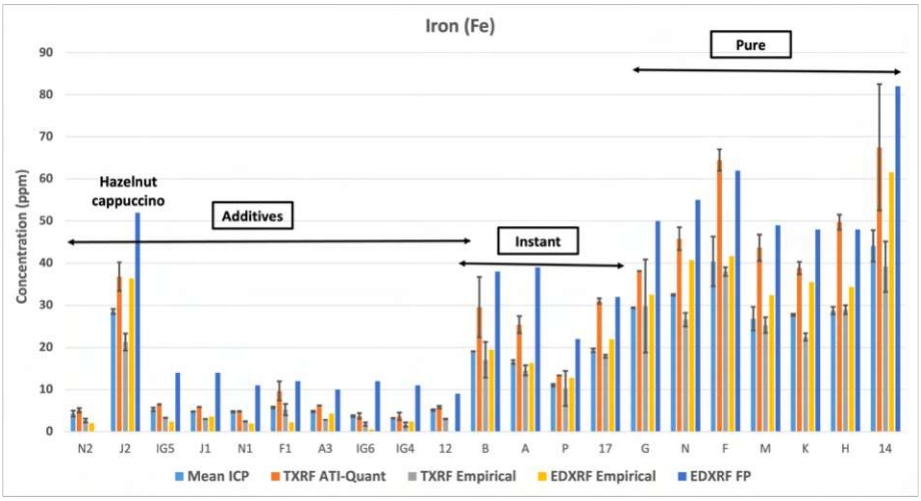

Figure 78: Comparison of the concentrations obtained with their standard deviation for Fe.

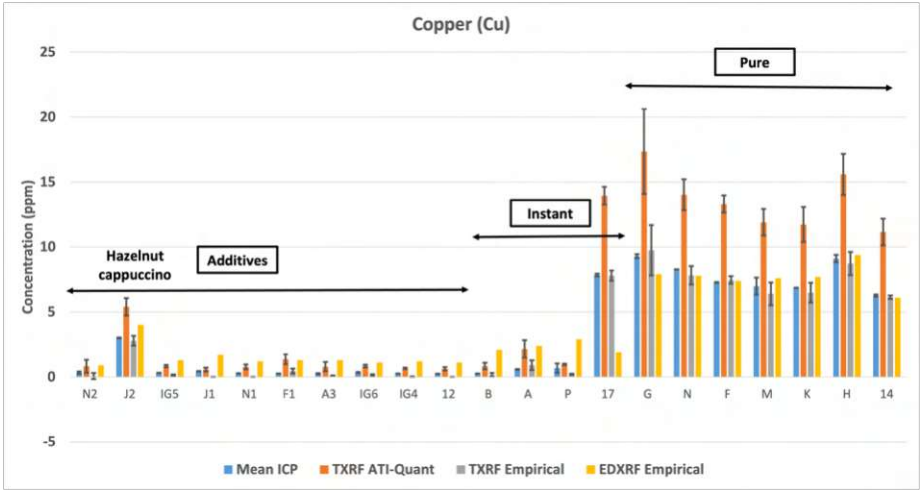

Figure 79: Comparison of the obtained concentrations with the standard deviations for Cu. The semi-empirical EDXRF FP approach is not shown because the values are too high and therefore interfere with the analysis of the other approaches.

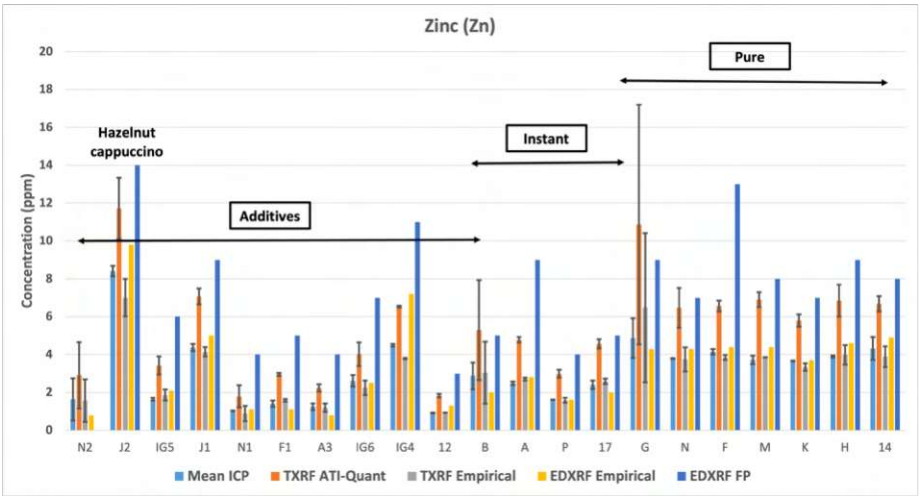

Figure 80: Comparison of the concentrations obtained with their standard deviation for Zn.

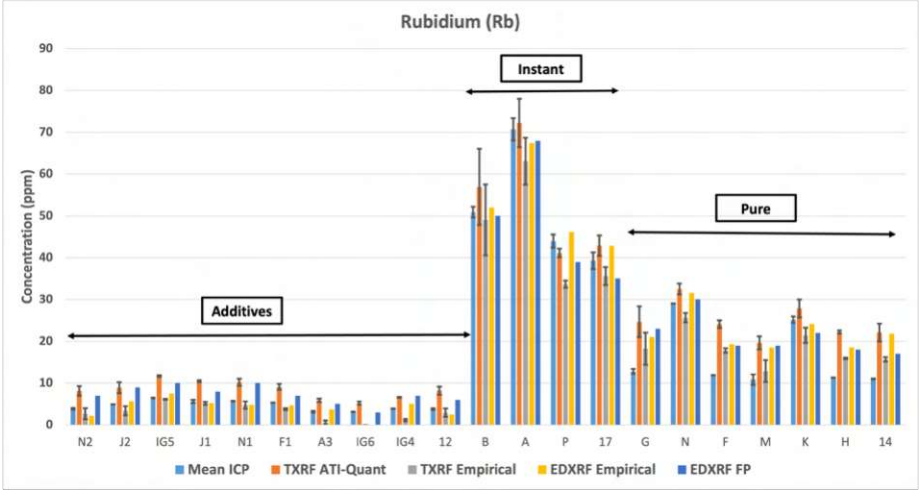

Figure 81: Comparison of the concentrations obtained with their standard deviation for Rb.

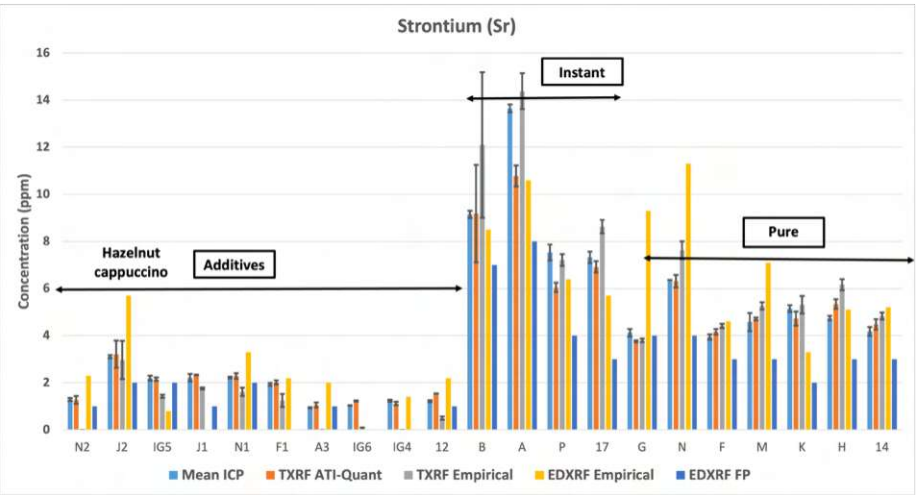

Figure 82: Comparison of the concentrations obtained with their standard deviation for Sr.

6 Final conclusion

In this diploma thesis, an EDXRF and a TXRF method were developed for the multi-element (K, Ca, Mn, Fe, Cu, Zn, Sr and Rb) analysis of coffee samples of different categories (pure coffee, pure instant coffee and coffee with additives such as milk, proteins, etc.).

In addition to elemental quantification and chemometic analysis, the sample preparation procedure was also studied in detail, as there was nor is a general consensus in the scientific literature. Evaluation of sample preparation for EDXRF showed best results with pellets of 2 g coffee grain powder with 0.2 g wax added (10% of sample mass). The TXRF approach used the digest previously prepared for ICP-OES analysis with the addition of 4 ppm Ga as an internal standard. The ICP-OES measurements were necessary because no CRMs are available for coffee and reference values were needed.

For both the TXRF and EDXRF methods, elemental quantification worked best using empirical calibration curves for the respective spectrometers. These curves used a set of coffee samples as empirical standards that had been previously analyzed by ICP-OES but were not otherwise included in the study. Comparison with the ICP-OES data showed acceptable agreement. The FP quantification approaches studied were promising, but particularly problematic for the trace elements Mn, Fe, Cu and Zn.

The chemometric approaches used to classify the coffee categories were PCA and PLS-DA. PCA showed a good clustering of the coffee categories when the elemental concentrations were used as variables, but not when the raw spectra were used as input. PLS-DA, on the other hand, worked well with the raw EDXRF spectra. The big advantage of this is that there is no need to quantify the spectra before analysis, which saves time. The author hopes that the results presented in this work can be used as a basis for further EDXRF and TXRF analyses not only of coffee but also of other organic materials in the future. The chemometric approaches may also provide the potential for origin analysis of coffees.

7 Acknowledgments

I would like to thank the Radiation Physics Group at the Institute of Atomic and Subatomic Physics of Christina Streli for the great working atmosphere and the always available advice. Many thanks to Dieter Ingerle and Peter Kregsamer for explaining the background of various XRF related topics.
I would especially like to thank Peter Wobrauschek for supervising this thesis, for his kindness, and for all that I have learned from him. His true passion for all aspects of X-ray physics is truly remarkable. From the bottom of my heart, I would like to thank my second supervisor, Eva Marguí from the University of Girona, for welcoming me so openly into her group at the Department of Chemistry and for creating such a great, international place to work. I would also like to thank Emili Besalu for his explanations and help with the chemometric analysis.

References

[1] International Coffee Organization. *The coffee development report 2021: The future of coffee – Investing in youth for a resilient and sustainable coffee sector*. 2021. URL: https://www.ico.org/documents/cy2022-23/coffee-development-report-2021.pdf%20(Access:%2015/02/23).

[2] P. Pohl et al. *Determination of the Elemental Composition of Coffee using Instrumental Methods*. Food Analytical Methods, 6, 598-613, 2013. DOI: 10.1007/s12161-012-9467-6.

[3] E.Marguí and R. Van Grieken. *X-Ray Fluorescence Spectrometry and Related Techniques: An Introduction*. Momentum Press, ISBN: 160650391X, 9781606503911, 2013.

[4] M. Oliveira et al. *Intra- and interspecific mineral composition variability of commercial instant coffees and coffee substitutes: Contribution to mineral intake*. Food Chemistry 130, 702, 2012. DOI: https://doi.org/10.1016/j.foodchem.2011.07.113.

[5] E. Olechno et al. *Coffee Infusions: Can They Be a Source of Microelements with Antioxidant Properties?* Antioxidants, 10, 1709, 2021. DOI: https://doi.org/10.3390/antiox10111709.

[6] E. Marguí et al. *Analytical potential of total reflection X-ray fluorescence (TXRF) instrumentation for simple determination of major and trace elements in milk powder samples*. Food Chemistry Volume 383, 132590, 2022. DOI: https://doi.org/10.1016/j.foodchem.2022.132590.

[7] R. Dalipi et al. *Analytical performance of benchtop total reflection X-ray fluorescence instrumentation for multielemental analysis of wine samples*. Spectrochimica Acta Part B: Atomic Spectroscopy Volume 120, Pages 37-43, 2016. DOI: https://doi.org/10.1016/j.sab.2016.04.001.

[8] E. Marguí et al. *Energy dispersive X-ray fluorescence spectrometry for the direct multi-element analysis of dried blood spots*. Spectrochimica Acta Part B: Atomic Spectroscopy Volume 139, 2018. DOI: https://doi.org/10.1016/j.sab.2017.11.003.

[9] E. Marguí et al. *Critical evaluation of the use of total reflection X-ray fluorescence spectrometry for the analysis of whole blood samples: application to patients with thyroid gland diseases*. Analytical and Bioanalytical

Chemistry volume 411, pages 1659–167, 2019. DOI: https://doi.org/10.1007/s00216-019-01618-3.

[10] J.L. Aleixandre-Tudo et al. *Chemometrics in food science and technology: A bibliometric study.* Chemometrics and Intelligent Laboratory Systems 222, 104514, 2022. DOI: https://doi.org/10.1016/j.chemolab.2022.104514.

[11] I. Allegretta et al. *TXRF spectral information enhanced by multivariate analysis: A new strategy for food fingerprint.* Food Chemistry 401, 134124, 2023. DOI: https://doi.org/10.1016/j.foodchem.2022.134124.

[12] M. Worku et al. *Differentiating the geographical origin of Ethiopian coffee using XRF- and ICP-based multi-element and stable isotope profiling.* Food Chemistry, 290, 295-307, 2019. DOI: https://doi.org/10.1016/j.foodchem.2019.03.135.

[13] Y. Fiamengos et al. *Are the elemental fingerprints of organic and conventional food different?* ED-XRF as screening technique, Journal of Food Composition and Analysis, 99, 103854, 2021. DOI: https://doi.org/10.1016/j.jfca.2021.103854.

[14] H.M. Feleke et al. *Energy Dispersive X-Ray Fluorescence Elemental Analysis of Roasted and Non- Roasted Ethiopian Coffee Specialty.* Journal of Environmental Science, Toxicology and Food Technology, 12, 51-70, 2018. URL: https://www.researchgate.net/publication/334724346_Energy_Dispersive_X-Ray_Fluorescence_Elemental_Analysis_of_Roasted_and_Non-Roasted_Ethiopian_Coffee_Specialty.

[15] J.S. Almeida et al. *Direct multielement determination of Cd, Pb, Fe, and Mn in ground coffee samples using energy dispersive X-ray fluorescence spectrometry.* X-Ray Spectrometry, 50, 2–8., 2021. DOI: https://doi.org/10.1002/xrs.3182.

[16] I. Orlić, J. Makjanić, and V. Valković. *Optimization of XRFS for the analysis of toxic elements and heavy metals in coffee products.* Journal of Radioanalytical and Nuclear Chemistry, Articles, Vol. 102, No. 1 (1986) 203-211), 1986. URL: https://link.springer.com/article/10.1007/BF02037961.

[17] S. J. Haswell and A. D. Walmsley. *Multivariate data visualization methods based on multi-elemental analysis of wines and coffees using total reflection X-ray fluorescence analysis*. Journal of Analytical Atomic Spectrometry 13, 131-134, 1998. URL: https://pubs.rsc.org/en/content/articlelanding/1998/ja/a705317g.

[18] M. Denni and D. Joseph. *Elemental Analysis of Indian Coffee Powder Samples using Hand Held X-Ray Fluorescence Spectrometer*. Madridge Journal of Analytical Sciences and Instrumentation, 4, 109-112, 2019. DOI: https://doi.org/10.18689/mjai-1000120.

[19] A.S. Machado et al. *Analysis of the quality of industrialized coffee powder using the techniques of computed microtomorgraphy and X-ray fluorescence*. X-ray spectrometry, 1-9, 2023. DOI: https://doi.org/10.1002/xrs.3326.

[20] M.A. Guazelli et al. *Direct multielement determination of Cd, Pb, Fe, and Mn in ground coffee samples using energy dispersive X-ray fluorescence spectrometry*. Journal of physics: Conference series 2340, 012004, 2022. DOI: https://doi.org/10.1088/1742-6596/2340/1/012004.

[21] M. Weinberger et al. *Critical evaluation of energy dispersive X-ray fluorescence spectrometry for multielemental analysis of coffee samples: sample preparation, quantification and chemometric approaches*. Submitted to the Journal of Food Chemistry in July 2023, Manuscript No: FOODCHEM-D-23-06473; not yet published at the time of writing this thesis., 2023.

[22] R. Klockenkaemper and A. von Bohlen (Eds.) *Total-Reflection X-Ray Fluorescence Analysis and Related Methods, 2nd edition*. John Wiley and Sons, Inc., Hoboken, New Jersey, 2014. DOI: doi:10.1002/9781118985953. URL: http://doi.wiley.com/10.1002/9781118985953.

[23] W. Demtroeder. *Experimentalphysik 3, 4. Auflage, pp. 253-258*. Springer Spektrum Verlag, 2010.

[24] P. Brouwer. *Theory of XRF: Getting acquainted with the principles*. PANalytical B.V., 3rd edition, ISBN: 90-9016758-7, 2010. URL: www.panalytical.com.

[25] S. Price et al. *Pair production*. Reference article, Radiopaedia.org (Accessed on 04 Sep 2023). DOI: https://doi.org/10.53347/rID-31661.

[26] E. Marguí et al. *High-energy polarized-beam EDXRF for trace metal analysis of vegetation samples in environmental studies*. Vol. 35. X-Ray Spectrometry, 2006, pp. 169–177. DOI: 10.1002/xrs.890.

[27] J. Machado et al. *Accuracy improvement in XRF analysis for the quantification of elements ranging from tenths to thousands ug.g-1 in human tissues using different matrix reference materials*. Journal of Analytical Atomic Spectrometry, 2020. DOI: 10.1039/d0ja00307g.

[28] G.R. Blumenthal and R.J. Gould. *Bremsstrahlung, synchrotron radiation, and compton scattering of high-energy electrons traversing dilute gases*. Reviews of modern Physics, Volume 42, No. 2, pp. 238-240., 1970. URL: https://www.fisgeo.unipg.it/~fiandrin/didattica_fisica/cosmic_rays1819/bibliography/blumenthal-gould.pdf.

[29] W. Demtroeder. *Experimentalphysik 3, 4. Auflage, pp. 86-88*. Springer Spektrum Verlag, 2010.

[30] C. Streli, D. Ingerle, and P. Wobrauschek. *Folienskriptum zur Vorlesung X-Ray Analytical Methods, 10. GIXRF+XRR = GIXA*. Technische Universität Wien, 2021.

[31] P. Kregsamer. *X-ray analytical methods, Skriptum zur Übung*. Technische Universität Wien, 2015.

[32] D. Krstajić. *Application of Total reflection X-ray fluorescence analysis of light elements down to Carbon*. reposiTUm, 2022. DOI: 10.34726/hss.2022.100800. URL: http://hdl.handle.net/20.500.12708/20162.

[33] L. Rachbauer. *Towards Quantification of Carbon in Nanoplastic Samples using TXRF: Optimization and Characterization of a Low-Z Spectrometer*. reposiTUm, 2020. DOI: 10.34726/hss.2020.84602. URL: https://repositum.tuwien.at/handle/20.500.12708/16047.

[34] C. Streli, D. Ingerle, and P. Wobrauschek. *Folienskriptum zur Vorlesung X-Ray Analytical Methods, 7. Quantitative X-ray Fluorescence Analysis Part 2*. Technische Universität Wien, 2021.

[35] D. Eichert. *The Fundamentals of Total Reflection X-ray Fluorescence*. Spectroscopy, Spectroscopy-08-01-2020, Volume 35, Issue 8, 2020. URL: https://www.spectroscopyonline.com/view/the-fundamentals-of-total-reflection-x-ray-fluorescence.

[36] K. Olbrich et al. *The first total reflection X-ray fluorescence round-robin test of rat tissue samples: Preliminary results*. Vol. 205. Spectrochimica Acta Part B: Atomic Spectroscopy, 2023, p. 106695. DOI: https://doi.org/10.1016/j.sab.2023.106695. URL: https://www.sciencedirect.com/science/article/pii/S0584854723000824.

[37] E. Marguí et al. *Potential of total-reflection X-ray spectrometry for multi-element analysis of biological samples using dilution or suspension sample preparation techniques*. X-Ray Spectrometry 51 (2022), pp. 230, 2022. DOI: https://doi.org/10.1002/xrs.3230.

[38] D. Ingerle. *Grazing incidence X-ray fluorescence combined with X-ray reflectivity: development of an evaluation software*. reposiTUm, 2017. DOI: 10.34726/hss.2017.35981. URL: https://repositum.tuwien.at/handle/20.500.12708/10375.

[39] D. Ingerle et al. *JGIXA — A software package for the calculation and fitting of grazing incidence X-ray fluorescence and X-ray reflectivity data for the characterization of nanometer- layers and ultra-shallow-implants*. Spectrochim. Acta Part B At. Spectrosc. 118, 20–28, 2016. DOI: doi:10.1016/j.sab.2016.02.010.

[40] *X-ray reflectometry (XRR), thickness, density and roughness for multilayers on wavers*. Rigaku. URL: https://www.rigaku.com/techniques/x-ray-reflectometry-xrr.

[41] *X-ray Reflectometry (XRR)*. Covalent Metrology. URL: https://covalent%5C%5Cmetrology.com/techniques/x-ray-reflectometry-xrr/,%2018.06.2022.

[42] L. Brunnbauer. *Liquid Inductively Coupled Plasma-Mass Spectrometry (ICP-MS)/Inductively Coupled Plasma-Optical Emission Spectroscopy (ICP-OES)*. Accessed on 05 Sep 2023. DOI: https://www.tuwien.at/en/tch/lalibs/techniques/icp-ms-icp-oes.

[43] C.B. Boss and K.J. Fredeen. *Concepts, instrumentation and techniques in inductively coupled plasma optical emission spectrometry*. Perkin Elmer Corp, 1997. URL: https://resources.perkinelmer.com/lab-solutions/resources/docs/gde_concepts-of-icp-oes-booklet.pdf.

[44] S.R. Khan, B. Sharma, and P. A. Chawla et al. *Inductively Coupled Plasma Optical Emission Spectrometry (ICP-OES): a Powerful Analytical Technique for Elemental Analysis*. Food Anal. Methods 15, 666–688, 2022. DOI: https://doi.org/10.1007/s12161-021-02148-4.

[45] S. Ghosh et al. *Inductively coupled plasma - Optical emission spectroscopy: A review*. Vol. 3. Asian J. Pharm. Ana., 2013, pp. 24–33. URL: https://www.researchgate.net/publication/288811956_Inductively_coupled_plasma_-_Optical_emission_spectroscopy_A_review.

[46] R. Thomas. *A beginner's guide to ICP-MS, Part VI — The Mass Analyzer*. Vol. 16. Spectroscopy, 2001. URL: http://scientificsolutions1.com/Beginners%20guide%20to%20ICP-MS.pdf.

[47] G. Thippa Reddy et al. *Analysis of Dimensionality Reduction Techniques on Big Data*. Vol. 8. IEEE Access, 2020, pp. 54776–54788. DOI: 10.1109/ACCESS.2020.2980942.

[48] G. L. Scheel et al. *Environmental stress evaluation of Coffea arabica L. leaves from spectrophotometric fingerprints by PCA and OSC–PLS–DA*. Vol. 12. 8. Arabian Journal of Chemistry, 2019, pp. 4251–4257. DOI: https://doi.org/10.1016/j.arabjc.2016.05.014. URL: https://www.sciencedirect.com/science/article/pii/S1878535216300685.

[49] D. Ruiz-Perez, H. Guan, and P. Madhivanan et al. *So you think you can PLS-DA?* BMC Bioinformatics 21 (Suppl 1), 2, 2020. DOI: https://doi.org/10.1186/s12859-019-3310-7.

[50] E. Besalú. *From Periodic Properties to a Periodic Table Arrangement*. Vol. 90. 8. Journal of Chemical Education, 2013, pp. 1009–1013. DOI: https://doi.org/10.1021/ed3004534.

[51] D. Ballabio and V. Consonni. *Classification tools in chemistry. Part 1: linear models. PLS-DA*. Vol. 5. The Royal Society of Chemistry, 2013, pp. 3790–3798. DOI: 10.1039/C3AY40582F. URL: http://dx.doi.org/10.1039/C3AY40582F.

[52] B. M. Salih Hasan and A. Mohsin Abdulazeez. *A Review of Principal Component Analysis Algorithm for Dimensionality Reduction*. Journal of soft comptuing and data mining, Vol. 2 No. 1, pp. 20-30, 2021. DOI: https://doi.org/10.30880/jscdm.2021.02.01.003.

[53] *Atomic radii of the elements, Wikipedia*. Accessed on 06 Sep 2023. URL: https://en.wikipedia.org/wiki/Atomic_radii_of_the_elements_(data_page)#:~:text=The%20atomic%20radius%20of%20a,equivalent%20definitions%20of%20atomic%20radius..

[54] J.C. Slater. *Atomic Radii in Crystals*. The Journal of Chemical Physics. 41 (10): 3199–3204. Bibcode:1964JChPh..41.3199S., 1964. DOI: doi:10.1063/1.1725697.

[55] S.G Bratsch and J.J. Lagowski. *Predicted stabilities of monatomic anions in water and liquid ammonia at 298.15 K*. Polyhedron. 5 (11): 1763–1770, 1986. DOI: doi:10.1016/S0277-5387(00)84854-8.

[56] P. W. Atkins and L. L. Jones. *Chemical Principles. The Quest for Insight, 5th ed.* W. H. Freeman and Company, New York, 2010. URL: https://archive.org/details/AtkinsChemicalPrinciples5thEdition/page/n3/mode/2up.

[57] A. Müller. *Eigenwerte und Eigenvektoren*. Berlin, Heidelberg: Springer Berlin Heidelberg, 2023, pp. 549–595. ISBN: 978-3-662-67866-4. DOI: 10.1007/978-3-662-67866-4_11. URL: https://doi.org/10.1007/978-3-662-67866-4_11.

[58] W. Auzinger et al. *Lineare Algebra für Technische Physik, Skriputum zur Vorlesung*. Technische Universität Wien, 2008, pp. 115–123.

[59] 1998 Colby College Chemistry. *Diagonalize a Symmetric Matrix*. Accessed on 06 Sep 2023. URL: https://www.colby.edu/chemistry/PChem/eigen.html.

[60] Royal Society of Chemistry. *Periodic table*. Accessed on 06 Sep 2023. URL: https://www.rsc.org/periodic-table.

[61] L. C. Lee, C. Y. Liong, and A. A. Jemain. *Partial least squares-discriminant analysis (PLS-DA) for classification of high-dimensional (HD) data: a review of contemporary practice strategies and knowledge gaps*. Vol. 143. The Royal Society of Chemistry, 2018, pp. 3526–3539. DOI: 10.1039/C8AN00599K. URL: http://dx.doi.org/10.1039/C8AN00599K.

[62] A. M. Molinaro, R. Simon, and R. M. Pfeiffer. *Prediction error estimation: a comparison of resampling methods*. Bioinformatics, Volume 21, Issue 15, Pages 3301–3307, 2005. DOI: https://doi.org/10.1093/bioinformatics/bti499.

[63] P. Geladi and B. R. Kowalski. *Partial least-square regression: a tutorial*. Analytica Chimica Acta, 186, 1-17, Elsevier Science Publishers B.V., 1986. URL: http://home.mit.bme.hu/~horvath/IDA/1-s2.0-0003267086800289-main.pdf.

[64] M. K. Moore. *Chapter 4 - Sex Estimation and Assessment*. Academic Press, 2013, pp. 91–116. ISBN: 978-0-12-385189-5. DOI: https://doi.org/10.1016/B978-0-12-385189-5.00004-2. URL: https://www.sciencedirect.com/science/article/pii/B9780123851895000042.

[65] Aglient Technologies. *Dual view ICP-OES minus the wait: Introducing the Agilent 5100 ICP-OES*. 2015. URL: https://www.agilent.com/Library/slidepresentation/Public/ASTS_2015_AtomicTour_5100_ICP-OES.pdf.

[66] Bruker AXS GmbH. *Product Sheet XRF 9, S2 RANGER with the New Generation XFlash® V5 Silicon Drift Detector*. URL: https://www.google.com/url?sa=t&rct=j&q=&esrc=s&source=web&cd=&ved=2ahUKEwjooLOi8omCAxVQ0AIHHbLPBSgQFnoECA8QAQ&url=https%3A%2F%2Fmy.bruker.com%2Facton%2Fct%2F2655%2Fp-008a%2FBct%2F-%2F-%2Fct16_1%2F1%2Fd%3Fsid%3DTV2%253AipYxvTPKi&usg=AOvVaw3epE9Kq%20M0UAHCpjnoUBJFp&opi=89978449.

[67] Bruker AXS GmbH. *S2 RANGER - Spectrometry Solutions*. URL: https://pdf.directindustry.com/pdf/bruker-axs-gmbh/s2-ranger-spectrometry-solutions/30028-686158.html.

[68] C. Streli et al. *A new total reflection X-ray fluorescence vacuum chamber with sample changer analysis using a silicon drift detector for chemical analysis*. Vol. 59. 8. 10th Symposium on Total Reflection X-Ray Fluorescence Analysis and 39th Discussion Meeting on Chemical Analysis. Spectrochimica Acta Part B: Atomic Spectroscopy, 2004, pp. 1199–1203. DOI: https://doi.org/10.1016/j.sab.2004.05.007. URL: https://www.sciencedirect.com/science/article/pii/S058485470400134X.

[69] C. Streli and P. Wobrauschek. *WOBISTRAX: A vacuum TXRF spectrometer with sample changer and two exchangeable excitation sources*. 2018. URL: http://www.ati.ac.at/fileadmin/files/research_areas/sarc/wobistrax_info.pdf.

[70] J. Prost. *Development and characterization of a new method for total-reflection X-ray fluorescence analysis of directly collected airborne particulate matter samples*. reposiTUm, 2018. DOI: https://doi.org/10.34726/hss.2018.37286.

[71] Amtek Inc. *X-123 Complete X-Ray Spectrometer with Si-PIN Detector*. URL: https://www.amptek.com/internal-products/x-123-complete-x-ray-spectrometer-with-si-pin-detector.

[72] R. Dalipi et al. *Multi-element analysis of vegetal foodstuff by means of low power total reflection X-ray fluorescence (TXRF) spectrometry*. Food Chemistry 218, 348-355, 2017. DOI: https://doi.org/10.1016/j.foodchem.2016.09.022.

[73] B. Grossmayer. *Softwarepaket zur quantitativen Röntgenfluoreszenzanalyse mittels Fundamentaler Parameter unter Verwendung von Röntgenoptiken*. Diplomathesis. Technische Universität Wien, 2009.

[74] P. Necker. *Quantitative X-ray fluorescence analysis of samples with various matrices using a universal data evaluation software*. Diplomathesis. Technische Universität Wien, 2017. URL: https://repositum.tuwien.at/handle/20.500.12708/5081.

[75] E. Holub. *Spectral correction for a rhodium-anode transmission X-ray tube. Quantitative X-ray fluorescence analysis and comparison with a side-window rhodium-anode tube*. Diplomathesis. Technische Universität Wien, 2020. URL: https://repositum.tuwien.at/handle/20.500.12708/1204.

[76] E. Marguí, I. Queralt, and R.Van Grieken. *Sample preparation in X-ray fluorescence Analysis*. Encyclopedia of Analytical Chemistry, John Willey Sons, Ltd., 2016. DOI: https://doi.org/10.1002/9780470027318.a6806m.pub3.

[77] D. V Čepo. et al. *Application of benchtop total-reflection X-ray fluorescence spectrometry and chemometrics in classification of origin and type of Croatian wines*. Food Chemistry: X 13, 100209, 2022. DOI: https://doi.org/10.1016/j.fochx.2022.100209.

[78] S. Panebianco et al. *Feasibility study of tomato fruit characterization by fast XRF analysis for quality assessment and food traceability*. Vol. 383. Food Chemistry, 2022. URL: https://www.sciencedirect.com/science/article/pii/S0308814622003260.

List of Figures

List of Tables

A Appendix: EDXRF

Potassium (K)							
Sample type	**Sample code**	**Mean ICP**	**SD ICP**	**EDXRF FP**	**Deviation (%) EDXRF FP / ICP**	**EDXRF emp.**	**Deviation (%) EDXRF emp./ ICP**
A	**N2**	4427	314	7260	-64	4347	2
A	**J2**	8663	89	12100	-40	10670	-23
A	**IG5**	9013	127	12200	-35	9285	-3
A	**J1**	9153	813	11400	-25	9648	-5
A	**N1**	8384	73	10200	-22	7329	13
A	**F1**	11404	423	14400	-26	12312	-8
A	**A3**	4973	199	8080	-62	5607	-13
A	**IG6**	4458	112	7000	-57	3978	11
A	**IG4**	5695	177	12500	-119	9409	-65
A	**12**	4151	271	6230	-50	2923	30
I	**B**	27154	701	28000	-3	27548	-1
I	**A**	36071	232	35400	2	33742	6
I	**P**	29831	1370	29800	0	30989	-4
I	**17**	24023	1294	24600	-2	24986	-4
P	**G**	15431	773	18600	-21	17224	-12
P	**N**	18613	120	21800	-17	21675	-16
P	**F**	16577	13	18000	-9	17831	-8
P	**M**	17050	1762	22300	-31	21483	-26
P	**K**	19986	521	21200	-6	21588	-8
P	**H**	15535	39	18900	-22	18392	-18
P	**14**	15039	167	17900	-19	17948	-19

Table 12: Concentrations obtained by ICP-OES, semi-empirical FP EDXRF and empirical EDXRF in ppm for K. Deviation is defined as (Mean ICP value - EDXRF value)/Mean ICP value * 100.

Calcium (Ca)							
Sample type	**Sample code**	**Mean ICP**	**SD ICP**	**EDXRF FP**	**Deviation (%) EDXRF FP / ICP**	**EDXRF emp.**	**Deviation (%) EDXRF emp./ ICP**
A	**N2**	625	1	672	-8	537	14
A	**J2**	1235	6	1670	-35	1221,1	1
A	**IG5**	436	2	283	35	487,2	-12
A	**J1**	1546	70	1880	-22	1522,6	2
A	**N1**	1710	16	2190	-28	1723,3	-1
A	**F1**	377	7	169	55	623,8	-65
A	**A3**	259	10	79	69	348,8	-35
A	**IG6**	677	26	680	0	644,2	5
A	**IG4**	1411	16	2820	-100	2066,9	-46
A	**12**	1156	31	1370	-18	1132,9	2
I	**B**	1046	7	1220	-17	1164,2	-11
I	**A**	920	15	957	-4	1323,3	-44
I	**P**	918	6	852	7	1345	-47
I	**17**	911	12	844	7	1069,4	-17
P	**G**	842	5	855	-2	798	5
P	**N**	891	6	926	-4	950,9	-7
P	**F**	864	12	960	-11	841,1	3
P	**M**	822	32	896	-9	984,5	-20
P	**K**	938	10	908	3	1004,2	-7
P	**H**	856	10	827	3	889,8	-4
P	**14**	878	20	872	1	856,7	2

Table 13: Concentrations obtained by ICP-OES, semi-empirical FP EDXRF and empirical EDXRF in ppm for Ca. Deviation is defined as (Mean ICP value - EDXRF value)/Mean ICP value * 100.

Manganese (Mn)							
Sample type	**Sample code**	**Mean ICP**	**SD ICP**	**EDXRF FP**	**Deviation (%) EDXRF FP / ICP**	**EDXRF emp.**	**Deviation (%) EDXRF emp./ ICP**
A	**N2**	1,29	0,05	N.D	-	0,3	77
A	**J2**	3,65	0,04	11	-201	6,5	-78
A	**IG5**	1,82	0,01	11	-505	0,3	83
A	**J1**	1,06	0,06	9	-747	2,3	-117
A	**N1**	1,76	0,03	N.D	-	0,3	83
A	**F1**	1,35	0,01	8	-494	2	-49
A	**A3**	0,73	0,03	5	-587	1,5	-106
A	**IG6**	0,63	0,02	7	-1004	0,3	53
A	**IG4**	0,75	0,00	8	-969	0,3	60
A	**12**	1,21	0,05	4	-231	0,8	34
I	**B**	20,79	0,48	38	-83	20,2	3
I	**A**	7,08	0,03	21	-196	9	-27
I	**P**	8,21	0,05	18	-119	8,1	1
I	**17**	19,84	0,65	29	-46	19,9	0
P	**G**	17,98	0,58	31	-72	16,4	9
P	**N**	20,71	0,12	34	-64	18,1	13
P	**F**	17,81	0,26	35	-97	16,9	5
P	**M**	14,55	1,40	27	-86	16	-10
P	**K**	18,42	0,11	28	-52	19,3	-5
P	**H**	17,17	0,02	31	-81	18,3	-7
P	**14**	11,51	0,07	24	-108	14,5	-26

Table 14: Concentrations obtained by ICP-OES, semi-empirical FP EDXRF and empirical EDXRF in ppm for Mn. Deviation is defined as (Mean ICP value - EDXRF value)/Mean ICP value * 100.

Iron (Fe)							
Sample type	**Sample code**	**Mean ICP**	**SD ICP**	**EDXRF FP**	**Deviation (%) EDXRF FP / ICP**	**EDXRF emp.**	**Deviation (%) EDXRF emp./ ICP**
A	**N2**	4,29	0,71	N.D	-	2	53
A	**J2**	28,50	0,62	52	-82	36,4	-28
A	**IG5**	5,27	0,42	14	-166	2,4	54
A	**J1**	4,76	0,07	14	-194	3,6	24
A	**N1**	4,74	0,16	11	-132	1,9	60
A	**F1**	5,74	0,17	12	-109	2,2	62
A	**A3**	4,78	0,15	10	-109	4,3	10
A	**IG6**	3,69	0,20	12	-225	0,5	86
A	**IG4**	3,20	0,08	11	-243	2,4	25
A	**12**	5,13	0,17	9	-75	N.D	-
I	**B**	19,07	0,00	38	-99	19,5	-2
I	**A**	16,51	0,42	39	-136	16,3	1
I	**P**	11,02	0,29	22	-100	12,7	-15
I	**17**	19,31	0,43	32	-66	21,9	-13
P	**G**	29,39	0,11	50	-70	32,5	-11
P	**N**	32,46	0,18	55	-69	40,8	-26
P	**F**	40,40	5,94	62	-53	41,7	-3
P	**M**	26,80	2,80	49	-83	32,4	-21
P	**K**	27,70	0,22	48	-73	35,5	-28
P	**H**	28,72	0,88	48	-67	34,3	-19
P	**14**	44,09	3,73	82	-86	61,6	-40

Table 15: Concentrations obtained by ICP-OES, semi-empirical FP EDXRF and empirical EDXRF in ppm for Fe. Deviation is defined as (Mean ICP value - EDXRF value)/Mean ICP value * 100.

Copper (Cu)							
Sample type	**Sample code**	**Mean ICP**	**SD ICP**	**EDXRF FP**	**Deviation (%) EDXRF FP / ICP**	**EDXRF emp.**	**Deviation (%) EDXRF emp./ ICP**
A	**N2**	0,33	0,09	9	-2631	0,9	-173
A	**J2**	3,00	0,03	14	-366	4	-33
A	**IG5**	0,32	0,02	11	-3391	1,3	-313
A	**J1**	0,44	0,02	12	-2641	1,7	-288
A	**N1**	0,28	0,00	10	-3454	1,2	-326
A	**F1**	0,26	0,01	11	-4116	1,3	-398
A	**A3**	0,25	0,03	10	-3917	1,3	-422
A	**IG6**	0,34	0,04	11	-3090	1,1	-219
A	**IG4**	0,28	0,00	11	-3890	1,2	-335
A	**12**	0,25	0,00	9	-3440	1,1	-333
I	**B**	0,26	0,01	11	-4146	2,1	-711
I	**A**	0,57	0,03	15	-2511	2,4	-318
I	**P**	0,68	0,35	10	-1368	2,9	-326
I	**17**	7,84	0,10	9	-15	1,9	76
P	**G**	9,31	0,15	26	-179	7,9	15
P	**N**	8,28	0,01	22	-166	7,8	6
P	**F**	7,28	0,02	27	-271	7,4	-2
P	**M**	6,99	0,66	21	-200	7,6	-9
P	**K**	6,87	0,01	20	-191	7,7	-12
P	**H**	9,11	0,29	24	-163	9,4	-3
P	**14**	6,26	0,08	19	-203	6,1	3

Table 16: Concentrations obtained by ICP-OES, semi-empirical FP EDXRF and empirical EDXRF in ppm for Cu. Deviation is defined as (Mean ICP value - EDXRF value)/Mean ICP value * 100.

Zinc (Zn)							
Sample type	**Sample code**	**Mean ICP**	**SD ICP**	**EDXRF FP**	**Deviation (%) EDXRF FP / ICP**	**EDXRF emp.**	**Deviation (%) EDXRF emp./ ICP**
A	**N2**	1,63	1,11	N.D	-	0,8	51
A	**J2**	8,41	0,27	14	-66	9,8	-16
A	**IG5**	1,65	0,07	6	-264	2,1	-27
A	**J1**	4,37	0,19	9	-106	5	-14
A	**N1**	1,03	0,01	4	-289	1,1	-7
A	**F1**	1,40	0,17	5	-257	1,1	22
A	**A3**	1,24	0,17	4	-222	0,8	36
A	**IG6**	2,61	0,30	7	-168	2,5	4
A	**IG4**	4,50	0,06	11	-144	7,2	-60
A	**12**	0,92	0,02	3	-227	1,3	-42
I	**B**	2,88	0,70	5	-74	2	30
I	**A**	2,48	0,10	9	-263	2,8	-13
I	**P**	1,61	0,01	4	-148	1,6	1
I	**17**	2,41	0,22	5	-108	2	17
P	**G**	4,87	1,04	9	-85	4,3	12
P	**N**	3,79	0,02	7	-85	4,3	-14
P	**F**	4,15	0,15	13	-213	4,4	-6
P	**M**	3,72	0,22	8	-115	4,4	-18
P	**K**	3,66	0,02	7	-91	3,7	-1
P	**H**	3,90	0,06	9	-131	4,6	-18
P	**14**	4,32	0,60	8	-85	4,9	-13

Table 17: Concentrations obtained by ICP-OES, semi-empirical FP EDXRF and empirical EDXRF in ppm for Zn. Deviation is defined as (Mean ICP value - EDXRF value)/Mean ICP value * 100.

Rubidium (Rb)							
Sample type	**Sample code**	**Mean ICP**	**SD ICP**	**EDXRF FP**	**Deviation (%) EDXRF FP / ICP**	**EDXRF emp.**	**Deviation (%) EDXRF emp./ ICP**
A	**N2**	3,87	0,21	7	-81	2,2	43
A	**J2**	4,91	0,01	9	-83	5,6	-14
A	**IG5**	6,49	0,08	10	-54	7,5	-16
A	**J1**	5,62	0,39	8	-42	5,2	7
A	**N1**	5,68	0,10	10	-76	4,8	15
A	**F1**	5,31	0,02	7	-32	4,7	11
A	**A3**	3,18	0,20	5	-57	3,7	-16
A	**IG6**	3,12	0,05	3	4	N.D	-
A	**IG4**	3,88	0,07	7	-80	5	-29
A	**12**	3,79	0,21	6	-58	2,5	34
I	**B**	50,91	1,28	50	2	52	-2
I	**A**	70,70	2,63	68	4	67,4	5
I	**P**	43,97	1,61	39	11	46,1	-5
I	**17**	39,30	1,98	35	11	42,8	-9
P	**G**	12,83	0,58	23	-79	21,1	-65
P	**N**	29,02	0,01	30	-3	31,6	-9
P	**F**	11,92	0,05	19	-59	19,3	-62
P	**M**	10,84	1,25	19	-75	18,5	-71
P	**K**	25,20	0,79	22	13	24,1	4
P	**H**	11,29	0,01	18	-59	18,6	-65
P	**14**	10,98	0,08	17	-55	21,8	-99

Table 18: Concentrations obtained by ICP-OES, semi-empirical FP EDXRF and empirical EDXRF in ppm for Rb. Deviation is defined as (Mean ICP value - EDXRF value)/Mean ICP value * 100.

Strontium (Sr)							
Sample type	**Sample code**	**Mean ICP**	**SD ICP**	**EDXRF FP**	**Deviation (%) EDXRF FP / ICP**	**EDXRF emp.**	**Deviation (%) EDXRF emp./ ICP**
A	**N2**	3,87	0,21	7	-81	2,2	43
A	**J2**	4,91	0,01	9	-83	5,6	-14
A	**IG5**	6,49	0,08	10	-54	7,5	-16
A	**J1**	5,62	0,39	8	-42	5,2	7
A	**N1**	5,68	0,10	10	-76	4,8	15
A	**F1**	5,31	0,02	7	-32	4,7	11
A	**A3**	3,18	0,20	5	-57	3,7	-16
A	**IG6**	3,12	0,05	3	4	N.D	-
A	**IG4**	3,88	0,07	7	-80	5	-29
A	**12**	3,79	0,21	6	-58	2,5	34
I	**B**	50,91	1,28	50	2	52	-2
I	**A**	70,70	2,63	68	4	67,4	5
I	**P**	43,97	1,61	39	11	46,1	-5
I	**17**	39,30	1,98	35	11	42,8	-9
P	**G**	12,83	0,58	23	-79	21,1	-65
P	**N**	29,02	0,01	30	-3	31,6	-9
P	**F**	11,92	0,05	19	-59	19,3	-62
P	**M**	10,84	1,25	19	-75	18,5	-71
P	**K**	25,20	0,79	22	13	24,1	4
P	**H**	11,29	0,01	18	-59	18,6	-65
P	**14**	10,98	0,08	17	-55	21,8	-99

Table 19: Concentrations obtained by ICP-OES, semi-empirical FP EDXRF and empirical EDXRF in ppm for Sr. Deviation is defined as (Mean ICP value - EDXRF value)/Mean ICP value * 100.

Sample type	Sample code	K	Ca	Mn	Fe	Cu	Zn	Sr	Rb
A	**N2**	4347	537	0,3	2	0,9	0,8	2,3	2,2
A	**J2**	10670	1221,1	6,5	36,4	4	9,8	5,7	5,6
A	**IG5**	9285	487,2	0,3	2,4	1,3	2,1	0,8	7,5
A	**J1**	9648	1522,6	2,3	3,6	1,7	5	0	5,2
A	**N1**	7329	1723,3	0,3	1,9	1,2	1,1	3,3	4,8
A	**F1**	12312	623,8	2	2,2	1,3	1,1	2,2	4,7
A	**A3**	5607	348,8	1,5	4,3	1,3	0,8	2	3,7
A	**IG6**	3978	644,2	0,3	0,5	1,1	2,5	0	0
A	**IG4**	9409	2066,9	0,3	2,4	1,2	7,2	1,4	5
A	**1**	5806	397,8	3,8	35,7	3,3	6,9	3,6	3,4
A	**2**	7956	508,2	0,9	4,1	1,2	1	1,1	16,1
A	**3**	6098	430,9	1,5	0,9	1,1	0,9	7,2	1,7
A	**4**	5037	345,2	0,3	1,1	1,4	1,1	0,6	0,1
A	**9**	2717	6286,3	7,1	10,1	1,8	15,7	6,1	4,6
A	**12**	2923	1132,9	0,8	0	1,1	1,3	2,2	2,5
A	**19**	15908	4808	10,5	13,1	4,2	19,1	1,6	26,4
I	**B**	27548	1164,2	20,2	19,5	2,1	2	8,5	52
I	**A**	33742	1323,3	9	16,3	2,4	2,8	10,6	67,4
I	**P**	30989	1345	8,1	12,7	2,9	1,6	6,4	46,1
I	**11**	30952	1305,7	5,5	11	2,7	2	6,5	34,7
I	**17**	24986	1069,4	19,9	21,9	1,9	2	5,7	42,8
P	**G**	17224	798	16,4	32,5	7,9	4,3	9,3	21,1
P	**N**	21675	950,9	18,1	40,8	7,8	4,3	11,3	31,6
P	**F**	17831	841,1	16,9	41,7	7,4	4,4	4,6	19,3
P	**M**	21483	984,5	16	32,4	7,6	4,4	7,1	18,5
P	**K**	21588	1004,2	19,3	35,5	7,7	3,7	3,3	24,1
P	**H**	18392	889,8	18,3	34,3	9,4	4,6	5,1	18,6
P	**5**	17293	820,5	15,5	36	8,7	4,5	5,9	23,3
P	**6**	17567	835,9	18,1	36,2	9	4,7	5	22,2
P	**7**	17520	830,8	16,9	38	8,2	4,5	3,8	21,9
P	**8**	17423	837,4	18,9	28,7	9,1	4,3	6	19,2
P	**10**	20751	953	19,7	34,4	8,2	3,6	11,5	30,3
P	**13**	17099	845,8	16,5	29,9	7,4	4,1	2,3	15,7

Table 20 continued from previous page

Sample type	Sample code	K	Ca	Mn	Fe	Cu	Zn	Sr	Rb
P	**14**	17948	856,7	14,5	61,6	6,1	4,9	5,2	21,8
P	**15**	16327	751,5	24,8	23,5	8,6	4,9	23,5	29,5
P	**16**	15345	772,5	32,9	26,9	8,5	5,6	4	17,4
P	**18**	20401	909,8	20,7	31,1	7,9	3,9	7,1	29,4

Table 20: Concentrations in ppm obtained by the EDXRF empirical calibration method used for PCA and PLS-DA.

B Appendix: TXRF

Potassium (K)											
Type of coffee	**Sample code**	**Mean ICP**	**SD ICP**	**Mean TXRF FP**	**SD TXRF FP**	**RSD (%) TXRF FP**	**Deviation TXRF FP / ICP**	**Mean TXRF emp.**	**SD TXRF emp.**	**RSD (%) TXRF emp.**	**Deviation TXRF emp. / ICP**
A	**N2**	4427	314	5567	578	10	-26	3606	886	25	19
A	**J2**	8663	89	8458	1544	18	2	7246	1832	25	16
A	**IG5**	9013	127	9398	66	1	-4	8538	9	0	5
A	**J1**	9153	813	7893	104	1	14	6746	224	3	26
A	**N1**	8384	73	7311	1782	24	13	5627	2251	40	33
A	**F1**	11404	423	12076	330	3	-6	11946	146	1	-5
A	**A3**	4973	199	6489	82	1	-30	4342	168	4	13
A	**IG6**	4458	112	4720	81	2	-6	2752	143	5	38
A	**IG4**	5695	177	5347	622	12	6	3091	664	21	46
A	**12**	4151	271	5360	179	3	-29	3535	264	7	15
I	**B**	27154	701	27154	5493	20	0	31061	6882	22	-14
I	**A**	36071	232	32949	3507	11	9	38144	4543	12	-6
I	**P**	29831	1370	25393	909	4	15	27635	1199	4	7
I	**17**	24023	1294	23730	440	2	1	26624	454	2	-11
P	**G**	15431	773	15647	1658	11	-1	15742	2278	14	-2
P	**N**	18613	120	19741	5	0	-6	21465	50	0	-15
P	**F**	16577	13	16562	1865	11	0	17591	2659	15	-6
P	**M**	17050	1762	15184	1130	7	11	15152	1628	11	11
P	**K**	19986	521	18704	252	1	6	19594	158	1	2
P	**H**	15535	39	16775	823	5	-8	17732	1142	6	-14
P	**14**	15039	167	16308	2048	13	-8	16996	1093	6	-13

Table 21: ICP-OES, FP TXRF and empirical TXRF concentrations in ppm for K. The deviation is defined as (Mean ICP value - EDXRF value)/Mean ICP value * 100; RSD = SD TXRF/Mean TXRF * 100.

Calcium (Ca)											
Type of coffee	**Sample code**	**Mean ICP**	**SD ICP**	**Mean TXRF FP**	**SD TXRF FP**	**RSD (%) TXRF FP**	**Deviation TXRF FP / ICP**	**Mean TXRF emp.**	**SD TXRF emp.**	**RSD (%) TXRF emp.**	**Deviation TXRF emp. / ICP**
A	**N2**	625	1	674	122	18	-8	625	87	14	0
A	**J2**	1235	6	1375	161	12	-11	1132	121	11	8
A	**IG5**	436	2	379	23	6	13	403	14	3	7
A	**J1**	1546	70	1716	218	13	-11	1372	162	12	11
A	**N1**	1710	16	1816	286	16	-6	1420	198	-	17
A	**F1**	377	7	355	20	6	6	385	5	1	-2
A	**A3**	259	10	178	3	1	31	249	13	5	4
A	**IG6**	677	26	655	35	5	3	600	27	5	11
A	**IG4**	1411	16	1368	54	4	3	1108	42	4	21
A	**12**	1156	31	1424	88	6	-23	1161	63	5	0
I	**B**	1046	7	1266	376	30	-21	1042	276	26	0
I	**A**	920	15	1132	137	12	-23	954	95	10	-4
I	**P**	918	6	952	49	5	-4	813	32	4	11
I	**17**	911	12	1124	26	2	-23	945	23	2	-4
P	**G**	842	5	835	36	4	1	727	15	2	14
P	**N**	891	6	1021	19	2	-15	875	16	2	2
P	**F**	864	12	962	66	7	-11	841	57	7	3
P	**M**	822	32	807	18	2	2	703	14	2	14
P	**K**	938	10	993	21	2	-6	836	9	1	11
P	**H**	856	10	994	40	4	-16	855	33	4	0
P	**14**	878	20	979	111	11	-11	845	30	4	4

Table 22: ICP-OES, FP TXRF and empirical TXRF concentrations in ppm for Ca. The deviation is defined as (Mean ICP value - EDXRF value)/Mean ICP value * 100; RSD = SD TXRF/Mean TXRF * 100.

Manganese (Mn)											
Type of coffee	**Sample code**	**Mean ICP**	**SD ICP**	**Mean TXRF FP**	**SD TXRF FP**	**RSD (%) TXRF FP**	**Deviation TXRF FP / ICP**	**Mean TXRF emp.**	**SD TXRF emp.**	**RSD (%) TXRF emp.**	**Deviation TXRF emp. / ICP**
A	**N2**	1,29	0,05	2,95	1,20	41	-128	0,32	0,84	259	75
A	**J2**	3,65	0,04	6,54	1,00	15	-79	3,27	0,71	22	10
A	**IG5**	1,82	0,01	3,45	1,06	31	-90	0,89	0,78	88	51
A	**J1**	1,06	0,06	2,75	0,20	7	-159	0,42	0,12	28	60
A	**N1**	1,76	0,03	2,46	0,24	10	-40	0,22	0,38	-	88
A	**F1**	1,35	0,01	2,70	0,45	17	-101	0,33	0,52	155	75
A	**A3**	0,73	0,03	2,52	0,55	22	-246	ND	-	-	-
A	**IG6**	0,63	0,02	1,71	0,25	15	-169	ND	-	-	-
A	**IG4**	0,75	0,00	1,65	0,12	7	-120	ND	-	-	-
A	**12**	1,21	0,05	3,21	0,70	22	-165	0,62	0,66	106	48
I	**B**	20,79	0,48	30,16	6,03	20	-45	21,89	4,69	21	-5
I	**A**	7,08	0,03	13,41	1,46	11	-89	8,65	1,23	14	-22
I	**P**	8,21	0,05	12,87	0,03	0	-57	8,15	0,06	1	1
I	**17**	19,84	0,65	30,62	1,61	5	-54	22,18	1,19	5	-12
P	**G**	17,98	0,58	25,58	5,18	20	-42	18,08	4,18	23	-1
P	**N**	20,71	0,12	27,51	0,38	1	-33	19,67	0,32	2	5
P	**F**	17,81	0,26	26,43	0,49	2	-48	18,99	0,66	3	-7
P	**M**	14,55	1,40	18,48	0,66	4	-27	13,33	0,49	4	8
P	**K**	18,42	0,11	25,39	1,25	5	-38	17,99	0,90	5	2
P	**H**	17,17	0,02	24,26	0,37	2	-41	17,13	0,37	2	0
P	**14**	11,51	0,07	19,77	2,31	12	-72	13,54	0,69	5	-18

Table 23: ICP-OES, FP TXRF and empirical TXRF concentrations in ppm for Mn. The deviation is defined as (Mean ICP value - EDXRF value)/Mean ICP value * 100; RSD = SD TXRF/Mean TXRF * 100.

Iron (Fe)											
Type of coffee	**Sample code**	**Mean ICP**	**SD ICP**	**Mean TXRF FP**	**SD TXRF FP**	**RSD (%) TXRF FP**	**Deviation TXRF FP / ICP**	**Mean TXRF emp.**	**SD TXRF emp.**	**RSD (%) TXRF emp.**	**Deviation TXRF emp. / ICP**
A	**N2**	1,29	0,05	2,95	1,20	41	-128	0,32	0,84	259	75
A	**J2**	3,65	0,04	6,54	1,00	15	-79	3,27	0,71	22	10
A	**IG5**	1,82	0,01	3,45	1,06	31	-90	0,89	0,78	88	51
A	**J1**	1,06	0,06	2,75	0,20	7	-159	0,42	0,12	28	60
A	**N1**	1,76	0,03	2,46	0,24	10	-40	0,22	0,38	-	88
A	**F1**	1,35	0,01	2,70	0,45	17	-101	0,33	0,52	155	75
A	**A3**	0,73	0,03	2,52	0,55	22	-246	ND	-	-	-
A	**IG6**	0,63	0,02	1,71	0,25	15	-169	ND	-	-	-
A	**IG4**	0,75	0,00	1,65	0,12	7	-120	ND	-	-	-
A	**12**	1,21	0,05	3,21	0,70	22	-165	0,62	0,66	106	48
I	**B**	20,79	0,48	30,16	6,03	20	-45	21,89	4,69	21	-5
I	**A**	7,08	0,03	13,41	1,46	11	-89	8,65	1,23	14	-22
I	**P**	8,21	0,05	12,87	0,03	0	-57	8,15	0,06	1	1
I	**17**	19,84	0,65	30,62	1,61	5	-54	22,18	1,19	5	-12
P	**G**	17,98	0,58	25,58	5,18	20	-42	18,08	4,18	23	-1
P	**N**	20,71	0,12	27,51	0,38	1	-33	19,67	0,32	2	5
P	**F**	17,81	0,26	26,43	0,49	2	-48	18,99	0,66	3	-7
P	**M**	14,55	1,40	18,48	0,66	4	-27	13,33	0,49	4	8
P	**K**	18,42	0,11	25,39	1,25	5	-38	17,99	0,90	5	2
P	**H**	17,17	0,02	24,26	0,37	2	-41	17,13	0,37	2	0
P	**14**	11,51	0,07	19,77	2,31	12	-72	13,54	0,69	5	-18

Table 24: ICP-OES, FP TXRF and empirical TXRF concentrations in ppm for Fe. The deviation is defined as (Mean ICP value - EDXRF value)/Mean ICP value * 100; RSD = SD TXRF/Mean TXRF * 100.

Copper (Cu)											
Type of coffee	**Sample code**	**Mean ICP**	**SD ICP**	**Mean TXRF FP**	**SD TXRF FP**	**RSD (%) TXRF FP**	**Deviation TXRF FP / ICP**	**Mean TXRF emp.**	**SD TXRF emp.**	**RSD (%) TXRF emp.**	**Deviation TXRF emp. / ICP**
A	**N2**	0,33	0,09	0,82	0,50	61	-148	0,07	0,23	316	78
A	**J2**	3,00	0,03	5,40	0,67	12	-80	2,79	0,38	13	7
A	**IG5**	0,32	0,02	0,84	0,09	11	-165	0,15	0,04	28	54
A	**J1**	0,44	0,02	0,58	0,15	26	-31	ND	-	-	-
A	**N1**	0,28	0,00	0,77	0,18	24	-174	ND	-	-	-
A	**F1**	0,26	0,01	1,36	0,38	28	-423	0,46	0,19	41	-75
A	**A3**	0,25	0,03	0,79	0,36	45	-216	0,12	-	-	51
A	**IG6**	0,34	0,04	0,83	0,11	13	-142	0,16	0,06	37	55
A	**IG4**	0,28	0,00	0,66	0,06	9	-139	0,03	0,02	78	90
A	**12**	0,25	0,00	0,63	0,13	21	-147	ND	-	-	-
I	**B**	0,26	0,01	0,84	0,25	30	-223	0,16	0,14	89	38
I	**A**	0,57	0,03	2,15	0,66	31	-275	0,90	0,38	42	-57
I	**P**	0,68	0,35	0,96	0,06	6	-40	0,20	0,04	22	71
I	**17**	7,84	0,10	13,95	0,69	5	-78	7,79	0,39	5	1
P	**G**	9,31	0,15	17,35	3,27	19	-86	9,76	1,94	20	-5
P	**N**	8,28	0,01	14,02	1,19	9	-69	7,82	0,70	9	6
P	**F**	7,28	0,02	13,31	0,66	5	-83	7,46	0,29	4	-2
P	**M**	6,99	0,66	11,91	1,03	9	-70	6,40	0,88	14	9
P	**K**	6,87	0,01	11,73	1,35	11	-71	6,49	0,77	12	5
P	**H**	9,11	0,29	15,60	1,58	10	-71	8,73	0,90	10	4
P	**14**	6,26	0,08	11,16	1,02	9	-78	6,13	0,13	2	2

Table 25: ICP-OES, FP TXRF and empirical TXRF concentrations in ppm for Cu. The deviation is defined as (Mean ICP value - EDXRF value)/Mean ICP value * 100; RSD = SD TXRF/Mean TXRF * 100.

Zinc (Zn)											
Type of coffee	**Sample code**	**Mean ICP**	**SD ICP**	**Mean TXRF FP**	**SD TXRF FP**	**RSD (%) TXRF FP**	**Deviation TXRF FP / ICP**	**Mean TXRF emp.**	**SD TXRF emp.**	**RSD (%) TXRF emp.**	**Deviation TXRF emp. / ICP**
A	**N2**	1,63	1,11	2,91	1,75	60	-78	1,57	1,13	72	4
A	**J2**	8,41	0,27	11,72	1,62	14	-39	7,01	0,99	14	17
A	**IG5**	1,65	0,07	3,42	0,48	14	-108	1,87	0,30	16	-13
A	**J1**	4,37	0,19	7,07	0,41	6	-62	4,15	0,25	6	5
A	**N1**	1,03	0,01	1,79	0,59	33	-74	0,88	0,40	45	14
A	**F1**	1,40	0,17	2,95	0,08	3	-111	1,58	0,07	4	-13
A	**A3**	1,24	0,17	2,24	0,20	9	-80	1,20	0,22	18	4
A	**IG6**	2,61	0,30	4,02	0,63	16	-54	2,25	0,38	17	14
A	**IG4**	4,50	0,06	6,53	0,06	1	-45	3,79	0,03	1	16
A	**12**	0,92	0,02	1,83	0,09	5	-100	0,93	0,01	1	-2
I	**B**	2,88	0,70	5,29	2,64	50	-84	3,04	1,64	54	-6
I	**A**	2,48	0,10	4,78	0,14	3	-93	2,71	0,08	3	-9
I	**P**	1,61	0,01	2,99	0,21	7	-85	1,59	0,14	9	2
I	**17**	2,41	0,22	4,57	0,24	5	-90	2,58	0,14	5	-7
P	**G**	4,87	1,04	10,87	6,33	58	-123	6,48	3,94	61	-33
P	**N**	3,79	0,02	6,47	1,04	16	-71	3,75	0,64	17	1
P	**F**	4,15	0,15	6,57	0,29	4	-58	3,84	0,13	3	7
P	**M**	3,72	0,22	6,90	0,39	6	-85	3,85	0,00	0	-4
P	**K**	3,66	0,02	5,80	0,33	6	-59	3,34	0,19	6	9
P	**H**	3,90	0,06	6,85	0,84	12	-76	3,99	0,51	13	-2
P	**14**	4,32	0,60	6,68	0,40	6	-55	3,89	0,54	14	10

Table 26: ICP-OES, FP TXRF and empirical TXRF concentrations in ppm for Zn. The deviation is defined as (Mean ICP value - EDXRF value)/Mean ICP value * 100; RSD = SD TXRF/Mean TXRF * 100.

Rubidium (Rb)											
Type of coffee	**Sample code**	**Mean ICP**	**SD ICP**	**Mean TXRF FP**	**SD TXRF FP**	**RSD (%) TXRF FP**	**Deviation TXRF FP / ICP**	**Mean TXRF emp.**	**SD TXRF emp.**	**RSD (%) TXRF emp.**	**Deviation TXRF emp. / ICP**
A	**N2**	3,87	0,21	8,14	1,12	14	-111	2,68	1,30	49	31
A	**J2**	4,91	0,01	8,90	1,32	15	-81	3,38	1,08	32	31
A	**IG5**	6,49	0,08	11,69	0,22	2	-80	6,16	0,10	2	5
A	**J1**	5,62	0,39	10,45	0,21	2	-86	5,15	0,33	6	8
A	**N1**	5,68	0,10	10,20	0,85	8	-80	4,73	0,88	19	17
A	**F1**	5,31	0,02	9,10	0,69	8	-71	3,77	0,24	6	29
A	**A3**	3,18	0,20	5,91	0,43	7	-86	0,62	0,50	80	80
A	**IG6**	3,12	0,05	5,21	0,41	8	-67	ND	-	-	-
A	**IG4**	3,88	0,07	6,62	0,13	2	-71	1,17	0,27	23	70
A	**12**	3,79	0,21	8,21	0,96	12	-117	2,94	0,97	33	22
I	**B**	50,91	1,28	56,93	9,10	16	-12	49,03	8,49	17	4
I	**A**	70,70	2,63	72,20	5,76	8	-2	63,09	5,63	9	11
I	**P**	43,97	1,61	41,11	1,03	3	6	33,69	0,85	3	23
I	**17**	39,30	1,98	42,87	2,45	6	-9	35,61	2,14	6	9
P	**G**	12,83	0,58	24,68	3,64	15	-92	18,26	3,83	21	-42
P	**N**	29,02	0,01	32,54	1,27	4	-12	25,65	1,13	4	12
P	**F**	11,92	0,05	24,11	0,93	4	-102	17,80	0,57	3	-49
P	**M**	10,84	1,25	19,62	1,55	8	-81	12,90	2,60	20	-19
P	**K**	25,20	0,79	27,88	2,12	8	-11	21,44	1,78	8	15
P	**H**	11,29	0,01	22,21	0,36	2	-97	15,92	0,17	1	-41
P	**14**	10,98	0,08	22,11	2,14	10	-101	15,68	0,51	3	-43

Table 27: ICP-OES, FP TXRF and empirical TXRF concentrations in ppm for Rb. The deviation is defined as (Mean ICP value - EDXRF value)/Mean ICP value * 100; RSD = SD TXRF/Mean TXRF * 100.

Strontium (Sr)											
Type of coffee	**Sample code**	**Mean ICP**	**SD ICP**	**Mean TXRF FP**	**SD TXRF FP**	**RSD (%) TXRF FP**	**Deviation TXRF FP / ICP**	**Mean TXRF emp.**	**SD TXRF emp.**	**RSD (%) TXRF emp.**	**Deviation TXRF emp. / ICP**
A	**N2**	1,29	0,06	1,27	0,16	13	1	ND	-	-	-
A	**J2**	3,11	0,06	3,21	0,58	18	-3	2,97	0,81	27	5
A	**IG5**	2,20	0,11	2,15	0,07	3	2	1,43	0,06	4	35
A	**J1**	2,21	0,16	2,33	0,01	0	-5	1,76	0,04	2	21
A	**N1**	2,22	0,04	2,29	0,12	5	-3	1,61	0,18	11	27
A	**F1**	1,93	0,06	2,02	0,09	4	-4	1,25	0,28	22	36
A	**A3**	0,94	0,02	1,05	0,11	11	-13	ND	-	-	-
A	**IG6**	1,03	0,01	1,23	0,02	1	-19	0,10	0,01	7	90
A	**IG4**	1,24	0,04	1,12	0,08	7	10	ND	-	-	-
A	**12**	1,22	0,04	1,53	0,01	0	-26	0,50	0,08	15	59
I	**B**	9,15	0,15	9,18	2,07	23	0	12,10	3,09	26	-32
I	**A**	13,65	0,16	10,78	0,45	4	21	14,38	0,76	5	-5
I	**P**	7,53	0,34	6,05	0,19	3	20	7,22	0,25	3	4
I	**17**	7,33	0,24	6,93	0,24	3	5	8,63	0,29	3	-18
P	**G**	4,13	0,16	3,76	0,04	1	9	3,80	0,08	2	8
P	**N**	6,36	0,01	6,31	0,27	4	1	7,63	0,38	5	-20
P	**F**	3,95	0,11	4,16	0,12	3	-5	4,41	0,09	2	-12
P	**M**	4,58	0,39	4,71	0,07	1	-3	5,26	0,16	3	-15
P	**K**	5,15	0,15	4,73	0,30	6	8	5,31	0,37	7	-3
P	**H**	4,75	0,10	5,34	0,21	4	-13	6,17	0,24	4	-30
P	**14**	4,18	0,19	4,48	0,22	5	-7	4,83	0,15	3	-16

Table 28: ICP-OES, FP TXRF and empirical TXRF concentrations in ppm for Sr. The deviation is defined as (Mean ICP value - EDXRF value)/Mean ICP value * 100; RSD = SD TXRF/Mean TXRF * 100.

Sample	Sample [g]	Vessel [g]	Total [g]	Digest [g]	DF
12,7	0,2506	11,7490	27,3863	15,6373	62,40
12,8	0,2576	11,6837	27,4669	15,7832	61,27
14,1	0,2540	11,7609	28,7936	17,0327	67,06
14,9	0,2540	11,7268	28,8512	17,1244	67,42
17,2	0,2502	11,6975	27,1470	15,4495	61,75
17, 1	0,2517	11,6601	27,9504	16,2903	64,72
A,7	0,2551	11,7486	28,9231	17,1745	67,32
A,8	0,2521	11,7395	27,7982	16,0587	63,70
A2, 1	0,2538	11,7470	28,4230	16,6760	65,71
A2, 2	0,2544	11,6958	28,2637	16,5679	65,13
A3,3	0,2508	11,6584	28,1467	16,4883	65,74
A3,4	0,2555	11,8208	27,2235	15,4027	60,28
B, 1	0,2549	11,7740	27,1352	15,3612	60,26
B,2	0,2526	11,7738	27,3099	15,5361	61,50
C, 4	0,2518	11,8292	28,2130	16,3838	65,07
C, 5	0,2584	11,7626	29,1351	17,3725	67,23
Carrot standard, 3	0,2079	11,7748	29,3532	17,5784	84,55
Carrot standard, 4	0,2047	11,7756	29,4379	17,6623	86,28
Carrot standard, 5	0,2190	11,7968	28,9577	17,1609	78,36
D, 6	0,2556	11,7872	28,5915	16,8043	65,74
D, 7	0,2508	11,7066	29,9883	18,2817	72,89
E, 7	0,2572	11,7197	27,7537	16,0340	62,34
E, 8	0,2528	11,6371	27,6362	15,9991	63,29
F,10	0,2543	11,7856	28,8070	17,0214	66,93
F,9	0,2533	11,6228	28,6967	17,0739	67,41
F1,5	0,2538	11,6271	28,5634	16,9363	66,73
F1,6	0,2536	11,7138	26,7743	15,0605	59,39
G, 1	0,2564	11,6987	27,6997	16,0010	62,41
G, 5	0,2526	11,7273	29,2169	17,4896	69,24
Green Tea, 6	0,2075	11,7457	28,1168	16,3711	78,90
Green Tea, 7	0,2045	11,7143	28,6219	16,9076	82,68
Green Tea, 8	0,2151	11,6783	29,0997	17,4214	80,99
H, 10	0,2547	11,7136	28,0815	16,3679	64,26
H, 9	0,2545	11,6314	28,7019	17,0705	67,07

Table 29 continued from previous page

Sample	Sample [g]	Vessel [g]	Total [g]	Digest [g]	DF
I, 2	0,2511	11,6950	27,3724	15,6774	62,43
I, 3	0,2568	11,6675	27,9974	16,3299	63,59
IG 5, 1	0,2520	11,5796	27,8800	16,3004	64,68
IG 5, 11	0,2532	11,6865	27,5578	15,8713	62,68
IG 6, 10	0,2586	11,7765	27,5385	15,7620	60,95
IG 6, 9	0,2511	11,7705	27,3483	15,5778	62,04
IG1,1	0,2534	11,6830	27,9720	16,2890	64,28
IG1,2	0,2506	11,6890	27,5285	15,8395	63,21
IG2, 3	0,2515	11,7433	27,9203	16,1770	64,32
IG2, 4	0,2545	11,7902	28,3059	16,5157	64,89
IG3, 10	0,2504	11,7302	28,6469	16,9167	67,56
IG3, 9	0,2572	11,7065	27,9623	16,2558	63,20
IG4, 5	0,2571	11,5888	29,0412	17,4524	67,88
IG4, 6	0,2509	11,7816	28,1504	16,3688	65,24
J, 11	0,2514	11,7605	27,9623	16,2018	64,45
J, 12	0,2545	11,7931	28,2331	16,4400	64,60
J1,3	0,2512	11,7264	27,5280	15,8016	62,90
J1,4	0,2573	11,6651	27,1960	15,5309	60,36
J2, 10	0,2559	11,8177	28,2353	16,4176	64,16
J2, 9	0,2533	11,7000	28,7412	17,0412	67,28
K, 3	0,2560	11,6745	28,5498	16,8753	65,92
K, 4	0,2572	11,7157	27,6227	15,9070	61,85
L, 5	0,2513	11,7865	27,9669	16,1804	64,39
L, 6	0,2592	11,7006	28,1032	16,4026	63,28
Leaves, 10	0,2181	11,7288	26,9310	15,2022	69,70
Leaves, 11	0,2114	11,7537	27,7442	15,9905	75,64
Leaves, 12	0,2201	11,6443	28,5739	16,9296	76,92
M,1	0,2525	11,7102	29,1417	17,4315	69,04
M,2	0,2540	11,7947	27,8117	16,0170	63,06
N, 11	0,2533	11,7374	28,2596	16,5222	65,23
N, 12	0,2518	11,7006	28,4286	16,7280	66,43
N1,5	0,2531	11,6718	27,6898	16,0180	63,29
N1,6	0,2505	11,7643	28,0031	16,2388	64,83

Table 29 continued from previous page

Sample	Sample [g]	Vessel [g]	Total [g]	Digest [g]	DF
N2, 11	0,2550	11,7448	28,0617	16,3169	63,99
N2, 12	0,2538	11,7217	28,9155	17,1938	67,75
N3, 3	0,2562	11,7809	28,3068	16,5259	64,50
N3, 4	0,2615	11,6602	27,3970	15,7368	60,18
P, 7	0,2511	11,7226	28,7760	17,0534	67,91
P, 8	0,2529	11,7864	28,4109	16,6245	65,74

Table 29: Dilution factors for coffee sample digests and CRMs.

Sample	Digest [g]	Digest + IS [g]	IS [g]	IS conc. [ppm]
12,7	1,2532	1,2790	0,0258	4,10
12,8	1,2147	1,2399	0,0252	4,13
14,10	1,2560	1,2825	0,0265	4,20
14,9	1,2397	1,2644	0,0247	3,97
17,1	1,2361	1,2620	0,0259	4,17
17,2	1,2641	1,2892	0,0251	3,96
A,7	1,2213	1,2464	0,0251	4,09
A,8	1,2590	1,2842	0,0252	3,99
A2,1	1,2469	1,2721	0,0252	4,03
A2,2	1,2664	1,2912	0,0248	3,91
A3,3	1,2383	1,2636	0,0253	4,07
A3,4	1,2477	1,2726	0,0249	3,98
B,1	1,2509	1,2761	0,0252	4,02
B,2	1,2474	1,2753	0,0279	4,45
C,4	1,2456	1,2692	0,0236	3,78
C,5	1,2186	1,2427	0,0241	3,94
Carrot standard, 3	1,2275	1,2527	0,0252	4,09
Carrot standard, 4	1,2052	1,2279	0,0227	3,76
Carrot standard, 5	1,2004	1,2246	0,0242	4,02
D,6	1,2382	1,2634	0,0252	4,06
D,7	1,2167	1,2423	0,0256	4,19
E,7	1,2037	1,2278	0,0241	3,99
E,8	1,1734	1,1988	0,0254	4,31

Table 30 continued from previous page

Sample	Digest [g]	Digest + IS [g]	IS [g]	IS conc. [ppm]
F,10	1,2151	1,2399	0,0248	4,07
F,9	1,1663	1,1909	0,0246	4,20
F1,5	1,2367	1,2637	0,0270	4,34
F1,6	1,2815	1,3042	0,0227	3,54
G,1	1,2486	1,2736	0,0250	3,99
G,5	1,2099	1,2352	0,0253	4,16
Green Tea, 6,1	1,2629	1,2862	0,0233	3,68
Green Tea, 6,2	1,2505	1,2756	0,0251	4,00
Green Tea, 7,1	1,2477	1,2703	0,0226	3,62
Green Tea, 7,2	1,2488	1,2719	0,0231	3,69
Green Tea, 8,1	1,2429	1,2679	0,025	4,01
Green Tea, 8,2	1,2429	1,2679	0,025	4,01
Green Tea, 8,3	1,2477	1,2728	0,0251	4,01
Green Tea, 8,4	1,2477	1,2728	0,0251	4,01
H,10	1,2495	1,2749	0,0254	4,05
H,9	1,2446	1,2700	0,0254	4,07
I,1	1,245	1,2699	0,0249	3,99
I,2	1,2503	1,2752	0,0249	3,97
IG1,1	1,2239	1,2491	0,0252	4,10
IG1,2	1,2555	1,281	0,0255	4,05
IG2,3	1,2435	1,2688	0,0253	4,05
IG2,4	1,2396	1,2656	0,0260	4,18
IG3,10	1,2285	1,2532	0,0247	4,01
IG3,9	1,2505	1,2757	0,0252	4,02
IG4,5	1,2235	1,2483	0,0248	4,04
IG4,6	1,1897	1,2150	0,0253	4,23
IG5,1	1,2146	1,2394	0,0248	4,07
IG5,11	1,1804	1,2055	0,0251	4,23
IG6,10	1,1782	1,2030	0,0248	4,19
IG6,9	1,1382	1,2004	0,0248	4,19
J,11	1,222	1,247	0,0250	4,08
J,12	1,2472	1,2723	0,0251	4,01
J1,3	1,2597	1,2852	0,0255	4,03

Table 30 continued from previous page

Sample	Digest [g]	Digest + IS [g]	IS [g]	IS conc. [ppm]
J1,4	1,2482	1,2718	0,0236	3,77
J2,10	1,2395	1,2640	0,0245	3,94
J2,9	1,2171	1,240	0,0229	3,76
K,3	1,1966	1,2218	0,0252	4,19
K,4	1,1966	1,2212	0,0246	4,10
L, 6	1,1723	1,1978	0,0255	4,33
L,5	1,1918	1,2169	0,0251	4,19
Leaves 10	1,0908	1,1167	0,0259	4,72
Leaves 11	1,2325	1,2580	0,0255	4,12
Leaves 12	1,2182	1,2409	0,0227	3,72
M, 1	1,2075	1,2326	0,0251	4,14
M,2	1,2731	1,2964	0,0233	3,65
N,11	1,2503	1,2755	0,0252	4,02
N,12	1,2475	1,2728	0,0253	4,04
N1,5	1,2543	1,2800	0,0257	4,08
N1,6	1,2155	1,2405	0,025	4,10
N2,11	1,2462	1,2711	0,0249	3,98
N2,12	1,2210	1,2465	0,0255	4,16
N3,3	1,2482	1,274	0,0258	4,12
N3,4	1,2590	1,2845	0,0255	4,04
P,7	1,2423	1,2672	0,0249	4,00
P,8	1,239	1,26422	0,0252	4,05

Table 30: Concentrations of the internal standard (Ga) in ppm in the digested coffee samples and in the digests of the certified reference materials.

Coffee type	Sample code	K	Ca	Mn	Fe	Cu	Zn	Rb	Sr
A	**N2**	3606	625	0,32	2,60	0,07	1,57	2,68	0,00
A	**J2**	7246	1132	3,27	21,27	2,79	7,01	3,38	2,97
A	**IG5**	8538	403	0,89	3,31	0,15	1,87	6,16	1,43
A	**J1**	6746	1372	0,42	3,00	0,00	4,15	5,15	1,76
A	**N1**	5627	1420	0,22	2,38	0,00	0,88	4,73	1,61
A	**F1**	11946	385	0,33	5,22	0,46	1,58	3,77	1,25
A	**A3**	4342	249	0,00	2,80	0,12	1,20	0,62	0,00
A	**IG6**	2752	600	0,00	1,73	0,16	2,25	0,00	0,10
A	**IG4**	3091	1108	0,00	1,63	0,03	3,79	1,17	0,00
A	**12**	3535	1161	0,62	3,01	0,00	0,93	2,94	0,50
I	**B**	31061	1042	21,89	17,03	0,16	3,04	49,03	12,10
I	**A**	38144	954	8,65	14,54	0,90	2,71	63,09	14,38
I	**P**	27635	813	8,15	10,26	0,20	1,59	33,69	7,22
I	**17**	26624	945	22,18	17,87	7,79	2,58	35,61	8,63
P	**G**	15742	727	18,08	29,81	9,76	6,48	18,26	3,80
P	**N**	21465	875	19,67	26,59	7,82	3,75	25,65	7,63
P	**F**	17591	841	18,99	37,98	7,46	3,84	17,80	4,41
P	**M**	15152	703	13,33	25,30	6,40	3,85	12,90	5,26
P	**K**	19594	836	17,99	22,44	6,49	3,34	21,44	5,31
P	**H**	17732	855	17,13	28,94	8,73	3,99	15,92	6,17
P	**14**	16996	845	13,54	39,15	6,13	3,89	15,68	4,83
P	**G**	17224	798	16,4	32,5	7,9	4,3	9,3	21,1
P	**N**	21675	950,9	18,1	40,8	7,8	4,3	11,3	31,6
P	**F**	17831	841,1	16,9	41,7	7,4	4,4	4,6	19,3
P	**M**	21483	984,5	16	32,4	7,6	4,4	7,1	18,5
P	**K**	21588	1004,2	19,3	35,5	7,7	3,7	3,3	24,1
P	**H**	18392	889,8	18,3	34,3	9,4	4,6	5,1	18,6
P	**5**	17293	820,5	15,5	36	8,7	4,5	5,9	23,3
P	**6**	17567	835,9	18,1	36,2	9	4,7	5	22,2
P	**7**	17520	830,8	16,9	38	8,2	4,5	3,8	21,9
P	**8**	17423	837,4	18,9	28,7	9,1	4,3	6	19,2
P	**10**	20751	953	19,7	34,4	8,2	3,6	11,5	30,3
P	**13**	17099	845,8	16,5	29,9	7,4	4,1	2,3	15,7

Table 31 continued from previous page

Coffee type	Sample code	K	Ca	Mn	Fe	Cu	Zn	Rb	Sr
P	**14**	17948	856,7	14,5	61,6	6,1	4,9	5,2	21,8
P	**15**	16327	751,5	24,8	23,5	8,6	4,9	23,5	29,5
P	**16**	15345	772,5	32,9	26,9	8,5	5,6	4	17,4
P	**18**	20401	909,8	20,7	31,1	7,9	3,9	7,1	29,4

Table 31: Concentrations in ppm obtained by the TXRF empirical calibration method used for PCA and PLS-DA.